Aus dem Institut für physiologische Genomik – Biomedical Center
der Ludwig-Maximilians-Universität München
Direktorin: Univ. Prof. Dr. Magdalena Götz

Functional Characterization of Murine Muscle Spindles: Modulatory Roles of Acetylcholine Receptors and of the Dystrophin-Associated Protein Complex

Dissertation
zum Erwerb des Doktorgrades der Naturwissenschaften
an der medizinischen Fakultät der
Ludwig-Maximilians-Universität zu München

vorgelegt von
Laura Gerwin

aus
Starnberg

2019

Mit Genehmigung der Medizinischen Fakultät
der Universität München

Betreuer : Prof. Dr. Stephan Kröger

Zweitgutachter(in): : Prof. Anja Horn-Bochtler

Dekan: Prof. Dr. med. dent. Reinhard Hickel

Tag der mündlichen Prüfung: 09.04.2020

Eidesstattliche Erklärung

Ich, Laura Gerwin, erkläre hiermit an Eides statt,
dass ich die vorliegende Dissertation mit dem Titel „Functional Characterization of Murine Muscle Spindles: Modulatory Roles of Acetylcholine Receptors and of the Dystrophin-Associated Protein Complex“
selbständig verfasst, mich außer der angegebenen keiner weiteren Hilfsmittel bedient und alle Erkenntnisse, die aus dem Schrifttum ganz oder annähernd übernommen sind, als solche kenntlich gemacht und nach ihrer Herkunft unter Bezeichnung der Fundstelle einzeln nachgewiesen habe.

Ich erkläre des Weiteren, dass die hier vorgelegte Dissertation nicht in gleicher oder in ähnlicher Form bei einer anderen Stelle zur Erlangung eines akademischen Grades eingereicht wurde.

München, den 24.04.2020

Laura Gerwin

Parts of this thesis have been published:

Gerwin L., Haupt C., Wilkinson K.A. and Kröger S. (2019). Acetylcholine receptors in the equatorial region of intrafusal muscle fibres modulate mouse muscle spindle sensitivity. *The Journal of Physiology* **597:** 1993-2006.

Gerwin L., Rossmanith S., Haupt C., Schultheiß J., Brinkmeier H., Bittner R.E. and Kröger S. (2020) Impaired Muscle Spindle Function in Murine Models of Muscular Dystrophy manuscript submitted for publication. *The Journal of Physiology* **598:** 1591-1609

Acknowledgements

The time as a PhD candidate has been a very intensive period of my life and I would like to thank all the people, who have supported me for their great help throughout the last years.
First, I would like to express my sincere gratitude to my supervisor Prof. Dr. Stephan Kröger for giving me the opportunity to work on these exciting projects and to be part of his research group. I am very grateful for providing me with all the equipment needed, for the excellent supervision, continuous scientific support and the chance to visit the lab of Prof. Katherine Wilkinson at SanJose State University.
I am very grateful to Prof. Wilkinson and her whole team for the lessons in electrophysiology and extracellular recordings, and for making the time in San Jose as enjoyable as it was. It was an amazing time and I will never forget it.
Moreover, I would like to thank Dr. Corinna Haupt for her constant help and guidance, for our fruitful discussions, for her scientific support whenever needed, and overall for her constant moral support and advice. I can´t express how grateful I am. Thank you so much.
I also want to thank the members of my thesis advisory committee Prof. Dr. Magdalena Götz, Prof. Dr. Benedikt Schoser, Prof. Dr. Bernd Sutor and Prof. Dr. Anja Horn-Bochtler for challenging scientific discussions and valuable feedback concerning the progress of my research.
I would also like to thank Dr. Andreas Thomae from the LMU bioimaging facility at the BMC for his great support and lessons in confocal microscopy. I would like to thank Hansruedi Brenner and Peter Grafe for many helpful discussions, Peter Fischer and Veit Witzemann for donating equipment, Heinrich Brinkmeier and Reginald E. Bittner for providing me with the mouse lines used in this study and of course Martina Bürkle for expert technical assistance.
I want to thank all the members of the lab Michel, Sarah, Hedi, Anna, Yina, Martina and especially Gerry for the great time, many loughs and our coffee breaks. It was great working with all of you.
I want to thank all my friends for always being there when needed.
Finally, I owe my deepest gratitude to my parents, my brother and Jean-Pierre. Thank you, for your constant support, love and encouragement. Thank you, for being on my side, for helping me through stressful times and not letting me give up. A special thanks to my brother for coding a program for analysing my data faster. This program saved my live.
You all never stopped believing in me and my thesis would have not been possible without you. Thank you so much.

Abbreviations

[ ]	Concentration
ACh	Acetylcholine
AChE	Acetylcholine Esterase
AChR	Acetylcholine Receptor
ACSF	Artificial cerebrospinal fluid
ADP	Adenosine diphosphate
ANOVA	analysis of variance
ATP	Adenosine triphosphate
BL10	C57BL10/10sc
BL6	C57BL6/J
Ca^{2+}	Calcium
CHT	High affinity choline transporter
Cy3	Cyanine dye 3
Cy5	Cyanine dye 5
DAPI	4',6-diamidino-2-phenylindole
DGC	dystrophin-glycoprotein complex
DI	Dynamic Index
DMD	Duchenne muscular dystrophy
DMD^{mdx}	C57BL10/10sc/Dmdx
DMD^{mdx}-*dysf*$^{-/-}$	Dmd^{mdx}SJL-dysf C57BL/6
DP	Dynamic Peak
DRG	Dorsal root ganglion
dysf$^{-/-}$	SJL-dysf C57BL/6
EDL	Extensor digitorum longus
GFP	green fluorescent protein
h	hour
H_2O	Hydrogen dioxide, water
HyDs	Hybrid detector system
Lo	Resting length of the EDL muscle
LSM	Laser scanning microscope
NMJ	neuromuscular junction
PBS	Phosphate Buffered Saline
PFA	Paraformaldehyde
RD	Resting Discharge

SR	Static Response
TS	Time Silenced
utro$^{-/-}$	C57BL10/10sc/Utro
vGluT1	vesicular glutamate Transporter 1
WLL	white light laser
WT	wildtype mice
α-BTX	alpha-bungarotoxin

Table of contents

Zusammenfassung

Für jede Form von koordinierten Bewegungen werden propriozeptive Informationen, wie z.B. die Muskelspannung oder die Position der Extremitäten im Raum benötigt. Die wichtigsten propriozeptiven Sensoren sind Muskelspindeln. Muskelspindeln sind komplexe, dehnungssensitive Mechanorezeptoren. Sie messen die Geschwindigkeit und das Ausmaß einer Dehnung von Skelettmuskelfasern. Muskelspindeln bestehen aus spezialisierten Skelettmuskelfasern, den so genannten Intrafusalfasern. Diese werden in ihrem Zentrum von einem sensorischen Neuron annulospiral umwunden. In diesem Bereich wird die Geschwindigkeit und das Ausmaß der Muskeldehnung in eine Aktionspotentialfrequenz kodiert, die proportional sowohl zum Ausmaß der Längenänderung als auch zu deren Geschwindigkeit ist. Beide polare Endigungen von Intrafusalfasern werden von einem γ-Motoneuron innerviert.

Im zentralen Bereich der Muskelspindel sind AChR im Bereich des Kontaktes zwischen sensorischer Afferenz und Intrafusalfaser konzentriert. Um die Funktion dieser AChR zu untersuchen, wurden extrazelluläre Ableitungen propriozeptiver Afferenzen von EDL-Muskeln aus Wildtypmäusen untersucht. Dafür wurden sowohl „ramp-and-hold“-Dehnungen als auch sinusoidale Vibrationen vor und nach Zugabe der AChR-Inhibitoren d-Tubocurarin und *α*-Bungarotoxin sowie Hemicholinium-3, einem Inhibitor der Cholinwiederaufnahme, durchgeführt. Nach Zugabe der Medikamente blieb die Aktionspotentialfrequenz in Ruhe konstant während sich die Aktionspotentialfrequenz bei Dehnung des Muskels erhöhte. Des Weiteren erhöhte sich die Aktionspotentialfrequenz bei sinusoidalen Vibrationen mit kleiner Amplitude in der Gegenwart von *α*-Bungarotoxin. Diese Ergebnisse deuten darauf hin, dass ACh die Muskelspindelfunktion während einer Muskeldehnung moduliert.

In einem zweiten Projekt habe ich die Muskelspindelfunktion in Mausmodellen für Muskeldystrophie untersucht. Zu der Gruppe der Muskeldystrophien werden verschiedene erbliche Krankheiten zusammengefasst, die alle durch eine progressive Degeneration und Schwäche der Skelettmuskulatur charakterisiert sind. Um zu untersuchen ob Intrafusalfasern ebenfalls betroffen sind, habe ich die Funktion und die Morphologie der Muskelspindeln von zwei Mausmodellen für Muskeldystrophie (Dystrophin- und Dysferlin-defiziente Mäuse) untersucht. Sowohl die Morphologie als auch die Anzahl der Muskelspindeln in Soleusmuskeln von dystrophischen Mäusen erscheint unverändert. Extrazelluläre Ableitungen von einzelnen sensorischen Ia-Afferenzen des EDL-Muskels während „ramp-and-hold“-Dehnung sowie während sinusoidaler Vibrationen zeigten, dass beide Mausmodelle eine erhöhte Aktionspotentialfrequenz bei der Ruhelänge des Muskels aufweisen, aber keine Änderung der Sensitivität während der dynamischen oder der

statischen Phase einer „ramp-and-hold“-Dehnung haben. Bei sinusoidalen Vibrationen mit kleiner Amplitude und langsamer Frequenz zeigten die dystrophischen Mausmodelle einen signifikanten Unterschied zu den Wildtypmäusen. Ein stärker ausgeprägter Phänotyp konnte in der DMD^{mdx}-*dysf*$^{-/-}$ Doppelmutante nicht festgestellt werden. Diese Ergebnisse zeigen, dass ein Fehlen von Dystrophin und/oder Dysferlin zu einer Veränderung in der Funktion der Muskelspindeln führt. Diese veränderte propriozeptive Funktion könnte zu den bei Patienten mit Muskeldystrophie beobachteten häufigen Stürzen und ihrem unsicheren Gang beitragen.

Um die Hypothese zu untersuchen, dass eine veränderte Konzentration von intrazellulärem Ca^{2+} eine Ursache für die veränderte Propriozeption sein könnte, wurden extrazelluläre Ableitungen der propriozeptiven Afferenz von EDL-Muskeln aus Wildtypmäusen in Gegenwart und Abwesenheit des AChE Inhibitors Neostigmin und des Calciumkanalblockers Nifedipin durchgeführt. Nach der Zugabe der Medikamente stieg die Aktionspotentialfrequenz in Ruhe, aber nicht während ramp-and-hold Dehnung an. Nach Zugabe von Neostigmin stieg auch die Aktionspotentialfrequenz während sinusiodaler Vibrationen mit kleiner Amplitude und langsamer Frequenz an. Die Ergebnisse dieser Experimente stützen die Hypothese einer Ca^{2+}-abhängigen Muskelspindelfunktion.

Zusammengefasst zeige ich, dass Mausmodelle für Muskeldystrophie eine veränderte Funktion der Muskelspindeln aufweisen, welche zur Gang- und Standunsicherheit in Dystrophiepatienten beitragen könnte. Diese Veränderungen könnten durch eine erhöhte intrazelluläre [Ca^{2+}] Konzentration in den Muskelzellen bedingt sein. Zudem zeige ich, dass die AChR im zentralen Bereich der Muskelspindel die Muskelspindelantwort während einer Dehnung modulieren.

Abstract

Coordinated movements require proprioceptive information, such as information about muscle tone as well as position and movement of extremities in space. The primary proprioceptive sensory receptors are muscle spindles. Muscle spindles are complex stretch-sensitive mechanoreceptors. They detect how much and how fast a muscle is lengthened. Muscle spindles consist of specialised skeletal muscle fibers, so called intrafusal fibers. In their central part, these fibers are surrounded by a proprioceptive afferent sensory neuron in an annulospiral shape. Here the speed as well as the length of the stretch is translated into action potential frequencies, which are proportional to the length change and the speed thereof. Both polar endings are innervated by efferent *γ*-motoneurons.

Previously it was shown that AChRs are concentrated in the polar region at the contact site between intrafusal fiber and sensory neuron. To investigate the function of these AChRs, extracellular recordings from single unit proprioceptive-afferents of wildtype murine extensor digitorum longus muscles in the absence of *γ*-motoneuron activity was performed. I investigated the response during ramp-and-hold stretches as well as during sinusoidal vibrations in the presence and absence of the AChR inhibitors d-tubocurarine, *α*-bungarotoxin or of the choline reuptake inhibitor hemicholinium-3. In the presence of either drug, the resting action potential discharge frequency was not altered but the stretch-evoked action potential frequencies were increased. Additionally, the firing rate during sinusoidal vibrations at low amplitudes was higher in the presence of *α*-bungarotoxin compared to control spindles. These results indicate that ACh modulates muscle spindle function during stretch in the central region of intrafusal fibers by possibly fine-tuning muscle spindle sensitivity.

As a second project, I investigated the morphology and function of muscle spindles from murine models of muscular dystrophies. Muscular dystrophies comprise a heterogeneous group of hereditary diseases, which are all characterised by progressive degeneration and weakness of skeletal muscles. Murine model systems for two distinct types of muscular dystrophy with very different disease etiologies, i.e. dystrophin- and dysferlin-deficient mice, were analysed. The total number and the overall structure of muscle spindles in soleus muscles of these mice appeared unchanged. Immunohistochemical analyses of wildtype muscle spindles revealed a concentration of dystrophin and β-dystroglycan in intrafusal fibers outside the region of contact to the sensory neuron. Moreover, extracellular recordings from single units of sensory afferents from muscle spindles of the extensor digitorum longus muscle were performed during ramp-and-hold stretches, as well as during sinusoidal vibrations. I demonstrate that mouse models for muscular dystrophy have an increased resting discharge but no change during

the dynamic or static phase of ramp-and-hold stretches. Mutant muscle spindles show a higher action potential firing rate during sinusoidal vibrations with small amplitudes and low frequencies. I observed no exacerbated phenotype in DMD^{mdx}- *dysf*$^{-/-}$ double transgenic mice compared to either single transgenic animal. These results demonstrate that a lack of dystrophin and or dysferlin lead to a change in muscle spindle function and suggest that an impaired proprioceptive feedback might contribute to the instable gait and the frequent falls in patients with muscular dystrophy.

To test the hypothesis that an increased intracellular calcium ion concentration [Ca^{2+}] in dystrophic muscles could cause the impaired proprioceptive function, extracellular recordings from single units of sensory afferents from muscle spindles of the extensor digitorum longus muscle were performed during ramp-and-hold stretches, as well as during sinusoidal vibrations in the presence and absence of the AChE inhibitor neostigmine and the calcium channel blocker nifedipine. After nifedipine and neostigmine administration an increased resting discharge but no change during the dynamic or static phase of ramp-and-hold stretches as well as a higher action potential firing rate during sinusoidal vibrations after neostigmine administration with small amplitudes and low frequencies was observed.

Overall, I show that murine models of muscular dystrophy have an impaired muscle spindle function, which could contribute to the instable gait and posture observed in patients with muscular dystrophy, that these changes could be due to an increased intracellular [Ca^{2+}] in muscles and that the AChR in the central part of the muscle spindles negatively modulates muscle spindle responses during stretch.

1 Introduction

Coordinated movements, including locomotion and their control, require proprioceptive information, like information about muscle tone as well as position and movement of extremities in space (Blecher et al., 2018, Dietz, 2002, Kröger, 2018, Tuthill and Azim, 2018). Proprioception is also required for realignment of fractured bones (Blecher et al., 2017a), for the maintenance of spinal alignment (Blecher et al., 2017b), as well as for basic locomotor recovery and circuit reorganisation after spinal cord injury (Takeoka et al., 2014). The primary proprioceptive sensory receptors are muscle spindles. They detect how much and how fast a muscle is lengthened (Kröger, 2018, Proske and Gandevia, 2012).

1.1 Muscle spindle structure

Muscle spindles were first characterised as sense organs by Sherrington in 1894 (Sherrington, 1894) in cats. In cat, they are approximately 6 - 10 mm long, localised within skeletal muscle tissue and consist of 4 - 12 specialised skeletal muscle fibers, the intrafusal fibers. In adult mice, muscle spindles are 200 - 400 µm long and consist of 3 - 5 specialised intrafusal muscle fibers (Lionikas et al., 2013). These intrafusal fibers lie in parallel with the force-generating extrafusal skeletal muscle fibers and are surrounded by a connective tissue capsule (Figure 1; Banks, 1994a, Bewick and Banks, 2015). Two types of intrafusal fibers can be distinguished, the nuclear chain and nuclear bag fibers. The nuclear bag fibers have diameters of 20 – 25 µm. Due to the high density of nuclei in the equatorial region, most of the contractile apparatus is replaced and only a circumferential ring of sarcomeres is left in the subsarcolemmal region. The function of the accumulation of nuclei is still unclear. Based on the specificity of the myosin ATPase isoform, they can be classified into bag1 and bag2 fibers (Banks, 1994b, Ovalle, 1972). The bag2 fibers are the largest intrafusal fibers and extend beyond the capsule. Bag1 fibers are shorter and their proprioceptive afferents respond maximally to the speed of changes in muscle fiber length (dynamic sensitivity), whereas bag2 fibers and nuclear chain fibers as well as their afferents respond to the amount of stretch. Nuclear chain fibers run entirely within the capsule and their diameter is between 10 – 12 µm (Banks, 1994b).

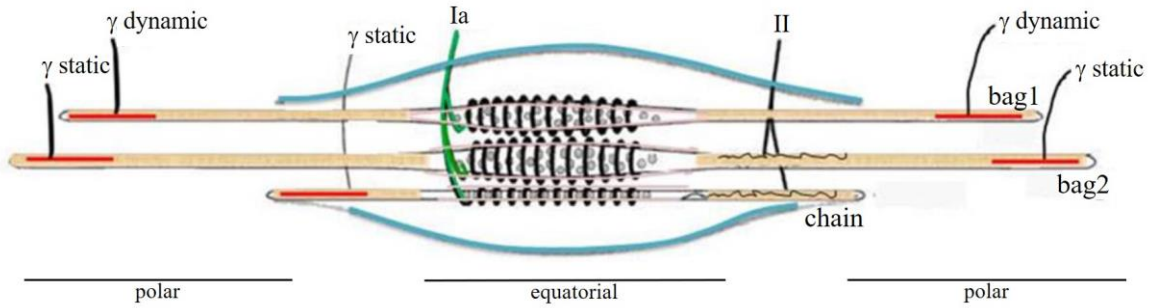

Figure 1: Scheme of a muscle spindle. The intrafusal fibers (beige) are surrounded by a connective tissue capsule (blue). All intrafusal fibers are innervated by an Ia-afferent (green) in the equatorial part. Bag2 and chain fibers are as well innervated by type II afferents (II) which flank the Ia-afferents. In the polar region chain and bag2 fibers are innervated by static γ-motoneurons (γ static, red line) and bag1 fibers by dynamic γ-motoneurons (γ dynamic, red line). Modified from Proske, 1997.

1.2 Muscle spindle innervation

Muscle spindles are innervated by afferent and efferent neurons. The equatorial (central) part of intrafusal muscle fibers is in close contact with two types of afferent proprioceptive sensory neurons (Banks, 2015), type Ia and type II afferents (Hunt, 1990). Both Ia and II afferent axons are myelinated and have a diameter of 4 – 20 µm in cats (Hunt, 1954). Ia afferent nerve fibers exhibit a conduction velocity of up to 120 m/sec in cats and innervate bag1, bag2 as well as chain fibers (Banks et al., 1982 ; Figure 1). They form the primary sensory nerve endings (Banks, 1986), called annulospiral endings, which are coiled around the equatorial region of the intrafusal fibers. In contrast, type II afferent sensory endings display a slower conduction velocity of 30 – 70 m/sec and innervate only bag2 and chain fibers (Banks et al., 1982). They form secondary sensory nerve endings which flank the Ia-afferents (Sonner et al., 2017). Ruffini described these secondary nerve endings, which have not been described in mice yet, in cats as “flower spray” endings (Ruffini, 1898). Afferent neurons generate action potentials with frequencies that are proportional to the size of the muscle stretch or to the speed of stretching (De-Doncker et al., 2003). The cell bodies of these pseudounipolar sensory neurons represent a minor fraction of all neurons in the dorsal root ganglion (DRG). They can be selectively labelled by using antibodies against the vesicular glutamate transporter 1 (vGluT1; Wu et al., 2004).

Besides the sensory neurons, intrafusal muscle fibers are at both polar regions innervated by efferent γ-motoneurons, the so-called fusimotor innervation (Figure 1; Banks, 1994b). These γ-motoneurons form a cholinergic synapse which appears functionally similar to the neuromuscular junction formed between α-motoneurons and extrafusal muscle fibers (Hunt and Kuffler, 1951a). Axons of γ-motoneurons enter the spindle together with the sensory fibers in the equatorial region of the spindle. Their cell bodies are localized in the ventral horn of the spinal cord (Ashrafi et al., 2012, Friese et al., 2009, Shneider et

al., 2009). These neurons represent about 30 % of all motoneurons in the ventral horn. Gamma-motoneurons function as gain control by inducing a contraction in the polar regions of the muscle spindle to exert tension on the central region of the muscle fiber (Proske, 1997, Banks, 1994a). This allows a continuous control of the mechanical sensitivity of muscle spindles over the wide range of lengths and velocities that occur during motor behaviours. This function is based on evidence provided by experiments by Hunt and Kuffler, who were the first to describe a short period of sensory nerve recordings without action potentials during the contraction of extrafusal fibers in which the γ-motoneuron innervation had been cut (Hunt and Kuffler, 1951a, Hunt and Kuffler, 1951b). They discovered that γ-motoneurons control the sensitivity of muscle spindles by regulating the length of intrafusal fibers. When extrafusal fibers are stretched, intrafusal fibers are stretched simultaneously and information about the stretch is transmitted by sensory nerves from muscle spindles to the spinal cord and to higher motor centres in the cortex and cerebellum. When extrafusal fibers contract, a passive loss in tension occurs in the intrafusal fibers and the muscle spindle is unresponsive to stretch. The simultaneous activation of γ-motoneurons cause the contraction of the polar regions of intrafusal fibers leading to a lengthening of the equatorial region of intrafusal fibers. Therefore, the co-activation of α- and γ-motoneurons maintains the tension of intrafusal fibers during the contraction of extrafusal muscle fibers. This ensures the sensitivity of muscle spindles during all phases of muscle relaxation and contraction (Hunt and Kuffler, 1951a).

1.3 The acetylcholine receptor in muscle spindles

How exactly the speed and the rate of stretching of the central part of the muscle spindle is transformed into action potential frequencies is still unknown. The Piezo2 channel is very likely an essential part of the transduction complex and the responsible channel for mechanotransduction at the central part of muscle spindles (Woo et al., 2015, Kröger, 2018). Little is known about the modulation of the transduction and transformation process (Bewick and Banks, 2015). Glutamate appears to be a positive regulator since exogenous glutamate enhanced stretch-induced Ia excitability and since Ia peripheral endings are enriched with glutamate-filled vesicles (Bewick et al., 2005).

A negative regulator of muscle spindle function has so far not been identified but acetylcholine (ACh) could be another neurotransmitter influencing muscle spindle sensitivity. Acetylcholine receptors (AChRs) are concentrated at the contact site of primary nerve endings with the intrafusal fiber at the central part of the muscle spindle (Zhang et al., 2014; see Figure 5). While the function of these cholinergic specialisations in this region is still unknown, the function of AChRs at the neuromuscular junction (NMJ), the contact site

between α-motoneuron and extrafusal fibers, is well characterised. In the pre-synaptic terminal of the motor axon ACh is stored in vesicles. Action potentials which are arriving at the axon terminal open voltage-sensitive calcium channels. The influx of calcium leads to a fusion of the synaptic vesicles with specific binding sites on the pre-synaptic nerve membrane (active zone) and a release of their contents into the synaptic cleft. Cooperative binding of 2 ACh molecules to the post-synaptic AChR on the extrafusal muscle fiber causes an above threshold depolarisation of the muscle fiber membrane and opens voltage-gated Na^+ channels which initiates an action potential that can spread over the surface of the muscle, initiating muscle contraction. The ACh in the synaptic cleft is quickly hydrolysed by ACh esterase (AChE) into acetate and choline. The free choline is transported back into the axon and used for the resynthesize of ACh (Auerbach, 2015, Taly et al., 2009). The transmission of the motoneuron action potential into a contraction of muscle fibers can be modulated at several sites. For example, the uptake of choline into the pre-synaptic terminal can be blocked by hemicholinium-3 (HC-3). This leads to a gradual paralysis because the ACh stored in the pre-synaptic terminal becomes exhausted with repeated stimulation (Bhattacharyya et al., 1988, Carpenter and Woodruff, 1987, Ferguson et al., 2004, Fukuda et al., 1972, Ganguly et al., 1978). The activity of the AChE, hydrolysing ACh, can be inhibited by neostigmine (Neely and Kohli, 2017). Whereas the binding of ACh to the AChR can be blocked by α-bungarotoxin (Dutertre et al., 2017) or d-tubocurarine (Fukuda et al., 1972, Ganguly et al., 1978, Smith and Albuquerque, 1967), leading to muscle paralysis. All these intervening effects are well described at the NMJ, but these drugs have not been tested in muscle spindles yet.

So far, the existence of the fetal (γ-subunit containing AChR) and the adult (ε-subunit containing AChR) forms of the AChR have been described in the central region of intrafusal fibers at the contact site with the sensory nerve ending (Zhang et al., 2014). Moreover, the AChR-associated protein rapsyn as well as the machinery for ACh uptake into vesicles and their exocytosis have been detected at the central part of the muscle spindle by immunohistochemistry (Zhang et al., 2014). Other studies described an excitatory effect of ACh and succinylcholine on muscle spindles, which is most likely due to a direct depolarising activity on intrafusal fibers via the γ-motoneuron endplate (for review Carr and Proske 1996). Accordingly, the function of the cholinergic specialisations in the equatorial region of intrafusal fibers remains unknown. One aim of this study was therefore to investigate the function of the AChRs at the central part of the muscle spindle by analysing muscle spindle afferent responses to stretch in the presence and absence of inhibitors of cholinergic transmission.

1.4 The effect of muscular dystrophies on the muscle spindle

Muscular dystrophies are a heterogeneous group of more than 30 different hereditary myogenic disorders that are all characterised by peripheral muscle weakness and a progressive loss of skeletal muscle tissue (Mercuri and Muntoni, 2013). The most common form is the Duchenne muscular dystrophy (DMD) which was first described in 1851 by Guillaume-Benjamin Duchenne. DMD affects approximately 1 in 5000 boys (Mah et al., 2014), making it one of the most common recessive disorders in the human population. The first symptoms of this disease, including progressive muscle wasting and weakness, appear in early childhood and the loss of skeletal muscle tissue leads to premature death in late adolescence (Emery, 1993, Meryon, 1852). The cause of DMD is a mutation in the *DMD* gene in the chromosomal region Xp21 leading to a loss of function of the sarcolemmal protein dystrophin (Kunkel et al., 1985, Ray et al., 1985, Waite et al., 2009).

Dystrophin is part of the dystrophin glycoprotein complex (DGC). This complex consists of several proteins and provides a framework which connects the extracellular matrix with the intracellular cytoskeleton (Chan et al., 1998, Ervasti, 2003, Ervasti and Campbell, 1991, Ozawa et al., 1998, Yoshida et al., 2000). A loss of dystrophin leads to a reduction or complete loss also of the remaining DGC components from the muscle fiber membrane and subsequently to an instability of the sarcolemma as well as sarcolemmal damage (Le Rumeur et al., 2010, Mercuri and Muntoni, 2013, Waite et al., 2012). This damage can be enhanced by muscle contractions and eventually leads to a degeneration and phagocytosis of the muscle fibers (Allikian and McNally, 2007). Due to several mechanisms, including changes in the regenerative capacity of satellite cells (Chang et al., 2016) and loss of signaling capacity of the DGC (Constantin, 2014), over time regeneration cannot compensate the degenerative loss of muscle tissue. This ultimately leads to a reduction of muscle mass, loss of contractile force and, in the case of Duchenne muscular dystrophy, to premature death of the affected person due to respiratory or cardiac muscle failure.

The degeneration of extrafusal fibres may lead to an increased instability of posture, an instable gait and frequent falls in patients with muscular dystrophy (Hsu and Furumasu, 1993, Pradhan et al., 2006, Chyatte et al., 1966). However, an altered proprioception might augment or contribute to the symptoms. Therefore, several studies investigated muscle spindle morphology in different mouse models for muscular dystrophy (Johnson and Ovalle, 1986, Nahirney and Ovalle, 1993, Gossrau and Grozdanovic, 1997, Ovalle and Dow, 1986) as well as in post-mortem material from DMD patients (Swash and Fox, 1976). In all cases muscle spindle morphology was mildly affected but spindles showed less severe signs of degeneration or regeneration compared to extrafusal muscle fibers. Spindles were slightly atrophic, and the connective tissue capsule appeared widened.

Analysis of the distribution of dystrophin showed a concentration at the central part of the muscle spindle between the contact region of the Ia-afferent and the intrafusal fiber (Figure 2; Nahirney and Ovalle, 1993).

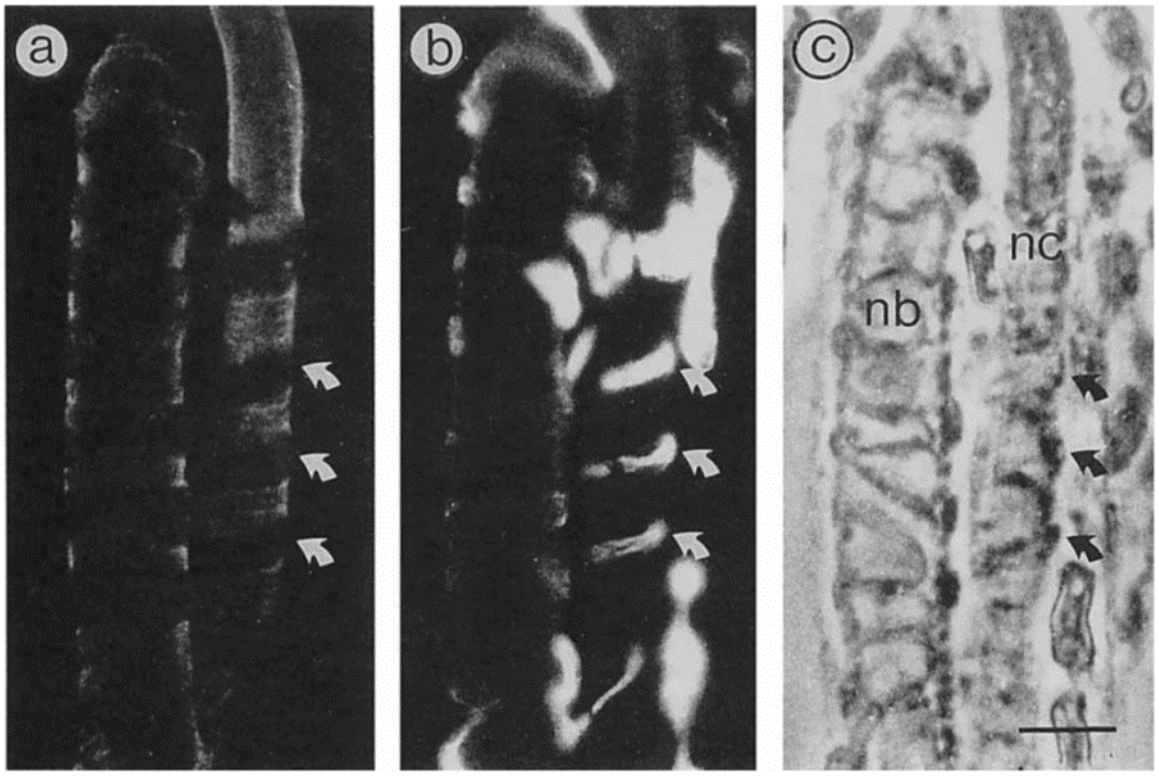

Figure 2: Distribution of dystrophin at the central part of the muscle spindle in mice. Dystrophin-deficient regions of the sarcolemma (arrows in a) are consistent with those areas in contact with the Ia-afferent sensory nerve endings (arrows in b). Phase contrast image (c) reveals a nuclear bag (nb) and a nuclear chain (nc) fiber. Bar = 10 µm, Reproduced with permission. (Nahirney and Ovalle, 1993).

This distribution suggested that dystrophin might not be part of the mechanotransduction system in the central region of the muscle spindle but could play a role in normal muscle spindle function. Moreover, the presence of dystrophin in muscle spindles suggested the possibility that muscle spindle function could be altered in dystrophic muscles.

Another form of muscular dystrophy is the dysferlinopathy. The phenotype of this disease is much milder compared to DMD with an onset between the second and third decade (Galassi et al., 1987, Barohn et al., 1998, Barohn et al., 1991, Rosales et al., 2010). A mutation in the *DYSF* gene on chromosome region 2p13 leads to a loss of dysferlin (Aoki et al., 2001, Bashir et al., 1998, Liu et al., 1998), a single pass transmembrane protein, which is an important component of the sarcolemmal membrane repair machinery (Anderson et al., 1999). Microlesions in the plasma membrane occur due to muscle mechanical activity or due to an adaptation to functional demands (Tidball, 2011). As a consequence, dysferlin-containing vesicles are recruited to the injury site in a calcium-dependent manner (Matsuda et al., 2012, Duann et al., 2015).

At the injury sites, dysferlin appears to promote the vesicle aggregation and fusion by a mechanism that depends on its association with anexins (McNeil, 2009). Moreover, dysferlin seems to be involved in Ca^{2+} homeostasis during mechanical stress (Kerr et al., 2013). A loss of dysferlin therefore leads to an impaired Ca^{2+} homeostasis and a disturbed membrane repair in skeletal muscles resulting in a degeneration of skeletal muscle fibers, eventually causing the muscle weakness.

In this part of my study, I investigated if an altered muscle spindle function can contribute to the phenotype of patients with muscular dystrophy. To this end, recordings of muscle spindle afferent responses to stretch were analysed in two mouse models for muscular dystrophy, the DMD^{mdx} mouse and the *dysf*$^{-/-}$ mouse. Both mouse lines will be introduced in the subsequent paragraphs.

1.5 Mouse models to study muscular dystrophy

1.5.1 The DMD^{mdx} mouse

In 1984 the first dystrophin-deficient mouse line arose due to a spontaneous mutation in a colony of C57BL/10 mice (Bulfield et al., 1984). The mutation in exon 23 of the dystrophin gene generates a premature stop codon and therefore to the absence of the full-length dystrophin. DMD^{mdx} mice die earlier compared to wildtype mice (Chamberlain et al., 2007) but the severity of the muscle degeneration differs from DMD patients. The degeneration of extrafusal fibers in DMD^{mdx} mice is slower and appears in waves followed by waves of regeneration (McGeachie et al., 1993; Haddix et al., 2018) which leads to an increased number of newly differentiated myofibers. They are characterised by centralised nuclei and an increased heterogeneity in myofiber diameter (Grounds and Torrisi, 2004, Messina et al., 2006). The absolute muscle force remains unchanged compared to wildtype mice whereas the relative force normalised to body weight decreases 20 – 50 % (Connolly et al., 2001, Messina et al., 2006, Raymackers et al., 2003). Moreover, calcium ion concentration ($[Ca^{2+}]$) in the subsarcolemmal compartment (Mallouk et al., 2000) and in the sarcoplastic reticulum (Robert et al., 2001) are increased. Despite the slightly less severe phenotype of DMD^{mdx} mice compared to DMD patients, the DMD^{mdx} mouse is recommended as the model of choice for proof-of-concept studies as well as for preclinical tests (Willmann et al., 2009).

1.5.2 The SJL-Dysf mouse

The SJL-Dysf (*dysf*$^{-/-}$) mouse is a model for dysferlinopathies, including the Miyoshi myopathy and limb girdle muscular dystrophy type 2B. These mice develop a mild, progressive myopathy (Bittner et al., 1999) due to a splice site mutation in the dysferlin gene. This leads to a deletion of 57 amino acids (Vafiadaki et al., 2001) and subsequently

to a reduction of 75 % of the dysferlin expression compared to wild type mice. The first signs of a progressive dystrophy appear at 2 months of age (Ho et al., 2004). Despite the residual 25 % of dysferlin, histological changes in these mice display many of the features also observed in patients (Hornsey et al., 2013).

1.5.3 The DMD^{mdx}-*dysf*$^{-/-}$ mouse

The DMD^{mdx}- *dysf*$^{-/-}$ mouse is a cross breading of the DMD^{mdx} and the *dysf*$^{-/-}$ mouse. This mouse model exhibits a more severe muscle pathology compared to DMD^{mdx} mice or *dysf*$^{-/-}$ mice. The onset of the muscle pathology occurs a lot earlier than in *dysf*$^{-/-}$ mice. These mice show a greater number of regenerating muscle fibers, higher serum creatine kinase levels and elevated Evans blue dye uptake into skeletal muscles compared to either DMD^{mdx} or *dysf*$^{-/-}$ mice. (Han et al., 2011). Moreover, the DMD^{mdx}-*dysf*$^{-/-}$ mice have a significant higher incidence to develop rhabdomyosarkomas compared the single mutant mice (Hosur et al., 2012, Schmidt et al., 2011).

1.5.4 The C57BL10/10sc/Utro mouse

The protein utrophin is a structural and functional autosomal paralogue of dystrophin (Love et al., 1989, Tinsley et al., 1992). It is localised at the sarcolemma during fetal development and confined to the NMJ in mature muscles (Lin and Burgunder, 2000). Studies have shown that utrophin overexpression can reduce or even prevent the dystrophic phenotype in DMD^{mdx} mice (Guiraud et al., 2015, Tinsley et al., 1998, Tinsley et al., 2011, Krag et al., 2004, Amenta et al., 2011, Kennedy et al., 2017). Thus, modulation of utrophin is a promising therapy for DMD patients (Guiraud et al., 2019). Utrophin-deficient mice C57BL10/10sc/Utro (*utro*$^{-/-}$) have a very mild phenotype and only subtle changes in skeletal muscle tissue (Deconinck et al., 1997, Grady et al., 1997), and were therefore used as controls.

2 Aims of the study

While the function of muscle spindles is relatively well understood, the molecules that mediate this function and potential mechanisms that modulate muscle spindle responses to stretch are poorly investigated. In my study, I characterised muscle spindles on the molecular level by addressing two main questions:

1. What is the function of the acetylcholine receptors in the central part of muscle spindles? To this end, I analysed muscle spindle Ia-afferent responses to stretch in the presence and absence of AChR inhibitors and inhibitors of cholinergic synaptic transmission.

2. What are the functional consequences of mutations in the DGC and in mouse models of dysferlinopathies? Do muscle spindle intrafusal fibers undergo similar rounds of degeneration and regeneration as extrafusal fibers? Can altered functional properties of dystrophic muscle spindles contribute to the unstable gait and frequent falls observed in dystrophic patients? To this end I analysed electrophysiological recordings from single unit Ia-afferent responses to stretch in a mouse model for DMD as well in other mouse models for muscular dystrophy.

3 Material and Methods

3.1 Chemicals

Chemical	Company	Catalog number
4',6-Diamidino-2-phenylindol Dihydrochloride (DAPI)	Carl Roth GmbH & Co. KG, Karlsruhe, Germany	6843.1
Albumin Fraction V	Carl Roth GmbH & Co. KG, Karlsruhe, Germany	8076.2
Aqua-Poly/Mount	Polysciences Europe GmbH	18606
$CaCl_2$	Carl Roth GmbH & Co. KG, Karlsruhe, Germany	CN93.2
D-Glucose	Sigma-Aldrich Chemie GmbH, Taufkirchen, Germany	G5146
KCl	Carl Roth GmbH & Co. KG, Karlsruhe, Germany	6781.3
Ketamine	Pfizer Inc., Berlin, Germany	
KH_2PO_4	Carl Roth GmbH & Co. KG, Karlsruhe, Germany	3904.1
$MgSO_4$	Carl Roth GmbH & Co. KG, Karlsruhe, Germany	0261.1
NaCl	Carl Roth GmbH & Co. KG, Karlsruhe, Germany	9265.1
$NaHCO_3$	Carl Roth GmbH & Co. KG, Karlsruhe, Germany	6885.1
Paraformaldehyde	Carl Roth GmbH & Co. KG, Karlsruhe, Germany	0335.1
Sodium borohydride	Sigma-Aldrich Chemie GmbH, Taufkirchen, Germany	71320
Sodium citrate	Sigma-Aldrich Chemie GmbH, Taufkirchen, Germany	W302600
Tissue Tec®	Sakura Finetek Europe, AJ Alphen an den Rijn, Netherland	TTEK
Triton® X-100	Sigma-Aldrich Chemie GmbH, Taufkirchen, Germany	9002-93-1
Tween20	Carl Roth GmbH & Co. KG, Karlsruhe, Germany	9127.1
Xylazine	Bayer AG, Leverkusen, Germany	

3.2 Artificial cerebrospinal fluid

Chemical	Concentration
$CaCl_2$	2,4 mM
D-Glucose	10,0 mM
KCl	1,9 mM
KH_2PO_4	1,2 mM
$MgSO_4$	1,3 mM
NaCl	128,0 mM
$NaHCO_3$	26,0 mM

3.3 Drugs for pharmacological experiments

Drug	Concen-tration	Equilibration time	Company	Catalog number
d-tubocurarine	30 µM	1 h	Sigma-Aldrich Chemie GmbH, Taufkirchen, Germany	T2379
Hemicholinium-3	10 µM	1 h	Sigma-Aldrich Chemie GmbH, Taufkirchen, Germany	H108
Neostigmine	10 µM	1 h	Sigma-Aldrich Chemie GmbH, Taufkirchen, Germany	N2126
Nifedipine	20 µM	4 h	Sigma-Aldrich Chemie GmbH, Taufkirchen, Germany	N7634
α-bungarotoxin	1,25 µM	3 h	Life Technologies, Carlsbad, California, USA	B1601

3.4 Antibodies

3.4.1 Primary Antibodies

Antibody	Host	Dilution	Company	Catalog number
anti-calcium channel L type DHPR α2 subunit	rabbit	1:100	Abcam plc, Cambridge, UK	ab80990
anti-dysferlin	rabbit	1:20	Abcam plc, Cambridge, UK	ab124684
anti-dystroglycan	mouse	1:75	Leica Biosystems, Nussloch, Germany	NCL-b-DG
anti-dystrophin	rabbit	1:20	Thermo Fisher Scientific Inc., Massachusetts, USA	RB-9024
anti-N_{av}1.4	rabbit	1:100	Abcam plc, Cambridge, UK	ab65165
anti-utrophin	mouse	1:4	Leica Biosystems, Nussloch, Germany	NCL-DRP2
anti-vesicular glutamate transporter 1	guinea pig	1:1000	Merck KGaA, Darmstadt, Germany	AB5905

3.4.2 Secondary Antibodies

Antibody	Host	Dilution	Company	Catalog number
anti-guinea pig Alexa Flour 647	donkey	1:300	Merck KGaA, Darmstadt, Germany	AP193SA6
anti-mouse Alexa Flour 488	goat	1:100	Thermo Fisher Scientific Inc., Massachusetts, USA	A11029
anti-mouse Alexa Flour 594	goat	1:500	Thermo Fisher Scientific Inc., Massachusetts, USA	A11032
anti-rabbit Alexa Flour 594	goat	1:100	Thermo Fisher Scientific Inc., Massachusetts, USA	A11037
α-Bungarotoxin conjugated with Alexa Flour 488	Bungarus multicinctus venom	1:100	Thermo Fisher Scientific Inc., Massachusetts, USA	B13422

3.5 Technical devices

Technical device	Type	Company
Ag/AgCl Electrode	0.015“(380 M)	Science Products GmbH, Hofheim, Germany
Amplifier	A-M Systems, Modell 1800	Science Products GmbH, Hofheim, Germany
Analog to Digital Board	Power Lab 8/35	ADInstruments, Oxford, UK
Binocular microscope	Leica MZ 75	Leica Camera, Wetzlar, Germany
Cryostat	LEICA CM3050S	Leica Biosystems, Nussloch, Germany
Electrode Glass	OD = 1,65 mm, ID = 0,75 mm	Dagan Corporation, Minneapolis, USA
Electrode holder	2 mm pin holder, narrow, with suction port and wire with 1.7 mm diameter	Science Products GmbH, Hofheim, Germany
Epifluorescence microscope	Module 700 with Imager M2, Power supply 232, HXP 120 C and camera AxioCam MRm	Carl Zeiss AG, Oberkochen, Germany
Fiber Optic Illuminator	1500 LCD	OLYMPUS, Munich, Germany
Force and Length Controller & Tissue Bath	300C-LR & 809B-IV	Aurora Scientific Europe, Dublin, Ireland
Laser-scanning confocal microscope	LSM 710 Module with AxioImagerZ.1, power supply 231, MCU 2008, HXP 120. Laser: Diode 405-30, HeNe633, DPSS 561-10 and Argon	Carl Zeiss AG, Oberkochen, Germany
Laser-scanning confocal microscope	SP8X WLL microscope with 405 nm laser, WLL2 laser (470 - 670 nm) and acusto-optical beam splitter	Leica Biosystems, Nussloch, Germany
Microforge	MF-900	Narishige Group, London, UK
Non-Sterile Suture	5/0	FINE SCIENCE TOOLS GmbH, Heidelberg, Germany
Pump	Masterflex L/S	Novodirect GmbH, Kehl, Germany
Pump Head	EASY-LOAD II	Novodirect GmbH, Kehl, Germany
Silver wire	99,99 %	Science Products GmbH, Hofheim, Germany

Stimulator	SD 9 / 701C	GRASS-Telefactor / Aurora Scientific Europe, Dublin, Ireland
Vertical Pipette puller	L/M-3P-A	List-Medical; Artisan Technology Group ® Champaign, Illinois, USA

3.6 Software

Software	**Company**
GraphPad Prism v.7	GraphPad Software, La Jolla California USA
ImageJ	public domain Java image processing program from NIH, USA (rsbweb.nih.gov/ij/)
Lab Chart Pro v.8.1.3	ADInstruments, Oxford, UK

3.7 Mice

Line	**Producer/Manufacturer**
C57BL6/J	Charles River Laboratories, Germany
C57BL10/10sc	University of Greifswald, Prof. Brinkmeier
C57BL10/10sc/DMD^{mdx}	University of Greifswald, Prof. Brinkmeier
C57BL10/10sc/Utro	University of Vienna, Prof. Bittner
Dmd^{mdx}SJL-dysf C57BL/6	University of Vienna, Prof. Bittner
SJL-dysf C57BL/6	University of Vienna, Prof. Bittner

4 Methods

4.1 Ethical Approval

Care and use of animals and all experimentations were approved by the German authorities and according to national law (§ 7 TierSchG; license Az.: 55.2-1-54-2532.8-160-13). All experiments were conducted in accordance with the guidelines of the Ludwig-Maximilians-University Munich. Additionally, all experimental protocols were designed to minimise suffering as well as the number of animals used in this study. At most five adult animals were housed in a sterile cage on a 12-hr light/dark cycle. Only male mice which were aged 10 -16 weeks with a weight of 22-30 grams were used in this study.

4.2 Immunofluorescence

4.2.1 Confocal images

Immunofluorescence stainings were performed as described previously (Zhang et al., 2014, Gerwin et al., 2019). To obtain muscle tissue for immunohistochemistry, mice were deeply anesthetised using ketamine and xylazine. Depth of anesthesia was assessed by the abolition of pedal reflexes. After transcardial perfusion with phosphate-buffered saline (PBS) followed by 4 % paraformaldehyde (PFA), the extensor digitorum longus muscle (EDL) was dissected. Muscles were post-fixed in 4 % PFA for 30 min to 2 h and afterwards incubated in 30 % sucrose in PBS overnight at 4°C. Fixed muscles were cryo-preserved in Tissue-Tek O.C.T. Compound and cryo-sectioned along the longitudinal axis at 20 - 30 µm thickness.

Frozen sections were washed 10 min in PBS and quenched 2 times in 1 mg/ml sodiumborohydrate for 4 min to reduce background signals. After an additional washing step, unspecific staining was blocked by incubating the sections in PBS containing 0.2 % Triton X-100 and 1 % bovine serum albumin (blocking solution) for 30 min at room temperature and incubated with the primary antibody in blocking solution at 4 °C overnight. After 3 washing steps, 10 min each, primary antibodies were detected by incubating the sections for 1 h with the appropriate secondary antibody, diluted in blocking solution. Sections were washed 10 min in PBS and the nuclei were stained using DAPI at a concentration of 2 µg/ml in blocking solution for 10 min.

Subsequent to 3 more washing steps in PBS for 10 min the sections were embedded in PolyAqua Mount mounting medium and analysed using a Zeiss LSM 710 laser scanning confocal microscope or a Leica SP8X WLL microscope. The LSM 710 was equipped with an Argon Laser (laser line 488 nm), a Diode (laser line 405 nm), a DPSS laser (561 nm) and a HeNe laser (633 nm). Confocal z-stack-images were generated using a 40x water

immersion objective (LD C-Apochromat 40x/1.1) and a multi-alkaline-based photomultiplier (PMT). Sequential recordings were performed to avoid bleed-through. The SP8X WLL microscope situated at the core facility bioimaging of the Biomedical Center was equipped with 405 nm laser, a WLL2 laser (470 - 670 nm) and an acusto-optical beam splitter. Sequentially scanned confocal Z-stacks of whole muscle spindles were obtained using 1 µm optical sections. Images were acquired with a 63x1.4 objective with an image pixel size of 80 nm. The following fluorescence settings were used: DAPI (excitation 405; emission 410-470), GFP (489; 492-550), Cy3 (558; 560-600) and Cy5 (650; 652-700). GFP and Cy3 were recorded with hybrid photo detectors (HyDs), DAPI and Cy5 with conventional photomultiplier tubes. Laser power levels, photomultiplier gain levels, scanning speed, and the confocal pinhole size were kept constant between experimental and control specimens. To avoid false positive results due to unspecific binding of secondary antibodies, negative control stainings were run in parallel. Digital processing of entire images, including adjustment of brightness and contrast, was performed by using the Java image processing program software package Fiji (Schindelin et al., 2012).

To improve the quality of staining using the anti-dysferlin antibody the staining protocol was enhanced by an antigen retrieval protocol (Roche et al., 2000). Sections were washed 10 min with PBS and incubated in 10 mM sodium citrate containing 0,05 % Tween20 (pH 6,0) at 90 °C for 30 min. After cooling down to 30 °C over 60 min, sections were washed 2 times in PBS for 5 min and then blocked and stained as described above.

4.2.2 Epifluorescence microscopy

To determine the number of muscle spindles whole soleus muscles were cryo-sectioned along the longitudinal axis at 20 - 30 µm thickness and stained with anti-vGluT1 and DAPI as described above. Each section was scanned by performing tile-scans and fused to one picture using the stitching tool at the epifluorescence microscope Zeiss Module 700. The number of muscle spindles for each individual muscle was counted. Muscle spindles were identified by morphological criteria, i.e. a positive staining of the annulospiral endings with anti-vGluT1 and the characteristic distribution of nuclei in nuclear chain and -bag fibers. 3 mice were analysed for each mouse line (Data from DMD^{mdx}-*dysf*$^{-/-}$ mice were compared to unpublished Data from Sarah Rossmanith from BL6, BL10 and DMD^{mdx} mice.)

4.3 Extracellular muscle spindle recordings

Proprioceptive sensory neuron responses to stretch were assayed using an isolated muscle-nerve preparation previously described (Franco et al., 2014, Wilkinson et al., 2012, Gerwin et al., 2019). Mice were sacrificed by cervical dislocation and the EDL muscle together with the deep peroneal branch of the sciatic nerve were dissected and afterwards placed in an oxygenated tissue bath containing artificial cerebrospinal fluid (ACSF).

The tendons were sutured to a fixed post and on the other end to a lever arm which was connected to a dual force and length controller allowing the simultaneous recording of muscle tension, muscle length and muscle spindle afferent discharges. The baseline muscle length (Lo) was defined as the length at which the maximal twitch contractile force was generated. The sensory activity was sampled using a suction electrode with a tip diameter of 50–70 µm, which was connected to an extracellular amplifier. A signal was classified as certainly being from a muscle spindle sensory afferent if it displayed a characteristic instantaneous frequency response to stretch as well as a pause during twitch contraction (Wilkinson et al., 2012, Gerwin et al., 2019).

4.3.1 Extracellular recordings from mouse models for muscular dystrophy

For every muscle spindle afferent recording (Figure 3A), a series of 27 ramp and hold stretches (Figure 3B; triplicates of each Lo plus 2.5 %, 5 % and 7.5 % Lo; ramp speed 20, 40 and 60 % Lo/sec; stretch duration: 4 sec with 45 sec intervals between each stretch), as well as 16 sinusoidal vibrations (amplitudes: 5 µm, 10 µm, 50 µm, 100 µm, each with a frequency of 10 Hz, 25 Hz, 50 Hz, 100 Hz for 9 sec) were recorded. The resting discharge (average baseline firing rate), the dynamic peak (highest firing rate during ramp – baseline firing rate), the dynamic index (highest firing rate during ramp – firing rate 0.45 to 0.55 sec into stretch), the static response (firing rate 3.25 to 3.75 sec into stretch – baseline firing rate) and the time of silence (time after the end of the ramp-and-hold stretch and the first action potential) were determined (Figure 3C). In addition to the stretch-evoked action potentials, the length and tension of the muscle were simultaneously recorded.

For the data analysis, individual sensory neurons were identified by spike shape and the interspike interval using the Spike Histogram feature of Lab Chart. Spindle afferent baseline firing rate (RD), dynamic peak (DP), dynamic index (DI) and the static stretch response (SR) were determined as described above. Only recordings in which a single individual muscle spindle afferent unit could be clearly identified were included in the analysis. Up to 3 different muscle spindle afferents were recorded from 1 EDL muscle (Gerwin et al., 2019, Wilkinson et al., 2012).

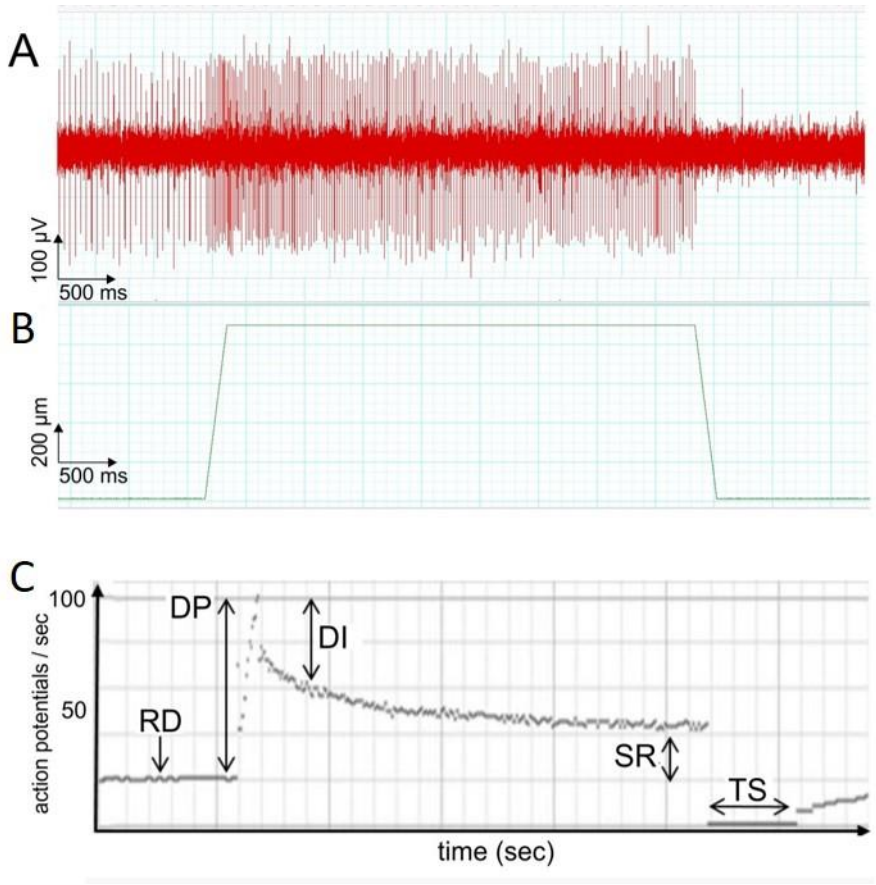

Figure 3: Data analysis of the action potential frequency of an exemplary muscle spindle Ia-afferent in response to a ramp-and-hold stretch. A: Change in action potential frequency of a muscle spindle Ia-afferent in response to stretch. B: Length change of the muscle during a ramp-and-hold stretch of the EDL. C: Action potentials/sec over time. Spindle afferent baseline firing rate (RD), dynamic peak (DP), dynamic index (DI), static stretch response (SR) and the pause of the firing rate after release of the stretch (TS) were determined.

Sinusoidal vibrations were analysed by comparing the number of action potentials during the 9 sec of each of the 16 vibrations between mutant mouse models with control animals. The values were expressed as impulses per 9 sec. Examples for 4 different vibrations are shown in Figure 4.

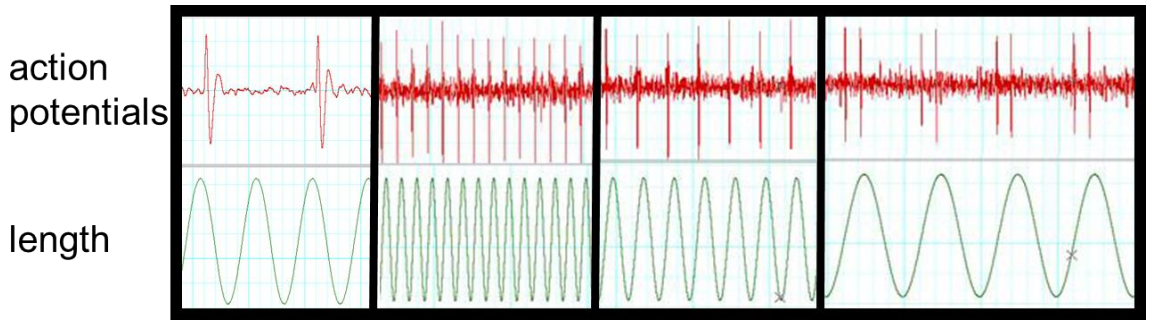

Figure 4: Examples of 4 different sinusoidal vibrations varying in vibrations frequency. The length change during each vibration is shown in green (lower panel) and the corresponding muscle spindle action potential frequency is shown in red (upper panel).

4.3.2 Extracellular recordings during pharmacological experiments

To ensure muscle spindle health, the experimental protocol was shortened during pharmacological experiments. For all muscle spindle afferent recordings, a series of only 9 ramp and hold stretches (triplicates of each Lo plus 2.5 %, 5 % and 7.5 % Lo; ramp speed 40 % Lo/sec; stretch duration: 4 sec with 45 sec intervals between each stretch), as well as 16 sinusoidal vibrations (amplitudes: 5 µm, 10 µm, 50 µm, 100 µm, each with a frequency of 10 Hz, 25 Hz, 50 Hz, 100 Hz for 9 sec) were recorded. Then a drug or 100 µL ACSF for control experiments was added to the oxygenated ACSF. After 1-4 h of equilibration depending on the drug, the response of the same muscle spindle afferent neuron was determined to the same series of three repetitions of each of the three ramp-and-hold stretches and 16 sinusoidal vibrations. Thus, a precise comparison of the stretch-evoked responses of individual single unit muscle spindle afferents in the absence and presence of each drug was possible.

For data analysis, individual sensory neurons were identified by spike shape and the interspike interval using the Spike Histogram feature of Lab Chart and RD, DP, DI as well as SR were determined as described above as well as the number of action potentials during the 9 sec of each sinusoidal vibration (Gerwin et al., 2019, Wilkinson et al., 2012). Only when an individual muscle spindle afferent unit could be unambiguously identified throughout the entire experiment the recording was included in the analysis.

4.3.3 Overall muscle health

At the end of each recording the muscle health checked. This was done by comparing the maximal contractile force during a tetanic stimulation (500 ms train, 120 Hz frequency, 0.5 ms pulse length, supramaximal voltage; Grass SD9 square pulse stimulator; Wilkinson et al., 2012) to the previously reported peak force of 23,466 N/cm² of the EDL (Brooks and Faulkner, 1988, Larsson and Edstrom, 1986). Neither the maximal force after tetanic stimulation nor the resting discharge varied significantly over the time course of the experiments. This leads to the suggestion that spindle afferents were not undergoing time dependent changes in firing properties and that the EDL muscle was returning to resting length after each stretch.

4.3.4 Statistical analysis

Exclusively single unit spindle afferent responses which were recorded without interruption throughout the entire experiment, i.e. before and after the addition of a drug, were included in the analysis. All statistical analyses were performed by using GraphPad Prism (v8; GraphPad Software, Inc., La Jolla, CA, USA). The level of significance (P-value) for all statistical tests was set at *$P < 0.05$, **$P < 0.01$, ***$P < 0.001$, **** $P < 0.0001$.

Date from wildtype mice were compared to data from mutant mouse lines by determining all parameters of ramp-and-hold stretches (baseline firing rate, dynamic peak, dynamic index and the static stretch response) as an average of three stretches for all mouse lines. Afterwards the values from mutant mouse lines were compared statistically by performing a one-way ANOVA (factor: mutation) with Dunnett's post hoc test to the wildtype (BL6 or BL10) control group. All values are reported as mean of the frequency (imp/sec) in a dot plot. Each dot represents an individual muscle spindle afferent.

To analyse sinusoidal vibrations, the total number of action potentials per 9 sec (imp/9 sec) for each of the 4 frequencies and 4 amplitudes were determined for all mouse lines. Data are presented as imp/9 sec in a dot plot. Each dot represents an independent experiment. Testing for statistical significance was done by using the three-way ANOVA (factors: mutation, amplitude and frequency). Additionally, all responses to the 16 different vibrations were compared individually with the one-way ANOVA (factor drug; Dunnett's multiple comparisons test) to the wildtype controls.

Data from pharmacological experiments, i.e. with hemicholinium-3, were statistically analysed as previously described by Gerwin et al. (2019). Baseline values for all parameters for ramp-and-hold stretches (resting discharge, dynamic peak, dynamic index and the static response) were determined as an average of three stretches before drug addition. After drug addition and equilibration, the firing frequencies were determined again from an average of three stretches. Action potential frequencies of individual muscle spindle afferents before drug addition were subtracted from the action potential frequencies after drug addition. In the no-drug control group the same time points within a ramp-and-hold stretch (RD, DP, DI and SR) were used to calculate the change in firing frequency. The mean of the overall changes in firing rate of all drug groups were compared statistically by using the one-way ANOVA (factor: drug) with Dunnett's post hoc test to the no-drug (ACSF) control group. All values are reported as mean of the action potential frequency change from pre- to post-drug addition (Δmean; imp/sec) in a dot plot. Each dot represents an individual muscle spindle afferent.

For sinusoidal vibrations, the total number of action potentials per 9 sec (imp/9 sec) for each of the 4 amplitudes and 4 frequencies before drug addition were subtracted from the corresponding values (imp/9 sec) after drug addition. Data are presented as Δimp/9 sec in a dot plot. Each dot represents an independent experiment. Statistical significance was determined by using the three-way ANOVA (factors: drug, frequency and amplitude). Furthermore, all responses to the 16 different vibrations were compared in the absence and presence of all drugs to the no drug control by using the one-way ANOVA (factor drug) with Dunnett's multiple comparisons test.

5 Results

5.1 Validation of the experimental protocol

Wilkinson et al. (2012) previously published an experimental protocol for extracellular recordings from muscle spindle afferents that I used in my thesis. To validate if my experimental setup and my method of analysis were comparable to the published data, I reproduced the results previously reported by the Wilkinson lab.

The EDL muscle from wildtype mice was dissected and the response of triplicates of 9 ramp-and-hold stretches were recorded. The results were then compared with the data from the literature (Wilkinson et al., 2012). No significant difference to the published data was observed for the resting discharge, dynamic peak, dynamic index or static response. Additionally, 16 sinusoidal vibrations were analysed, and the data showed the same distribution of multiple, harmonic, subharmonic and no entrainment as described by Wilkinson et al. (2012). Collectively, these results strongly suggest that my experimental setup and my method of analysis were comparable to those published previously by the Wilkinson lab. This provided strong confidence to further analyse muscle spindle afferent responses to stretch under various experimental conditions.

5.2 The AChR at the central part of the muscle spindle

5.2.1 Distribution of the AChR at the central part of the muscle spindle

The presence of mRNA which codes for the α- and ε-subunit of the AChR in the equatorial part of intrafusal muscle fibers as well as a concentration of α-, γ- and ε-subunit-containing AChRs at the contact site of the sensory nerve terminal and the intrafusal muscle fibers were reported previously (Sanes et al., 1991, Hippenmeyer et al., 2002, Zhang et al., 2014). Therefore, I investigate the distribution of the AChRs with respect to the sensory nerve terminal in detail in sections from the M. soleus. I stained these sections with fluorescently labelled α-bungarotoxin and anti-vGluT1 antibodies. A subsequent high-resolution confocal microscopic analysis of the equatorial region of the intrafusal muscle fibers revealed a precise codistribution of the AChRs with the vGluT1 immunoreactivity (Figure 5). A similar distribution of AChRs was observed in muscle spindles from EDL, quadriceps and soleus muscles. This positive fluorescent labelling represents a concentration of the AChRs in the intrafusal fiber plasma membrane at the contact region with the sensory nerve terminal as was previously described by Zhang et al. (2014). Some α-bungarotoxin labelling could be observed in the area of the intrafusal muscle fibre membrane between the annulospiral endings. Overall, a similar spatial distribution of the AChRs was detected in nuclear bag as well as in nuclear chain fibres from a number of different muscles (Gerwin et al., 2019).

Thus, a concentration of AChRs appears to be a general characteristic for the contact site between sensory nerve ending and intrafusal plasma membrane.

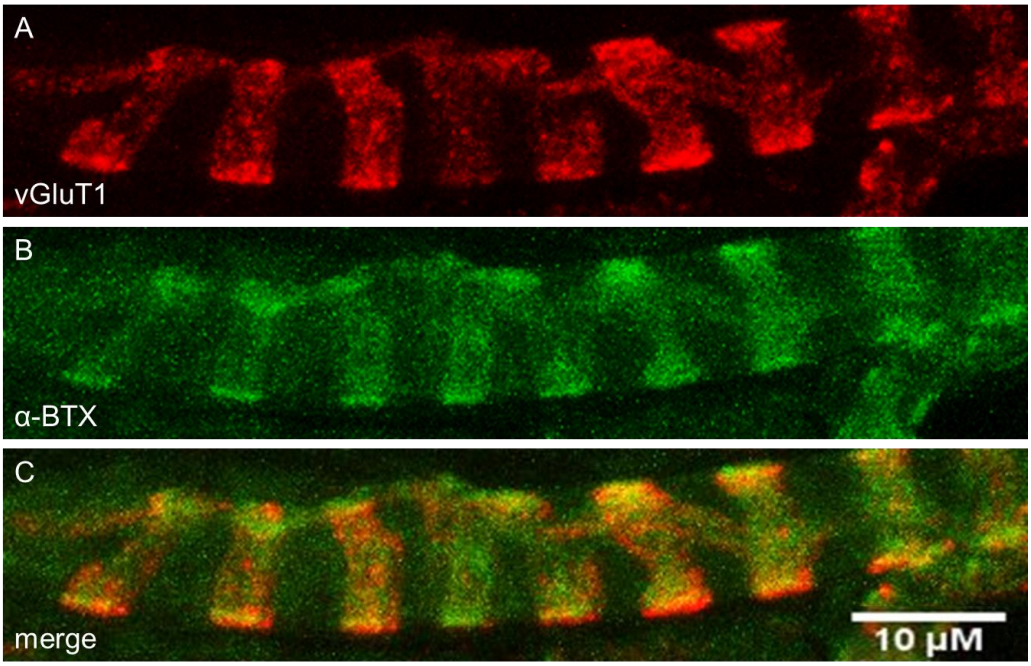

Figure 5: AChRs colocalise with the sensory nerve terminals at the central region of muscle spindles. A and B, high-resolution confocal z-scan of the distribution of AChRs (green channel, A) and the sensory nerve terminal shown by anti-VGluT1 immunoreactivity (red channel, B) in the equatorial region of a nuclear chain fiber of a soleus muscle. C, the precise overlap of both staining patterns at the contact site between sensory neuron and intrafusal muscle fiber can be seen in the merged image (Gerwin et al., 2019).

5.2.2 Effect of AChR blockers and hemicholinium-3 on action potential frequencies during ramp-and-hold stretches

To investigate the function of the AChRs at the contact site between sensory nerve terminal and intrafusal muscle fibre, I analysed individual muscle spindle afferent responses to ramp-and-hold stretches in the presence and absence of the AChR blockers d-tubocurarine and α-bungarotoxin (Figure 6). Firing rates were analysed at four different time points (Figure 6D) before (RD) and during (DP, DI, SR) the stretch each before and after drug administration. Figure 6 shows the action potentials during a ramp-and-hold stretch (Figure 6C) of one representative muscle spindle afferent neuron before (Figure 6A) and after (Figure 6B) the administration of 1.25 µM α-bungarotoxin. Figure 6E shows an exemplary image of the action potential firing frequency of a single proprioceptive sensory unit. The responses to a ramp-and-hold stretch before (green dots) and after (grey dots) addition of α-bungarotoxin (α-Btx) can be seen. The administration of α-bungarotoxin did not influence the resting discharge and the variation of RD frequencies were not larger than the normal variation of the frequency during the time course of the experiment. In contrast, DP, DI and SR were substantially increased after α-bungarotoxin administration (Gerwin et al., 2019).

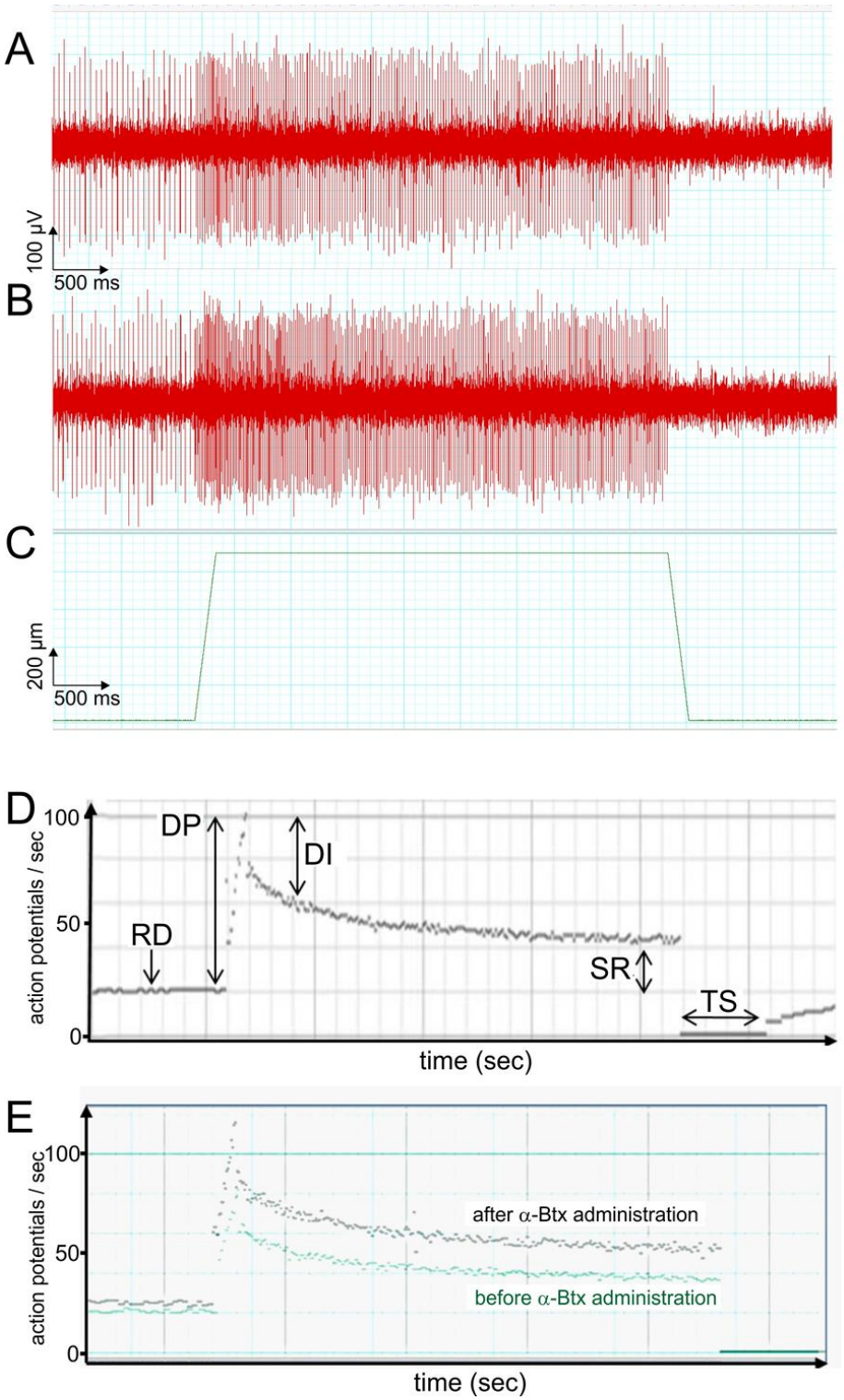

Figure 6: An inhibition of AChRs increases the stretch-evoked sensory afferent action potential firing frequencies. A and B, action potentials of the same muscle spindle proprioceptive afferent during a ramp-and-hold stretch (C) in the absence (A) and presence (B) of α-bungarotoxin. (C) A ramp-and-hold stretch of 4 sec with a ramp speed of 40 % Lo/sec and a length change of 7.5 % Lo. (D) The response of a muscle spindle afferent to a ramp-and-hold stretch to illustrate the four different parameters that were analysed before and during the stretch: resting discharge (RD), dynamic peak (DP), dynamic index (DI) and static response (SR). (E) representative image of the action potential firing frequency of the same proprioceptive sensory unit in response to a ramp-and-hold stretch before (green dots) and after (grey dots) the addition of α-bungarotoxin (α-Btx). α-bungarotoxin did not influence RD but DP, DI and SR were increased (Gerwin et al., 2019).

The action potential frequencies of DP, DI and SR changed with the length of the stretch. In Figure 7 these changes are shown for one exemplary spindle recording of ACSF, α-bungarotoxin and d-tubocurarine. The imp/sec before drug administration were subtracted from the imp/sec after drug administration for RD, DP, DI and SR. The values are expressed as Δmean imp/sec for triplicates of 2.5, 5 and 7.5 % Lo stretch length change, respectively. The RD did not differ between control experiments and the drug experiments (Fig. 8A). In contrast, the frequency of DP, DI and SR in the presence of α-bungarotoxin or d-tubocurarine increased significantly with increasing lengths (Fig. 8 B-D) whereas the frequencies of ACSF-control remained constant at all length changes. Since the most significant changes in frequency where observed at a stretch length of 7.5 % Lo these stretches were used for my subsequent statistical analysis.

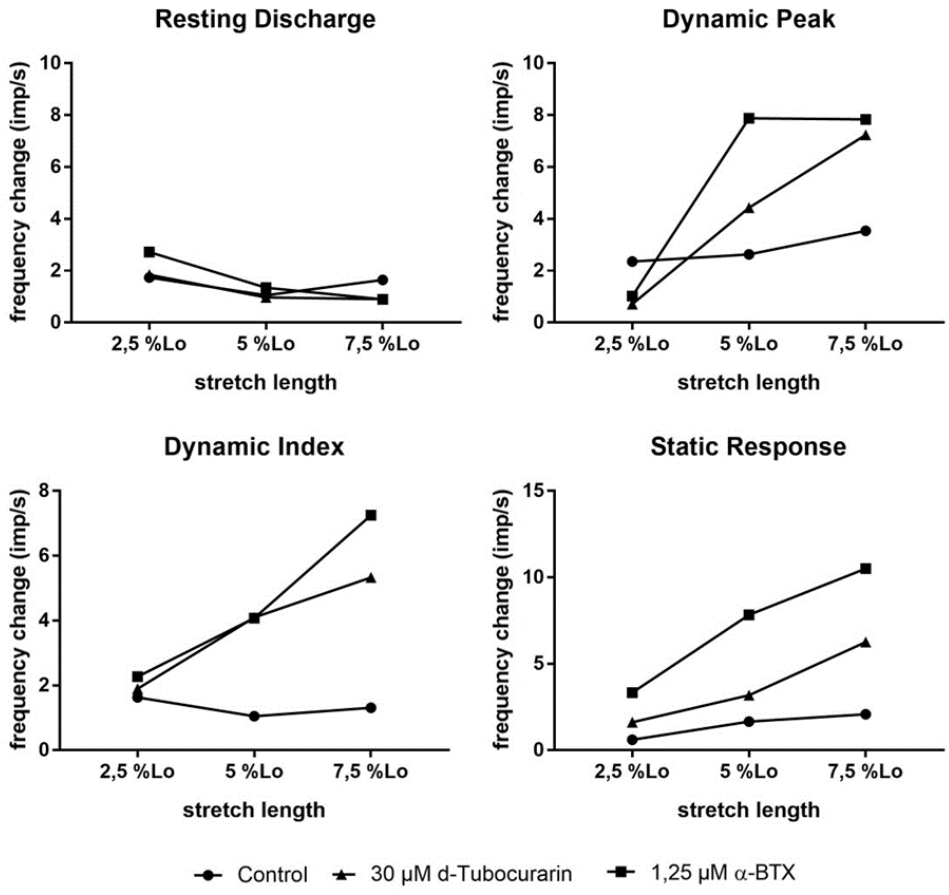

Figure 7: Firing frequencies increased with stretch length after administration of AChR blockers. The imp/sec before drug administration during ramp-and-hold stretches of 2.5, 5 and 7.5 % Lo stretch length change were subtracted from the imp/sec after drug administration for RD, DP, DI and SR. The values are expressed as Δmean imp/sec for triplicates of each 2.5, 5 and 7.5 % Lo stretch length change. No changes in frequency can be observed at RD (A) after administration of ACSF or a drug whereas at DP (B), DI (C) and SR (D) an increase of frequency is observed with stretch length after drug administration. In contrast, no increase is observed after ACSF administration during stretch.

To investigate the function of AChRs at the contact region between the sensory nerve terminal and the intrafusal muscle fiber, I analysed individual muscle spindle afferent responses to a ramp-and-hold stretch (Lo plus 7.5 % of Lo; ramp speed 40 % Lo/sec), before and after the addition of the AChR blockers d-tubocurarine and α-bungarotoxin, as well as the choline uptake inhibitor hemicholinium-3 (Gerwin et al., 2019). At four different time points before (RD) and during (DP, DI and SR) the stretch the action potential firing frequency were analysed in detail. Neither drug influenced the resting discharge (Figure 8A). In contrast, all drugs increased the action potential firing frequency during a ramp-and-hold stretches (Figure 8 B-D) compared to the action potential frequencies of the same muscle spindle afferents before drug addition. The overall effect of the drugs was analysed by using the one-way ANOVA (factor: drug). No differences for the resting discharge (P= 0.0610), but statistically significant differences for the dynamic peak (P = 0.0100), dynamic index (P = 0.0204) and static response (P = 0.0459) were revealed.

For a better comparison of the specific effect of the individual drugs, the results were expressed as Δmean. This Δmean represents the mean of the difference in frequency (imp/sec) before compared to after drug addition. Neither AChR inhibitor had an effect on the resting discharge (Δmean control: 2.092 imp/sec; Δmean d-tubocurarine: 1.346 imp/sec; Δmean α-bungarotoxin: 4.758 imp/sec; Dunnett's post hoc test relative to ACSF control: P = 0.9664, control vs. d-tubocurarine; P = 0.4313, control vs. α-bungarotoxin; Figure 8A). Nevertheless, the dynamic peak (Δmean control: −12.04 imp/sec; Δmean d-tubocurarine: 9.992 imp/sec; Δmean α-bungarotoxin: 26.53 imp/sec; Figure 8B) as well as the dynamic index (Δmean control: −5.413 imp/sec; Δmean d-tubocurarine: 2.78 imp/sec; Δmean α-bungarotoxin: 5.799 imp/sec; Figure 8C) were increased after drug addition compared to the same muscle spindle afferent before drug addition. The observed differences were statistically significant for the dynamic peak (P = 0.0442, control vs. d-tubocurarine; P = 0.0027, control vs. α-bungarotoxin; Figure 8B) as well as for the dynamic index (P = 0.0412, control vs. d-tubocurarine; P = 0.0073, control vs. α-bungarotoxin; Figure 8C). Moreover, α-Bungarotoxin also significantly increased the static response (Δmean control: −5.581 imp/sec; Δmean α-bungarotoxin: 18.69 imp/sec; P = 0.0169, control vs. α-bungarotoxin; Figure 9D), whereas d-Tubocurarine did not affect the static response (Δmean d-tubocurarine: 8.276 imp/sec; P = 0.2122, control vs. d-tubocurarine). Overall, these results demonstrate a higher instantaneous frequency and a higher sensitivity of muscle spindle responses to ramp-and-hold stretches in the presence of both AChR inhibitors.

Hemicholinium-3 (HC-3) blocks the high-affinity uptake of choline into nerve terminals, including α-motoneuron terminals at the neuromuscular junction (Yu and Van der Kloot, 1991). Therefore, an application of HC-3 to neuromuscular junctions results in an

inhibition of ACh synthesis and release (Carpenter and Woodruff, 1987). To investigate if the blockade of vesicular acetylcholine uptake and release through HC-3 influenced the proprioceptive afferent responses to stretch I analysed muscle spindle firing frequency in response to ramp-and-hold stretches before and after the addition of the drug. I observed no effect of HC-3 on the resting discharge before and after drug addition (Δmean control: 2.092 imp/sec; Δmean HC-3: −1.612 imp/sec; P = 0.235; Figure 8A). These data demonstrate that HC-3, like both tested AChR inhibitors before, did not activate γ-motoneuron endplates or had an effect on muscle spindle sensory afferents at resting length. However, the parameters analysed during the ramp-and-hold stretches, dynamic peak (Δmean control: −12.04 imp/sec; Δmean HC-3: 26.7 imp/sec; Figure 8B) and dynamic index (Δmean control: −5.413 imp/sec; Δmean HC-3: 16.35 imp/sec; Figure 8C) were significantly increased (Dunnett's post hoc test relative to ACSF control; dynamic peak P = 0.0111; dynamic index P = 0.0071). I did not observe an effect of HC-3 on the static response (Δmean control: −5.581 imp/sec; Δmean HC-3: 8.867 imp/sec; static response P = 0.228; Figure 8D).

Overall, these results demonstrate that muscle spindle afferent firing rates in response to stretch can be modulated by ACh uptake, synthesis and release. This modulation leads to an increase of the afferent firing rates in the response to stretch.

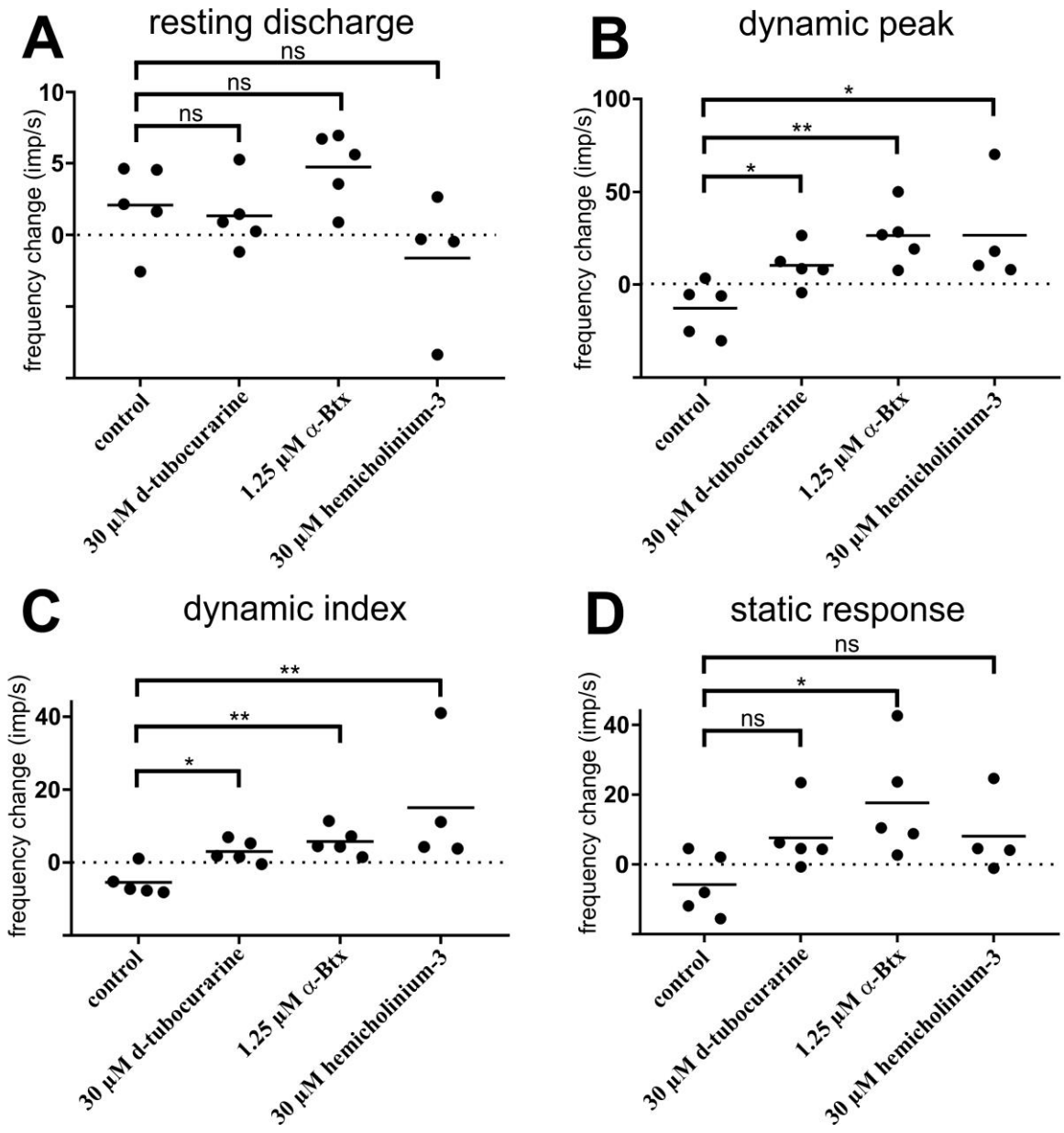

Figure 8: Neither d-Tubocurarine, α-bungarotoxin nor hemicholinium-3 have an effect on the resting discharge frequency but increase the firing rate during ramp-and-hold stretches.
The effect of d-tubocurarine, α-bungarotoxin or hemicholinium-3 on stretches of 7.5 % of Lo on single proprioceptive afferents was determined before and after the addition of each drug. The values (imp/sec) before drug addition were subtracted from the values after drug addition. The results are presented in a dot plot with each dot representing an individual muscle spindle afferent. Mean values are indicated as horizontal line. Five spindles, each from a different mouse, were analysed in the presence and absence of α-bungarotoxin or d-tubocurarine (n = 5). Four mice were evaluated in the presence and absence of hemicholinium-3 (n = 4) and control values represent muscle spindle activities where ACSF was added instead of a drug (n = 5). Addition of either drug had no influence on RD (A) but increased the firing frequencies during DP (B) and DI (C). SR was also increased after α-Bungarotoxin administration (D). Statistical significance was evaluated using one-way ANOVA (factor: drug) with Dunnett's post hoc corrections. *<0.05, **<0.01, ***<0.001, ****<0.0001. (Gerwin et al., 2019)

Table 1: Mean values (frequencies in imp/sec) ± SD of the responses to ramp-and-hold stretches before and after administration of ACSF, α-bungarotoxin, d-tubocurarine or HC-3 (Gerwin et al., 2019).

	Mean (imp/sec)							
	Control		α-Bungarotoxin		d-Tubocurarine		HC-3	
	Before	After	Before	After	Before	After	Before	After
RD	13,0 ± 6,0	15,1 ± 5,8	18,4 ± 4,4	23,2 ± 5,8	16,4 ± 3,6	17,8 ± 2,4	20,8 ± 1,5	19,2 ± 2,8
DP	94,2 ± 20,6	88,0 ± 31,5	56,8 ± 21,6	83,3 ± 34,5	60,5 ±23,5	70,5 ± 7,8	50,5 ± 14,7	77,2 ± 12,8
DI	37,3 ± 9,3	34,2 ± 11,6	27,9 ± 10,3	33,7 ± 10,4	27,3 ± 8,6	30,1 ± 9,2	26,1 ± 5,3	42,5 ± 5,4
SR	42,2 ± 12,9	40,3 ± 18,3	17,7 ± 7,4	36,4 ± 22,9	21,5 ±10,5	29,8 ±16,2	15,6 ± 1,8	24,4 ± 5,5

5.2.3 Effect of d-tubocurarine, α-bungarotoxin and hemicholinium-3 on action potential frequencies during sinusoidal vibrations

To analyse the function of the AChRs specifically during the dynamic response of a stretch, I determined the effect of both AChR blockers and of HC-3 on muscle spindle afferent responses to sinusoidal vibrations varying in displacement as well as in frequency as previously described (Gerwin et al., 2019). The tested stimuli included four different frequencies (10, 25, 50 and 100 Hz) and four different amplitudes (5, 10, 50 and 100 µm). In contrast to the ramp-and-hold stimuli, sinusoidal vibrations test the dynamic responsiveness at much smaller length changes and, thus, relatively selectively activate Ia-afferents (Brown et al., 1967).

Ia-afferent units show a narrow time range to spike during the stretching phase of a sinusoidal vibration (phase lock). Therefore, I investigated if d-tubocurarine or α-bungarotoxin changed this firing pattern. In the presence of either d-tubocurarine or α-bungarotoxin, I did not observe a change in the phase locking. Thus, the exact time point during a vibration at which an action potential was generated did not change significantly in the presence of the drug (Figure 9). Wilkinson et. al. described that the units fire preferentially in the stretch phase of the cycle (Wilkinson et al., 2012). However, the units in this study fired preferentially at the peak of the stretch or during the release phase of the vibration.

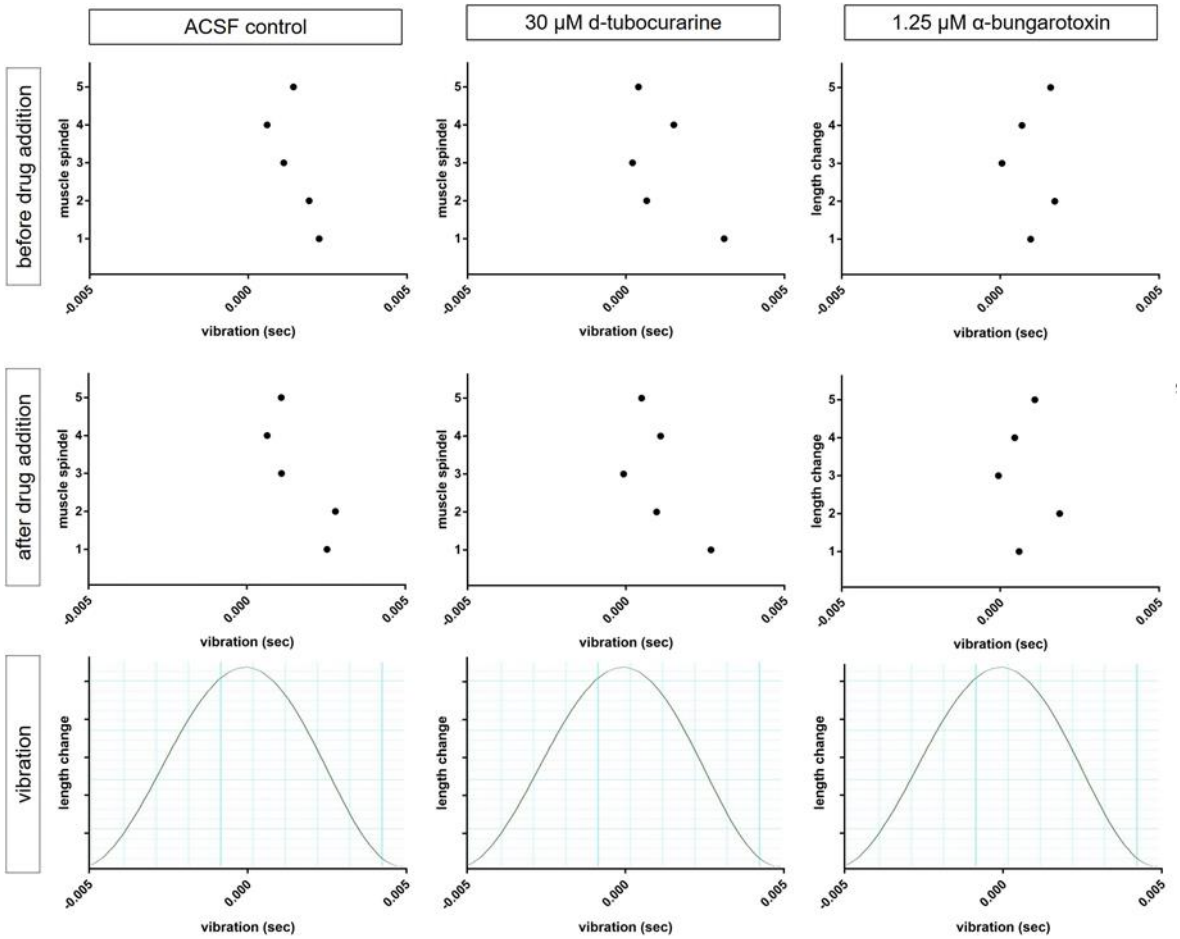

Figure 9: AChR inhibitors do not change the firing pattern of muscle spindles during sinusoidal vibrations. The time range to spike of Ia-afferents during a sinusoidal vibration (lower panel, upward deflection corresponds to lengthening of the muscle) is shown before (upper panel) and after drug or ACSF administration (middle panel). No differences are observed after drug or ACSF administration or between the groups. Each dot represents a single muscle spindle afferent unit before and after drug or ACSF administration.

Moreover, I observed an increase in firing frequency in response to sinusoidal vibrations after addition of all three drugs. Statistical analysis with the three-way ANOVA (factors: drug, amplitude and frequency) showed a significant change of the frequency before and after drug addition for the factor drug ($P = 0.0003$). The changes in the factors amplitude ($P = 0.6465$) and frequency ($P = 0.0602$) were not statistically significant. The effect was also significant for the drug by frequency analysis ($P = 0.0176$) but the drug by amplitude ($P = 0.5672$), the amplitude by frequency ($P = 0.7768$) or the drug by amplitude and frequency analysis ($P = 0.522$) were not significant.

Moreover, each of the 16 sinusoidal vibrational stimuli was analysed individually before and after drug addition by using the one-way ANOVA with Dunnett's multiple comparison test. This analysis revealed that the frequency were significantly increased in the presence of α-bungarotoxin. This increase appeared particularly at high frequencies (50 and 100 Hz) and small amplitudes (5 and 10 µm; Figure 10 B and C) but not at higher

amplitudes (50 and 100 µm; Figure 10 D and E) compared to the ACSF control. I detected no significant change in the presence of d-tubocurarine or HC-3 (Figure 10 B–E).

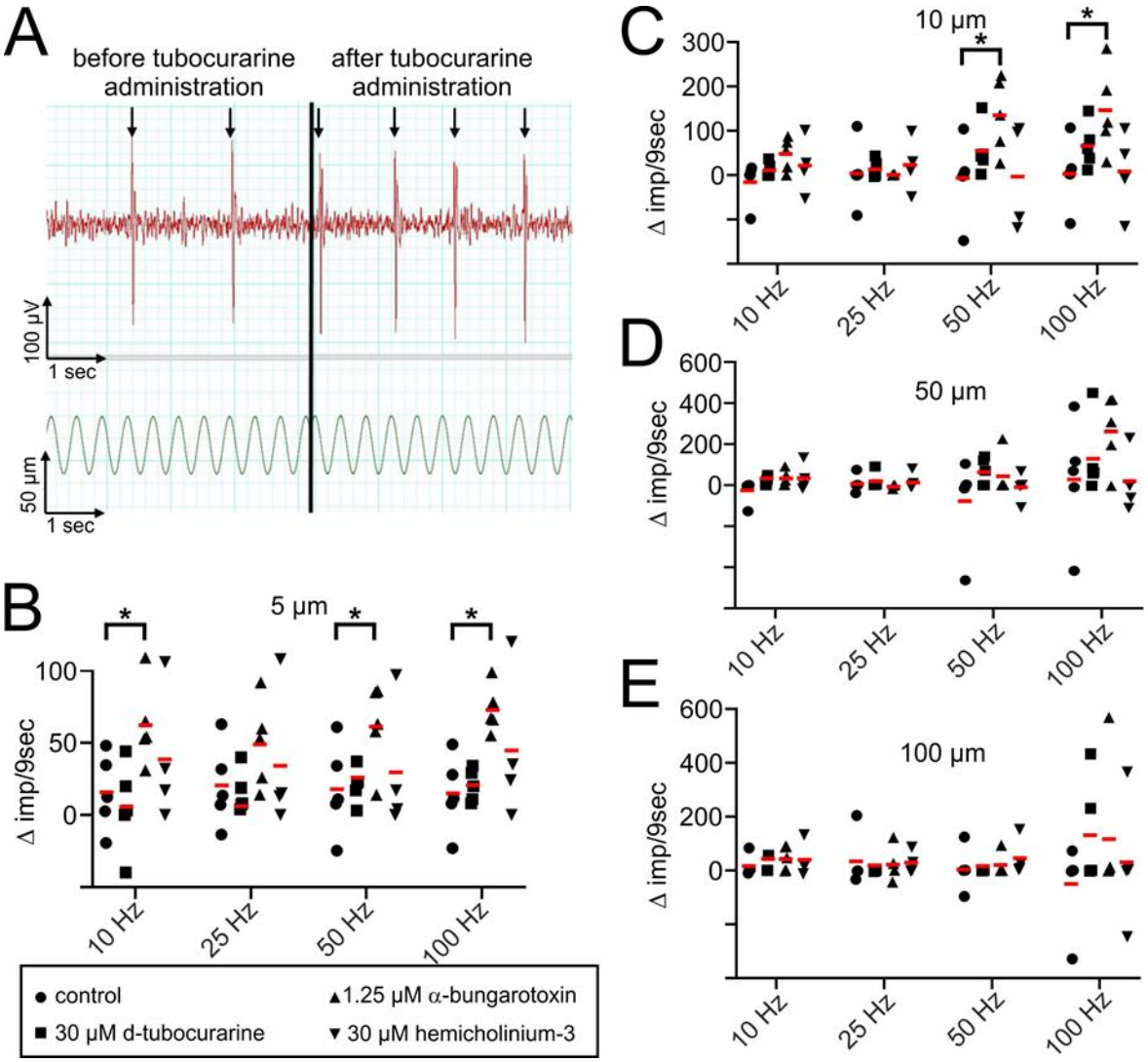

Figure 10: Responses of muscle spindle sensory afferents to sinusoidal vibrations in the presence and absence of cholinergic inhibitors. (A) Individual action potentials of an exemplary muscle spindle afferent in response to sinusoidal length changes (displayed below). In the absence of d-tubocurarine the muscle spindle afferent entrained with every 4th vibration (left side) whereas after drug addition the firing frequency increased and entrained with every 2nd vibration (right side). (B–E) Quantification of the 16 different sinusoidal vibrations (5, 25, 50 and 100 µm amplitude with each 10, 25, 50 and 100 Hz frequency). The impulses before drug, or ACSF for the control group, addition were subtracted from the impulses after drug addition (imp/9 sec) and presented as dot in a dot plot. Each dot represents an individual muscle spindle afferent. The mean of 5 (ACSF, α-bungarotoxin or d-tubocurarine) or 4 (hemicholinium-3) individual experiments is indicated as red line. Statistically significance was determined by using the one-way ANOVA (factor: drug) with Dunnett's post hoc test to the no drug control. Only significant changes are indicated *<0.05, **<0.01, ***<0.001, ****<0.0001. (Gerwin et al., 2019).

The absolute values (imp/9 sec ± SD) of the responses to sinusoidal vibrational stimuli are shown in Table 2. Overall, the effect of all three drugs on muscle spindle afferent responses to sinusoidal vibrations further support the hypothesis of a role for AChRs in modulating muscle spindle function during the dynamic phase of a muscle stretch.

Table 2: Mean values (in impulses per 9 sec) ± SD of the responses of muscle spindle afferents to all 16 sinusoidal vibrations before and after administration of ACSF, α-bungarotoxin, d-tubocurarine or HC-3 (Gerwin et al., 2019).

		Amplitude			
Frequency		5 µm	10 µm	50 µm	100 µm
Control					
10 Hz	Before	119,5 ± 61,6	148,3 ± 80,2	155,9 ± 83,8	176,3 ± 56,7
	After	135,2 ± 49,6	133,8 ± 46,8	130,4 ± 42,7	191,6 ± 60,1
25 Hz	Before	122,9 ± 65,4	207,5 ± 68,1	221,5 ± 39,1	234,5 ± 13,4
	After	143,2 ± 58,2	211,8 ± 26,4	229,4 ± 8,3	267,6 ± 76,9
50 Hz	Before	125,2 ± 67,5	241,4 ± 89,6	433,2 ± 257,1	448,4 ± 71,4
	After	143,0 ± 56,3	234,4 ± 38,6	358,6 ± 79,8	454,6 ± 8,7
100 Hz	Before	124,2 ± 66,9	232,8 ± 95,2	455,8 ± 239,1	887,9 ± 231,2
	After	138,8 ± 56,4	236,4 ± 43,3	484,6 ± 220,3	716,2 ± 210,8
α-Bungarotoxin					
10 Hz	Before	182,5 ± 29,8	144,8 ± 43,9	162,0 ± 35,5	162,4 ± 36,2
	After	208,6 ± 57,4	191,8 ± 51,2	195,2 ± 52,7	207,4 ± 66,8
25 Hz	Before	158,8 ± 60,4	202,2 ± 44,6	206,8 ± 36,9	224,8 ± 0,4
	After	207,8 ± 49,3	203,2 ± 45,1	202,8 ± 44,4	246,2 ± 55,1
50 Hz	Before	156,2 ± 68,3	221,4 ± 69,6	344,8 ± 131,0	386,6 ± 88,7
	After	217,4 ± 54,0	355,8 ± 128,7	390,0 ± 119,5	405,4 ± 90,2
100 Hz	Before	155,6 ± 57,1	233,2 ± 79,4	385,0 ± 159,8	729,0 ± 290,4
	After	228,6 ± 62,2	378,6 ± 149,8	651,4 ± 303,1	767,0 ± 267,5
d-Tubocurarine					
10 Hz	Before	147,2 ± 32,4	137,2 ± 40,0	141,6 ± 40,9	168,6 ± 22,8
	After	152,6 ± 31,2	148,6 ± 39,4	161,4 ± 24,6	180,2 ± 1,0
25 Hz	Before	155,2 ± 36,0	198,2 ± 44,4	207,8 ± 36,9	227,0 ± 1,7
	After	170,8 ± 26,7	211,2 ± 28,1	227,4 ± 1,6	227,0 ± 2,1
50 Hz	Before	161,4 ± 38,6	223,6 ± 56,8	337,0 ± 99,4	450,4 ± 0,5
	After	181,8 ± 34,9	279,4 ± 97,2	403,0 ± 62,0	450,2 ± 0,4
100 Hz	Before	157,6 ± 34,7	227,4 ± 65,2	378,4 ± 91,9	637,8 ± 215,0
	After	178,0 ± 32,5	294,4 ± 92,2	509,2 ± 207,7	672,4 ± 211,5
HC-3					
10 Hz	Before	190,7 ± 12,8	209,7 ± 7,3	212,3 ± 17,4	207,3 ± 17,9
	After	242,3 ± 65,2	255,0 ± 52,2	251,7 ± 43,9	267,0 ± 46,6
25 Hz	Before	183,7 ± 20,0	220,7 ± 8,0	330,3 ± 1,2	317,7 ± 2,0
	After	229,7 ± 60,8	267,0 ± 46,8	358,0 ± 36,1	365,7 ± 34,9
50 Hz	Before	174,0 ± 18,7	228,7 ± 82,4	379,3 ± 93,2	600,3 ± 87,0
	After	229,3 ± 60,9	258,7 ± 88,1	400,7 ± 75,8	656,0 ± 25,6
100 Hz	Before	181,7 ± 16,5	228,3 ± 73,6	381,7 ± 240,9	704,0 ± 247,7
	After	227,0 ± 71,6	266,7 ± 102,1	436,7 ± 210,7	826,7 ± 134,2

5.3 Altered muscle spindle function in murine models of muscular dystrophy

Duchenne muscular dystrophy is a disease that leads to an increased degeneration of muscle fibers. Histological hallmarks of the disease are variable fiber calibre as well as centralised nuclei, a loss of extrafusal muscle fibers and an infiltration of connective tissue and fat cells. It is unclear if intrafusal fibers are similarly affected as extrafusal muscle fibers. There are conflicting reports regarding the morphology of intrafusal muscle fibers in patients with muscle dystrophy and it cannot be excluded that some of the morphological changes are due to post-mortem damage and other, age-related degenerative processes (Gossrau and Grozdanovic, 1997, Johnson and Ovalle, 1986, Nahirney and Ovalle, 1993, Ovalle and Dow, 1986, Swash and Fox, 1976). In any case, patients with Duchenne muscular dystrophy fall and trip more often compared to healthy control groups (Hsu and Furumasu, 1993, Pradhan et al., 2006) and a functional analysis of muscle spindles has not been performed yet. To investigate if intrafusal fibers are similarly affected by the mutation as are extrafusal fibers, I analysed the morphology and function of adult muscle spindles in several mouse models for muscular dystrophies.

5.3.1 Dystrophin at the central part of the muscle spindle

The distribution of dystrophin in the central part of muscle spindles in mice has been previously described (Nahirney and Ovalle, 1993) and it was reported that dystrophin is concentrated in the area between the contact region of the sensory nerve terminal with the intrafusal fiber and is excluded from the area of contact to the sensory nerve terminal. To investigate the exact distribution of dystrophin in mouse models with respect to the sensory nerve terminal of the muscle spindle, I analysed sections stained with anti-dystrophin and anti-vGluT1 antibodies. High resolution confocal microscopic analysis of the central region of intrafusal muscle fibers, demonstrated an alternating staining pattern of dystrophin and the sensory nerve terminal (Figure 11). This indicates a concentration of dystrophin in the intrafusal fiber between the contact region of the sensory nerve terminal and the intrafusal fibers of mice, similar to what has been described by Nahirney and Ovalle.

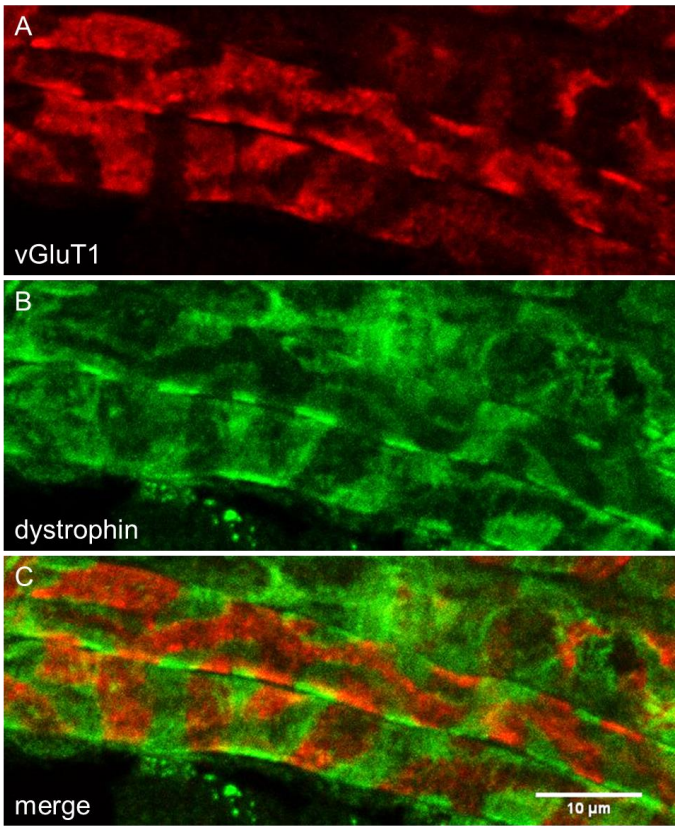

Figure 11: Distribution of dystrophin at the central part of the muscle spindle. Dystrophin (B, green panel) is concentrated in the area between the contact region of the sensory nerve terminal (A, red panel) with the intrafusal fiber. Nuclear chain fiber, Scale bar = 10 µm.

5.3.2 The dystrophin-associated glycoprotein complex at the central part of the muscle spindle

Dystrophin is part of the dystrophin-associated glycoprotein complex (DGC). In the sarcolemma of extrafusal fibers this complex has the function to connect the extracellular matrix with the intracellular cytoskeleton and by this secures mechanical stability of the sarcolemma during contraction (Chan et al., 1998, Ervasti, 2003, Ervasti and Campbell, 1991, Ozawa et al., 1998, Yoshida et al., 2000). To study if other components of the DGC are present at the central part of the muscle spindle and if they codistribute with dystrophin, I analysed sections stained with anti-beta-dystroglycan antibodies. Confocal microscopic analysis of the central region of intrafusal muscle fibers, demonstrated an alternating staining pattern of beta-dystroglycan immunoreactivity and the sensory nerve terminal (Figure 12), comparable to the staining pattern obtained with antibodies against dystrophin (Figure 11). This indicates a codistribution of beta-dystroglycan and dystrophin in the intrafusal fiber and suggests the presence of the DGC at the central part of the muscle spindle.

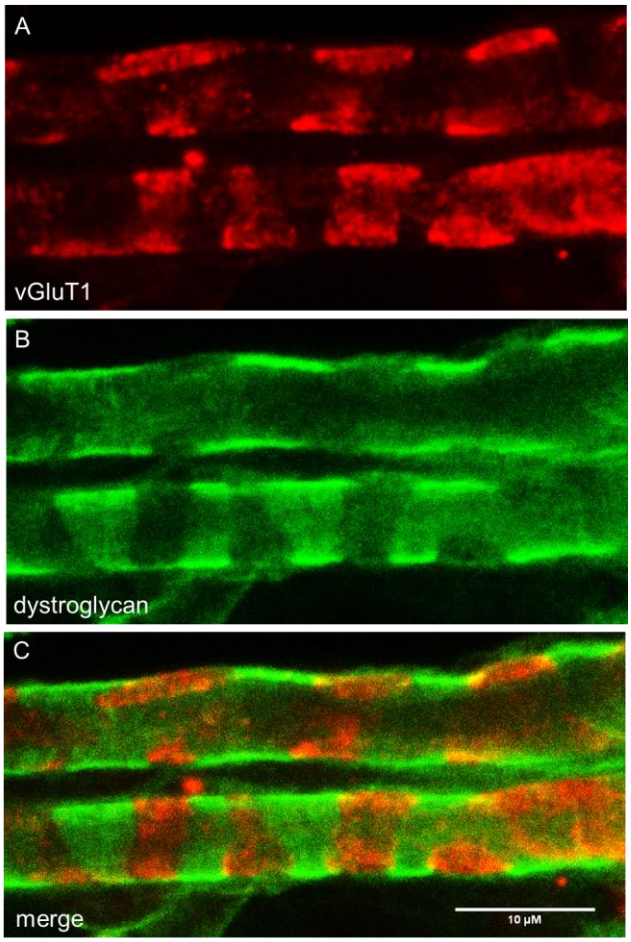

Figure 12: Distribution of beta-dystroglycan at the central part of the muscle spindle. Beta-dystroglycan (B, green panel) is concentrated in the area between the contact region of the sensory nerve terminal (A, red panel) with the intrafusal fiber, comparable with the staining pattern of dystrophin. Nuclear chain fiber, Scale bar = 10 µm.

5.3.3 Utrophin at the central part of the muscle spindle

The DGC has a differential composition at different regions along the extrafusal fiber. At the neuromuscular junction, dystrophin is replaced by an autosomal homologue named utrophin (Pilgram et al., 2010). In contrast, extrajunctional regions of the extrafusal fiber plasma membrane contain a DGC with dystrophin. To investigate if utrophin is present at the central part of the muscle spindle, I analysed sections stained with anti-utrophin antibodies. No signal with anti-utrophin antibodies was detected at the equatorial part of intrafusal fibers (Figure 13), suggesting an absence of utrophin at this area of the muscle spindle. Extrafusal fibers stained in parallel with the intrafusal fibers show a strong immunoreactivity at neuromuscular junctions (data not shown), demonstrating the specificity of the antibodies.

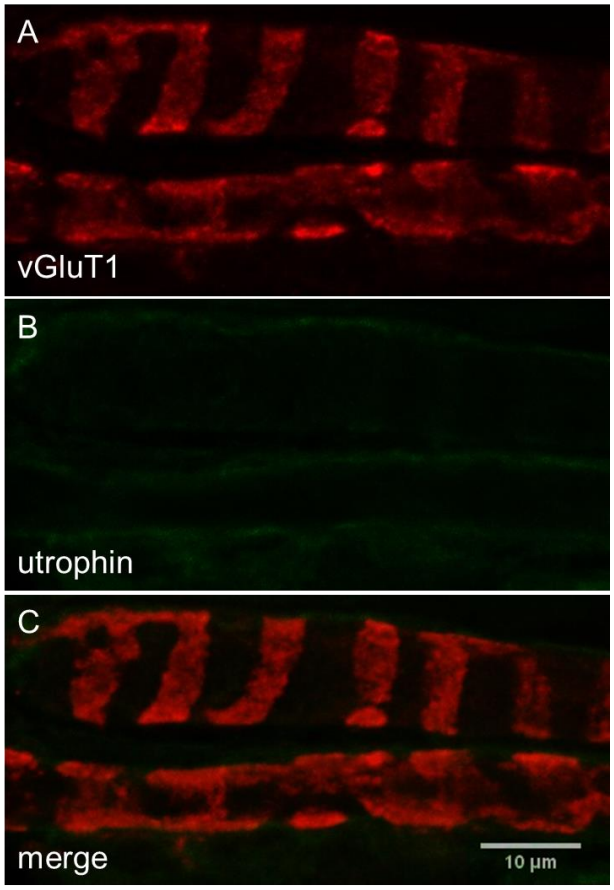

Figure 13: Distribution of utrophin at the central part of the muscle spindle. Utrophin (B, green panel) is not concentrated at the central part of the muscle spindle. The annulospiral ending is stained with anti-VGluT1 (A, red panel). Nuclear chain fiber, Scale bar = 10 µm.

5.3.4 The morphology of the central part of the muscle spindle in DMD^{mdx}-mice

The DMD^{mdx}-mouse has a mutation in the DMD gene, leading to an absence of dystrophin in extrafusal fibers. Thus, this mouse line is a model to study Duchenne muscular dystrophy in rodents. The absence of dystrophin in skeletal muscles leads to an increased degeneration of muscle fibers with typical signs of degenerative and regenerative processes. These include variable fiber calibre as well as centralised nuclei and loss of extrafusal fibers. To study if the absence of dystrophin also affects the morphology of the central part of the muscle spindle, I analysed sections from wildtype (WT) and DMD^{mdx} mice stained with anti-vGluT1 and anti-dystrophin antibodies. Sections of utrophin$^{-/-}$ mice (*utro*$^{-/-}$) were used as control, since utrophin was not detectable in this region of the muscle spindle.

The same distribution and apparent intensity of the anti-vGluT1 staining of the sensory nerve terminal were observed in WT, *utro*$^{-/-}$ and DMD^{mdx}-mice (Figure 14), suggesting a similar morphology of the annulospiral endings in these three mouse-lines. Additionally, the same distribution of dystrophin could be observed in WT and *utro*$^{-/-}$ mice and – as expected – no dystrophin immunofluorescence was detected in DMD^{mdx} mice.

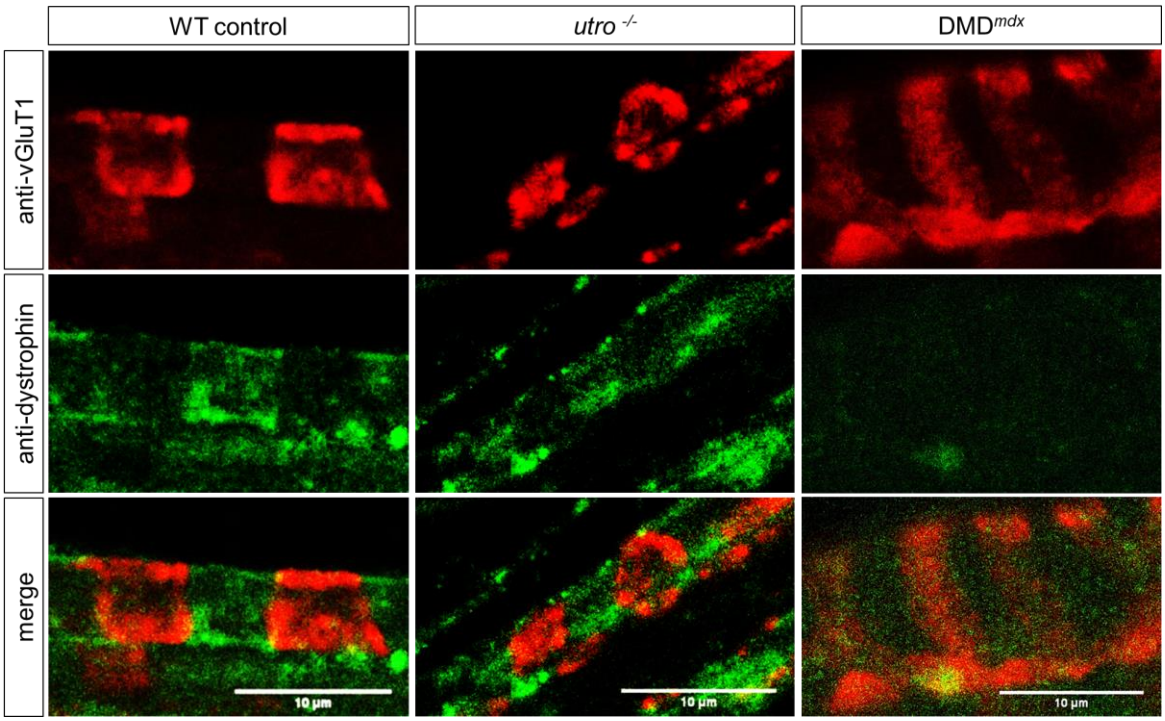

Figure 14: Distribution of dystrophin at the central part of the muscle spindle in DMD^{mdx}- and *utro*$^{-/-}$ mice. Dystrophin (green panel) is concentrated at the central part of the muscle spindle in the area between the contact region of the sensory nerve terminal with the intrafusal fiber in WT and *utro*$^{-/-}$ mice. No positive staining for dystrophin was observed in DMD^{mdx}-mice due to the knockout of dystrophin. The annulospiral ending was stained with anti-VGluT1 (red panel). No difference in the distribution of VGluT1 was discovered between the three mouse models. WT and *utro*$^{-/-}$ mice nuclear chain fiber, DMD^{mdx}-mice nuclear bag fiber, Scale bar = 10 µm.

To further investigate the molecular composition and the distribution of the DGC in the central region of muscle spindles from DMD^{mdx} mice, I analysed sections from WT and DMD^{mdx}-mice stained with anti-vGluT1 and anti-beta-dystroglycan antibodies. Sections of *utro*$^{-/-}$ mice were used as additional control. Again, the same distribution and intensity of the anti-vGluT1 staining of the sensory nerve terminal were observed in WT, *utro*$^{-/-}$ and DMD^{mdx} mice (Figure 15), suggesting a similar composition and subcellular distribution of the DGC in intrafusal fibers of wildtype and mutant mice. Furthermore, the overall distribution of the anti-beta-dystroglycan immunoreactivity was comparable in WT, *utro*$^{-/-}$ and DMD^{mdx} mice, suggesting that the absence of Dystrophin did apparently not impact the general subcellular concentration of β-dystroglycan. I noticed however that the β-dystroglycan distribution was slightly more diffuse in both mutant mice and not as clear compared to the wildtype-mice.

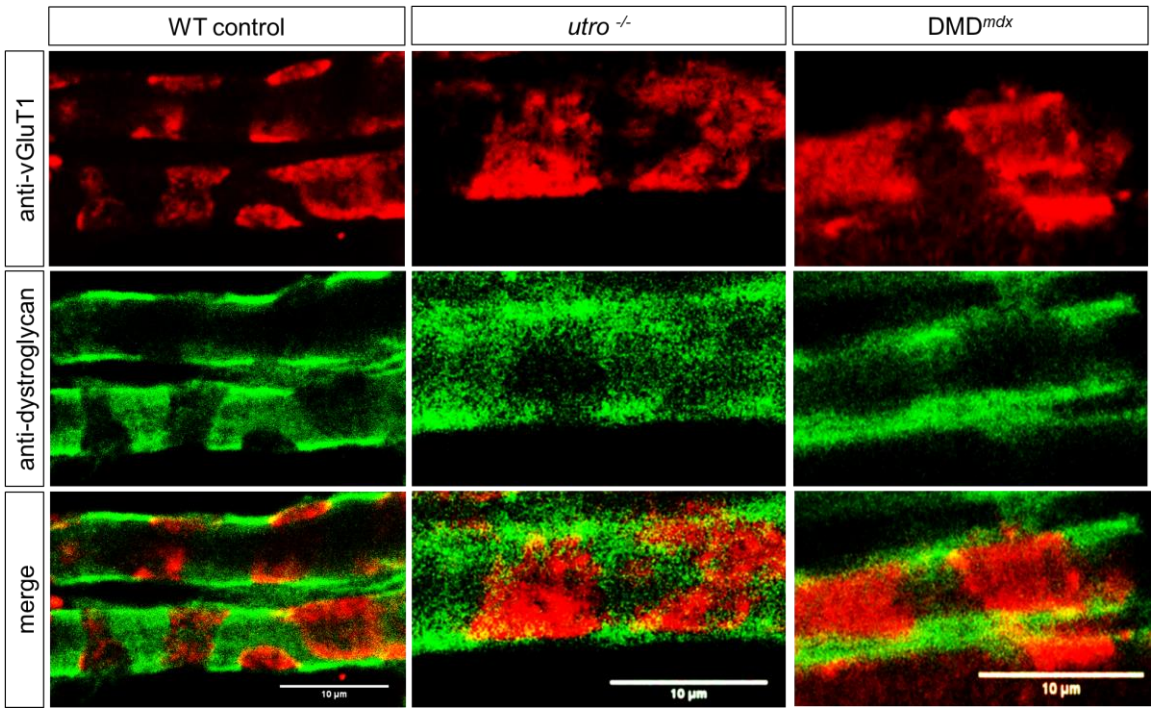

Figure 15: Distribution of beta-dystroglycan at the central part of the muscle spindle in DMD^{mdx}- and *utro*$^{-/-}$-mice. Beta -dystroglycan (green panel) is concentrated at the central part of the muscle spindle in the area between the contact region of the sensory nerve terminal with the intrafusal fiber in WT, DMD^{mdx}- and *utro*$^{-/-}$ mice. The annulospiral ending is stained with anti-vGluT1 (red panel). No differences in the distribution of VGlutT1 were observed between the three mouse models. However, the β-dystroglycan immunoreactivity in DMD^{mdx} mice was slightly more diffuse compared to the other mouse lines. WT, DMD^{mdx}- and *utro*$^{-/-}$ mice nuclear chain fiber, Scale bar = 10 µm.

5.3.5 Muscle spindle function in DMD^{mdx}-mice

Intrafusal fibers appeared to be morphologically less affected in DMD^{mdx}-mice compared to extrafusal fibers. I did not observe gross structural changes in the annulospiral endings between wildtype and the different mutant mice. To investigate if muscle spindle function is altered in DMD^{mdx}- and *utro*$^{-/-}$ mice, I analysed individual muscle spindle afferent unit responses to a ramp-and-hold stretch (Lo plus 7.5 % of Lo; ramp speed 40 % Lo/sec). Four different time points examining firing rates before (RD) and during (DP, DI and SR) the stretch from mutant mice were analysed in detail and compared to the results from wildtype mice (see Figure 3 for details). Analysis of the overall effect of the mutation using the one-way ANOVA (factor: mutation) revealed a statistically significant difference for the resting discharge ($P < 0.0001$), but no significant differences for the dynamic peak ($P = 0.2353$), dynamic index ($P = 0.3157$) and static response ($P = 0.3465$).

The resting discharge of the DMD^{mdx}-mice was significantly increased compared to wildtype and *utro*$^{-/-}$ mice (mean BL10: 13.7 imp/sec; mean *utro*$^{-/-}$: 13.6 imp/sec; mean DMD^{mdx}: 26.0 imp/sec; Dunnett's post hoc test relative to DMD^{mdx} mice: $P < 0.0001$, DMD^{mdx} vs. BL10; $P < 0.0001$, DMD^{mdx} vs. *utro*$^{-/-}$; Figure 16 A). However, dynamic peak (mean

BL10: 89.1 imp/sec; mean *utro*$^{-/-}$: 81.9 imp/sec; mean DMD^{mdx}: 114.5 imp/sec; Dunnett's post hoc test relative to DMD^{mdx} mice: P = 0.3549, DMD^{mdx} vs. BL10; P = 0.1855, DMD^{mdx} vs. *utro*$^{-/-}$; Figure 16 B), dynamic index (mean BL10: 44.9 imp/sec; mean *utro*$^{-/-}$: 40.4 imp/sec; mean DMD^{mdx}: 53.6 imp/sec; Dunnett's post hoc test relative to DMD^{mdx} mice: P = 0.5206, DMD^{mdx} vs. BL10; P = 0.2364, DMD^{mdx} vs. *utro*$^{-/-}$; Figure 16 C) and static response (mean BL10: 27.6 imp/sec; mean *utro*$^{-/-}$: 29.0 imp/sec; mean DMD^{mdx}: 40.0 imp/sec; Dunnett's post hoc test relative to DMD^{mdx} mice: P = 0.3186, DMD^{mdx} vs. BL10; P = 0.3856, DMD^{mdx} vs. *utro*$^{-/-}$; Figure 16 D) were not increased compared to the wildtype control. Overall, the results demonstrate a higher firing frequency of DMD^{mdx}-mice muscle spindle responses at resting length compared to wildtype mice. These results also demonstrate that a loss of dystrophin affects muscle spindle afferent firing rates at resting length. The absolute values of the mean muscle spindle afferent frequencies for each of the three mouse lines are given in Table 3 together with the corresponding standard deviations.

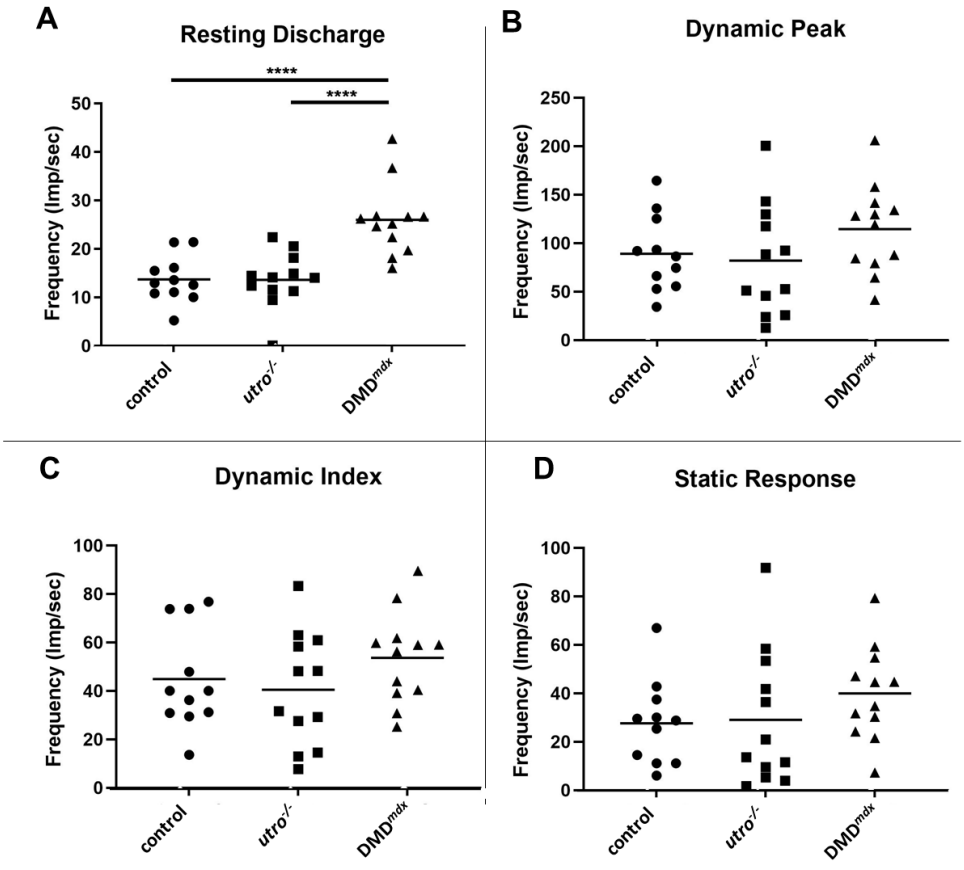

Figure 16: Muscle spindle function in DMD^{mdx}- and *utro*$^{-/-}$ mice compared to WT mice. (A) RD was significantly increased in DMD^{mdx}-mice compared to WT (control) or *utro*$^{-/-}$ mice. DP (B), DI (C) and SR (D) were not changed in DMD^{mdx}-mice compared to WT or *utro*$^{-/-}$ mice. Each dot represents an individual muscle spindle signal, mean values are indicated as black line. Control: N=6, n=11; *utro*$^{-/-}$: N=7, n=12; DMD^{mdx}: N=6, n=12; One-way ANOVA with Dunnett's multiple comparison test: *<0.05, **<0.01, ***<0.001, ****<0.0001. Only significant changes are indicated.

Table 3: Mean values (frequencies in imp/sec) ± SD from BL10, *utro*$^{-/-}$- and DMD^{mdx} mice in response to ramp-and-hold stretches.

	Mean (imp/sec)		
	BL10	*utro*$^{-/-}$	DMD^{mdx}
RD	13.7 ± 4.8	13.6 ± 5.7	26.0 ± 7.5
DP	89.1 ± 39.2	81.9 ± 57.1	114.5 ± 45.3
DI	44.9 ± 21.0	40.4 ± 23.5	53.6 ± 18.8
SR	27.6 ± 17.5	29.0 ± 27.9	40.0 ± 19.2

DP and SR were calculated depending on the RD values (see 4.3.1). Since RD values are changed significantly in DMD^{mdx}-mice compared to WT and *utro*$^{-/-}$ mice I tested if DP and SR still remain unchanged in DMD^{mdx}-mice compared to WT and *utro*$^{-/-}$ mice if RD-values are not subtracted from DP or SR values. Therefore, DP was determined as highest firing rate during ramp and SR was determined as firing rate at 3.25 to 3.75 sec into stretch. Again, no significant differences were observed between mutant and WT mice when the non-normalised values were compared. The results are summarised in Table 4.

Table 4: Mean values (frequencies in imp/sec, not depending on RD) ± SD of DP and SR from BL10, *utro*$^{-/-}$ and DMD^{mdx}-mice in response to ramp-and-hold stretches.

	Mean (imp/sec)		
	BL10	*utro*$^{-/-}$	DMD^{mdx}
DP	102.8 ± 39.6	91.2 ± 56.7	132.1 ± 39.8
SR	44.3 ± 16.3	41.2 ± 28.5	65.9 ± 22.8

To study the muscle spindle function of DMD^{mdx}-mice with respect to the dynamic phase of a muscle stretch, I analysed the muscle spindle afferent discharge response to sinusoidal vibrations varying in both displacement and frequency. I observed an increase in firing frequencies in response to sinusoidal vibrations for DMD^{mdx} mice compared to WT and *utro*$^{-/-}$ mice. Statistical analysis using a three-way ANOVA (factors: mutation, amplitude and frequency) showed that the change of frequency was significant for the factor mutation ($P = 0.0192$), amplitude ($P < 0.0001$) and frequency ($P < 0.0001$).

Additionally, each of the 16 vibrational stimuli from DMD^{mdx}-mice were compared to the corresponding values from WT and *utro*$^{-/-}$ mice with a one-way ANOVA and Dunnett´s multiple comparison test. This analysis revealed that the frequencies from DMD^{mdx}-mice were significantly increased at small amplitudes (5 µm, Figure 17 A) and low frequencies (10 Hz and 25 Hz, Figures 17 B, C and D) compared to WT- and *utro*$^{-/-}$ mice. The absolute values (imp/9 sec ± SD) for the responses to all 16 sinusoidal vibrations are shown in Table 5.

Collectively, the analysis of the response of wildtype and dystrophic mice to sinusoidal vibrational stimuli revealed an altered sensitivity of dystrophic mice compared to wildtype mice at vibrations with low frequencies and small amplitudes.

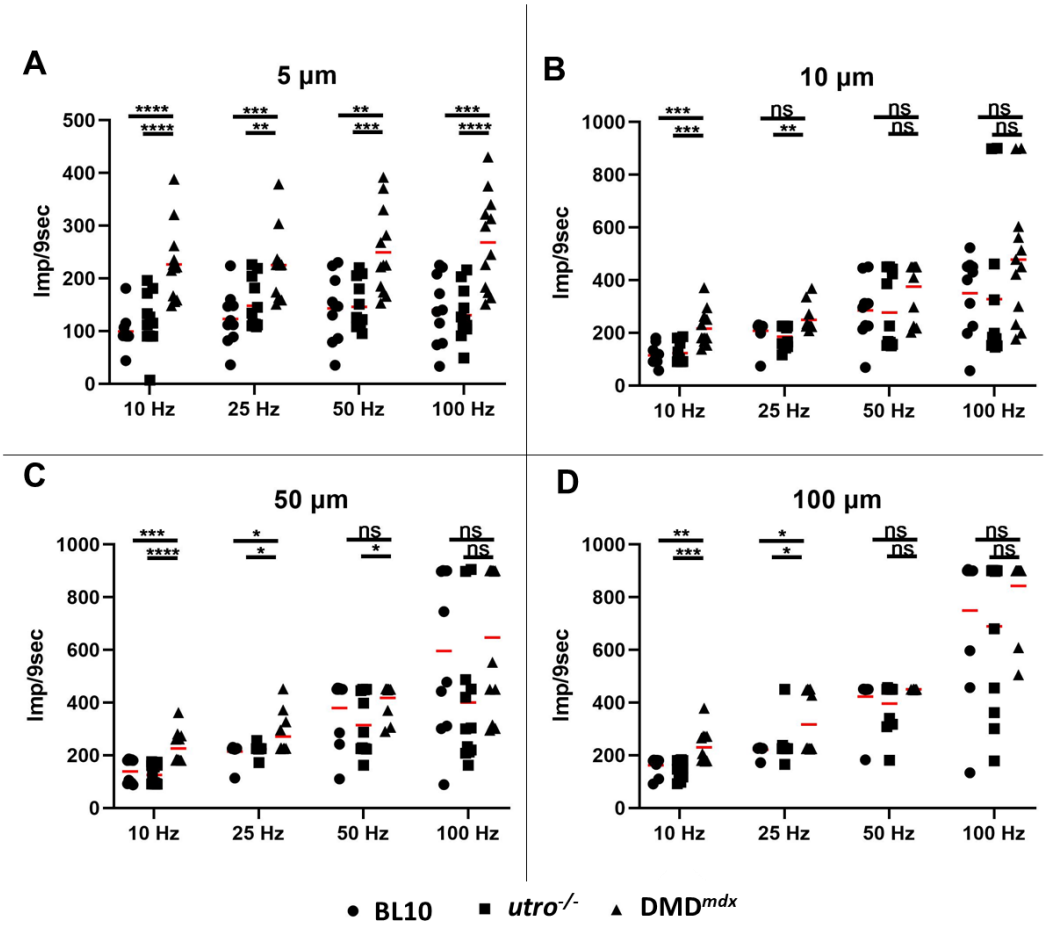

Figure 17: Muscle spindle response to sinusoidal vibrations in BL10 (Control), *utro*$^{-/-}$ and DMD^{mdx}-mice. DMD^{mdx}-mice show a significantly higher firing frequency in response to small sinusoidal vibrations (A) and slow frequencies (10 Hz and 25 Hz; B-D) compared to BL10 and *utro*$^{-/-}$ mice. Control: N=5, n=12; *utro*$^{-/-}$: N=7, n=12; DMD^{mdx}: N=6, n=12; Mean is indicated as red bar; one-way ANOVA with Dunnett´s multiple comparison-test, P-values: *<0.05, **<0.01, ***<0.001, ****<0.0001.

Table 5: Mean values (in impulses per 9 sec) ± SD of the responses of muscle spindle afferents to all 16 sinusoidal vibrations from BL10, *utro*$^{-/-}$ and DMD^{mdx}-mice.

	Amplitude			
Frequency	5 µm	10 µm	50 µm	100 µm
BL10				
10 Hz	90.3 ± 19.5	114.2 ± 37.9	138.5 ± 46.3	162.4 ± 33.3
25 Hz	123.0 ± 51.0	208.0 ± 47.9	214.7 ± 35.4	221.4 ± 17.4
50 Hz	143.0 ± 63.5	285.7 ± 112.2	379.6 ± 123.2	423.3 ± 84.4
100 Hz	140.1 ± 66.5	350.3 ± 148.0	596.6 ± 308.0	749.3 ± 268.3
***utro*$^{-/-}$**				
10 Hz	117.0 ± 51.1	123.2 ± 41.0	125.1 ± 37.1	149.4 ± 33.8
25 Hz	148.1 ± 46.5	185.6 ± 42.0	223.3 ± 18.4	240.1 ± 68.5
50 Hz	146.0 ± 45.3	276.8 ± 137.9	314.2 ± 113.7	396.3 ± 89.1
100 Hz	130.0 ± 47.8	327.6 ± 282.5	400.0 ± 256.2	689.8 ± 283.6
DMD^{mdx}				
10 Hz	226.6 ± 71.2	216.0 ± 68.3	226.0 ± 60.4	230.1 ± 62.8
25 Hz	225.1 ± 64.9	249.8 ± 50.7	271.3 ± 75.6	317.0 ± 113.3
50 Hz	249.4 ± 80.4	375.3 ± 106.0	418.3 ± 60.8	450.4 ± 1.0
100 Hz	268.3 ± 91.5	478.1 ± 242.1	647.3 ± 273.8	842.8 ± 135.3

5.3.6 Differences in muscle spindle function in BL6 and BL10 mice

To investigate if the reduced sensitivity during ramp-and-hold stretches and during sinusoidal vibrations of DMD^{mdx}-mice was directly due to the loss of the protein dystrophin or due to secondary effects in the dystrophic muscles, I analysed a mouse model with a different kind of muscular dystrophy, a dysferlinopathy. These mice also exhibit a degeneration of extrafusal fibers due to a loss of function of dysferlin, a protein which is important for membrane repair in muscles. The components of the DGC are not altered in this mouse line.

These mice were bred on a C57/BL6 background whereas the DMD^{mdx}- and *utro*$^{-/-}$ mice were bred on a BL10 background. Therefore, I initially determined if the response to stretch of mice with BL6 or BL10 background is similar. To this end, I compared muscle spindle afferent responses to stretch in both mouse lines. All parameters analysed were highly comparable between C57BL/6 and C57BL/10 animals and I detected no significant difference between both mouse lines (Figure 18). This demonstrates that muscle spindles from both mouse lines have very similar functional properties and therefore the subsequent results from mouse models with dysferlinopathy can be compared to the results from the DMD^{mdx}-mice.

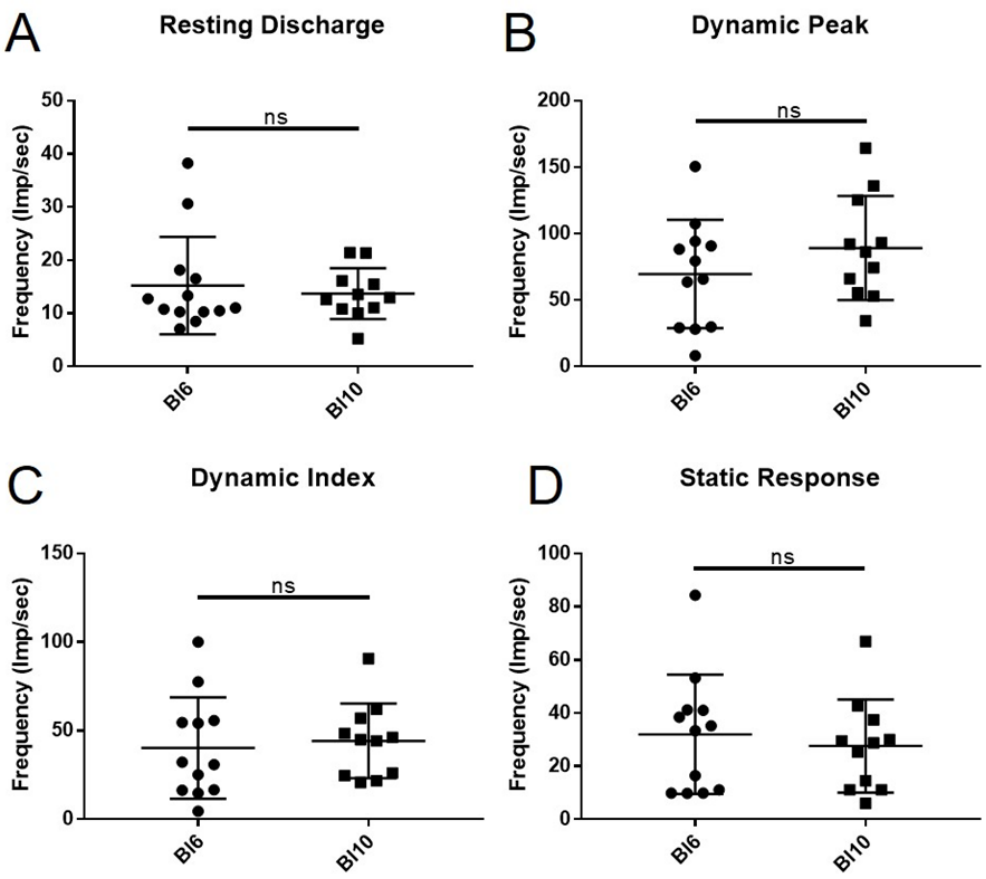

Figure 18: Differences in muscle spindle function between BL6 and BL10 mice in response to ramp-and-hold stretches. No differences between BL6 and BL10 mice in RD (A), DP (B), DI (C) or SR (D) were observed. BL6: N=5, n=12; BL10: N=7, n=12; Mean ± standard deviation; Student's t-test, P-values: *<0.05, **<0.01, ***<0.001, ****<0.0001.

5.3.7 Dysferlin at the central region of the muscle spindle

To investigate if dysferlin is present at the membrane of intrafusal fibers and to investigate it`s subcellular distribution, I analysed sections stained with anti-dysferlin and anti-VGluT1 antibodies. High resolution confocal microscopic analysis of the equatorial region of intrafusal muscle fibers demonstrated anti-dysferlin immunoreactivity at the sarcolemmal membrane, in particular in the contractile region of intrafusal fibers (Figure 19 arrows). A comparable distribution was observed in extrafusal fibers (arrowheads in Fig. 19 B, C). This indicates a comparable subcellular distribution of dysferlin in intrafusal and extrafusal fibers (Figure 19).

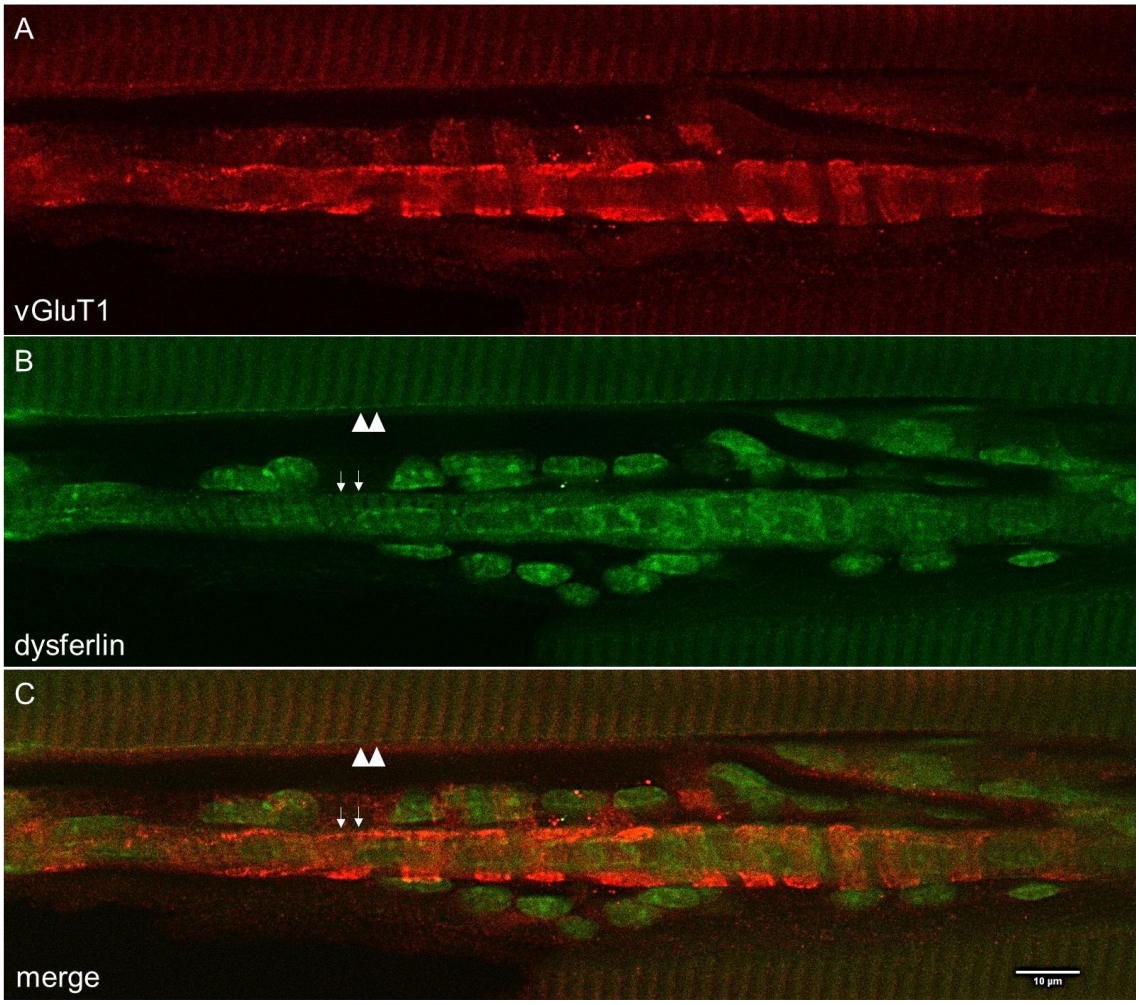

Figure 19: Distribution of Dysferlin in extrafusal and intrafusal fibers. Dysferlin (green, panel B) is concentrated at the sarcolemma of extrafusal (arrow heads) and intrafusal fibers (arrows) in an alternating pattern. The Ia-afferent of the muscle spindle is stained with anti-VGluT1 (red, panel A). An unspecific binding of the anti-dysferlin antibody at nuclei was observed (panel B). Scale bar = 10 µm.

5.3.8 The morphology of the central part of the muscle spindle in Dysferlin$^{-/-}$ mice

The Dysferlin$^{-/-}$ (*dysf*$^{-/-}$) mouse is a mouse model to study dysferlinopathies (Bittner et al., 1999). This mouse line has a mutation that leads to a similar phenotype as in DMD^{mdx}-mice, i.e. an increased degeneration and loss of extrafusal muscle fibers. To investigate if a loss of dysferlin affects the morphology of the central part of muscle spindles, I analysed sections from WT and *dysf*$^{-/-}$ mice stained with anti-vGluT1 and anti-dysferlin antibodies. Sections of DMD^{mdx}-*dysf*$^{-/-}$ double transgenic mice were used to investigate if the phenotype is additive.

A comparable distribution and intensity of the anti-vGluT1 staining of the sensory nerve terminal were observed in WT, *dysf*$^{-/-}$ and DMD^{mdx} *dysf*$^{-/-}$ mice (Figure 20), suggesting a rather normal morphology of the annulospiral ending in these three mouse lines. As expected, no dysferlin signal was observed in either mutant mice.

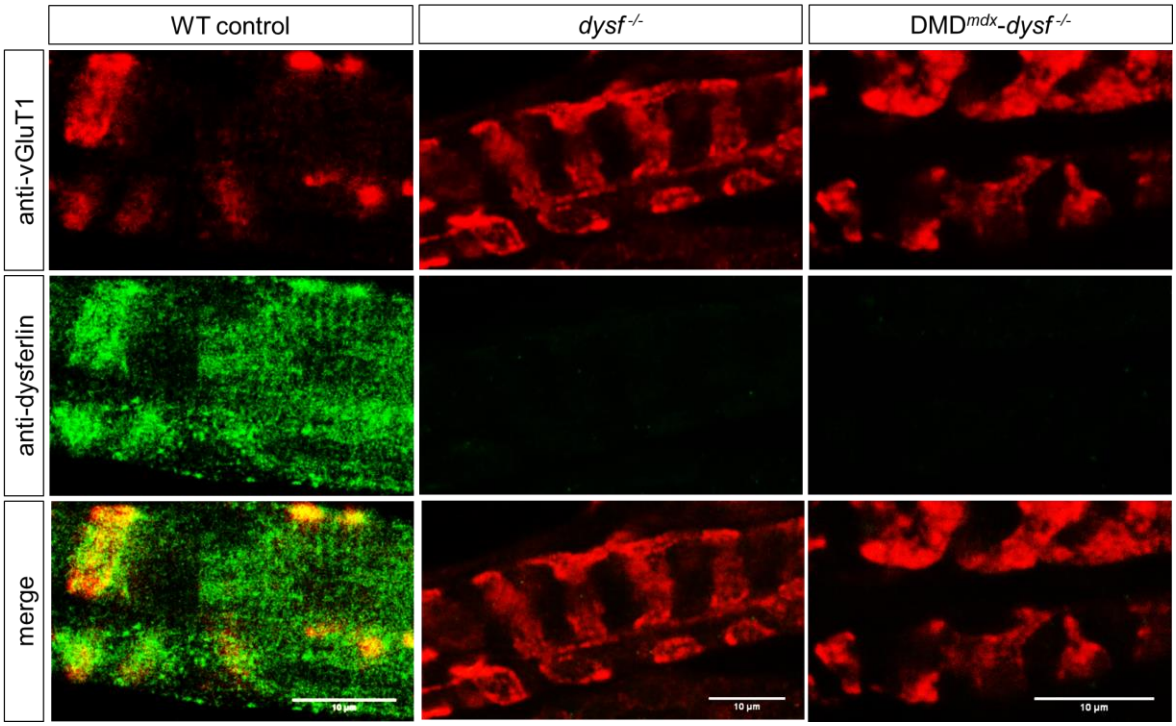

Figure 20: Distribution of dysferlin in intrafusal fibers of *dysf*$^{-/-}$ and DMD^{mdx}-*dysf*$^{-/-}$ mice compared to WT mice. Dysferlin (green panel) is concentrated at the sarcolemma of intrafusal fibers at the central region in an alternating pattern (green) whereas no positive staining was seen in both mutant lines despite of the 25 % of residual dysferlin in theses mice. The annulospiral ending was stained with anti-VGluT1 (red). All shown intrafusal fibers are chain fibers. Scale bar = 10 µm.

To further characterise the morphology and the distribution of the DGC at the central part of the muscle spindle of *dysf*$^{-/-}$ mice, I analysed sections from WT and mutant mice stained with anti-vGluT1 and either anti-dystrophin or anti-beta-dystroglycan antibodies. Similar to the other immunohistochemical analyses, I observed the same distribution and intensity of the anti-vGluT1 staining of the sensory nerve terminal in WT, *dysf*$^{-/-}$ and DMD^{mdx}-*dysf*$^{-/-}$ mice (Figures 21 and 22), supporting the hypothesis that the morphology of the annulospiral endings in these three mouse-lines was unaffected by the respective mutation.

Furthermore, the distribution of the anti-beta-dystroglycan immunoreactivity was unchanged in the mutant mice compared to wildtype mice, indicating a mutation-independent distribution of beta-dystroglycan. The distribution of the anti-dystrophin immunoreactivity was unchanged in the *dysf*$^{-/-}$ mice compared to the WT mice, indicating that the lack of dysferlin did not affect the distribution of dystrophin and of the DGC. No dystrophin immunoreactivity was detected in the DMD^{mdx}-*dysf*$^{-/-}$ mice due to the genetic ablation of this protein.

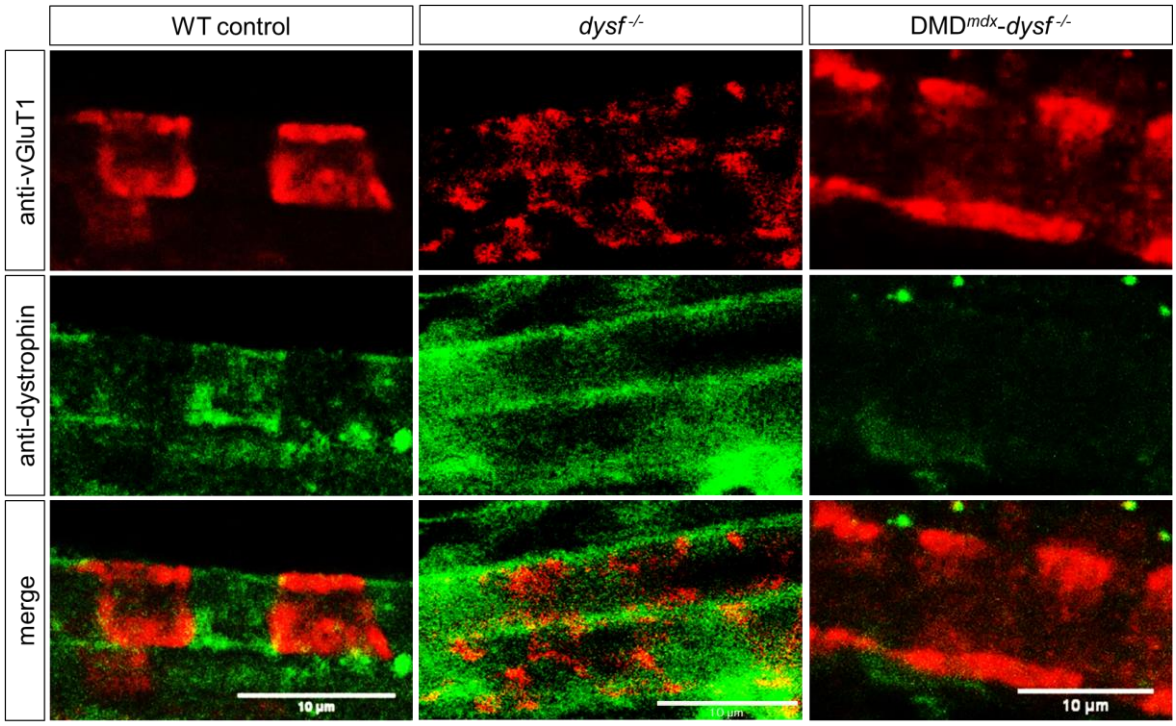

Figure 21: Distribution of dystrophin at the central part of muscle spindles in *dysf*$^{-/-}$ and DMD^{mdx}-*dysf*$^{-/-}$ mice compared to WT mice. Dystrophin (green panel) is concentrated in the area between the contact region of the Ia-afferent with the intrafusal fiber in wildtype and *dysf*$^{-/-}$ mice. No positive fluorescent signal of the anti-dystrophin antibody was observed in DMD^{mdx}-*dysf*$^{-/-}$ mice due to the knockout of this protein in this line. The annulospiral ending was stained with anti-VGluT1 (red panel). Scale bar = 10 µm.

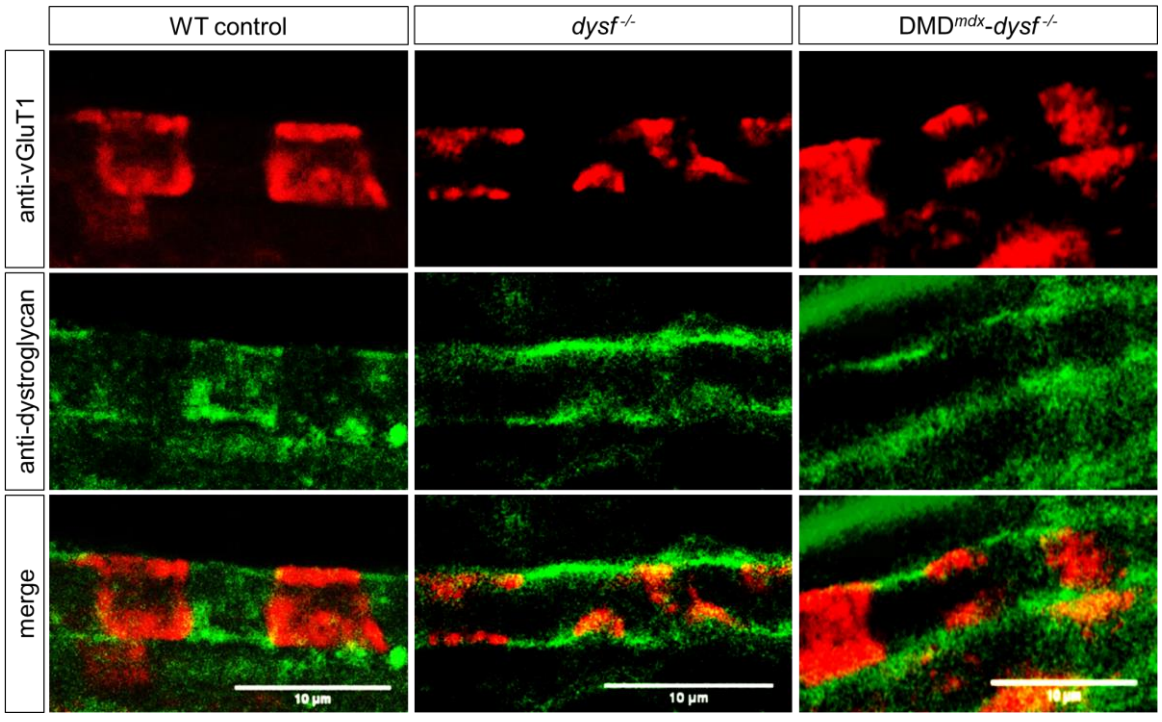

Figure 22: Distribution of beta-dystroglycan in *dysf*$^{-/-}$ and DMD^{mdx}-*dysf*$^{-/-}$ mice compared to WT mice. Beta-dystroglycan (red panel) is concentrated in the area between the contact region of the Ia-afferent (green panel) with the intrafusal fiber. Scale bar = 10 µm

5.3.9 Muscle spindle function in *dysf*$^{-/-}$ mice

The morphology of the annulospiral endings of the *dysf*$^{-/-}$ and DMD^{mdx} *dysf*$^{-/-}$ mice appeared unchanged compared to wildtype mice. To investigate if muscle spindle function is altered in *dysf*$^{-/-}$ and DMD^{mdx}-*dysf*$^{-/-}$ mice, I analysed individual muscle spindle afferent unit responses to a ramp-and-hold stretch (Lo plus 7.5% of Lo; ramp speed 40% Lo/sec). Four different time points examining firing rates before (RD) and during (DP, DI and SR) the stretch from mutant mice were analysed in detail and compared to the results from wildtype mice (C57BL/6). Analysis of the overall effect of the mutation using the one-way ANOVA (factor: mutation) revealed a statistically significant difference for the resting discharge ($P = 0.0002$), but no significant differences for the dynamic peak ($P = 0.4357$), dynamic index ($P = 0.5032$) or static response ($P = 0.3413$).

The resting discharge of the *dysf*$^{-/-}$ and DMD^{mdx} *dysf*$^{-/-}$ mice was significantly increased compared to wildtype mice (mean BL6: 9.0 imp/sec; mean *dysf*$^{-/-}$: 18.1 imp/sec; mean DMD^{mdx}-*dysf*$^{-/-}$: 18.3 imp/sec; Dunnett's post hoc test relative to BL6-mice: $P = 0.0009$, BL6 vs. *dysf*$^{-/-}$; $P = 0.0003$, BL6 vs. DMD^{mdx}-*dysf*$^{-/-}$; Figure 23 A). However, dynamic peak (mean BL6: 94.9 imp/sec; mean *dysf*$^{-/-}$: 94.9 imp/sec; mean DMD^{mdx}-*dysf*$^{-/-}$: 75.1 imp/sec; Dunnett's post hoc test relative to BL6-mice: $P > 0.9999$, Bl6 vs. *dysf*$^{-/-}$; $P = 0.4329$, BL6 vs. DMD^{mdx}-*dysf*$^{-/-}$; Figure 23 B), dynamic index (mean BL6: 45.3 imp/sec; mean *dysf*$^{-/-}$: 45.0 imp/sec; mean DMD^{mdx}-*dysf*$^{-/-}$ *:* 36.0 imp/sec; Dunnett's post hoc test relative to BL6 mice: $P = 0.9991$, BL6 vs. *dysf*$^{-/-}$; $P = 0.4854$, BL6 vs. DMD^{mdx}-*dysf*$^{-/-}$; Figure 23 C) and static response (mean BL6: 39.5 imp/sec; mean *dysf*$^{-/-}$: 35.0 imp/sec; mean DMD^{mdx}-*dysf*$^{-/-}$: 26.6 imp/sec; Dunnett's post hoc test relative to BL6 mice: $P = 0.8344$, BL6 vs. *dysf*$^{-/-}$; $P = 0.2573$, BL6 vs. DMD^{mdx}-*dysf*$^{-/-}$ *;* Figure 23 D) were not increased compared to wildtype control mice. The absolute values of the mean muscle spindle afferent frequencies for each of the three mouse lines are given in Table 6 including the corresponding standard deviations. Overall, the results demonstrate a higher firing frequency of *dysf*$^{-/-}$ and DMD^{mdx}-*dysf*$^{-/-}$ mice muscle spindles at resting length compared to wildtype mice.

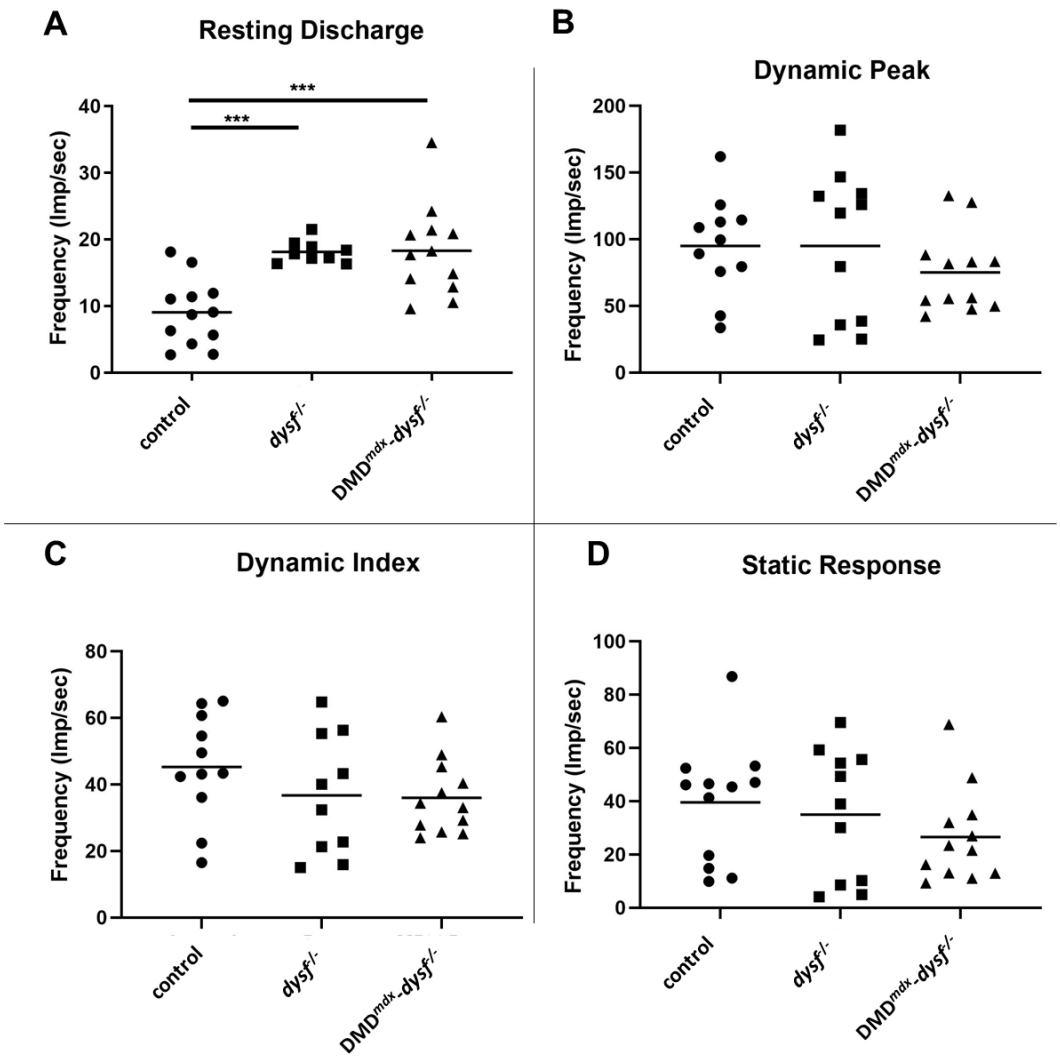

Figure 23: Muscle spindle responses to ramp-and-hold stretches in *dysf*$^{-/-}$ and DMD^{mdx}-*dysf*$^{-/-}$ mice compared to WT mice. The RD (A) is significantly increased in both mutant lines compared to the WT control. In contrast, the DP (B), the DI (C) and the SR (D) are not changed compared to WT mice. Control: N=6, n=11; *dysf*$^{-/-}$: N=6, n=11; DMD^{mdx}-*dysf*$^{-/-}$: N=5, n=12; Mean is indicated is black bar. One-way ANOVA with Dunnett´s multiple comparison test; P-values: *<0.05, **<0.01, ***<0.001, ****<0.0001. Only significant changes are indicated.

Table 6: Mean values (frequencies in imp/sec) ± SD from BL6, *dysf*$^{-/-}$ and DMD^{mdx}-*dysf*$^{-/-}$ mice in response to ramp-and-hold stretches.

	Mean (imp/sec)			
	RD	DP	DI	SR
BL6	9.0 ± 5.0	94.9 ± 36.8	45.3 ± 16.0	39.5 ± 22.3
dysf$^{-/-}$	18.1 ± 1.7	94.9 ± 56.1	45.0 ± 32.3	35.0 ± 24.5
DMD^{mdx}-*dysf*$^{-/-}$	18.3 ± 6.8	75.1 ± 30.3	36.0 ± 11.1	26.6 ± 17.7

DP and SR were calculated depending on the RD values (see 4.3.1). Since RD values are changed significantly in *dysf*$^{-/-}$ and DMD^{mdx}-*dysf*$^{-/-}$ mice compared to WT mice I tested if DP and SR still remain unchanged in *dysf*$^{-/-}$ and DMD^{mdx}-*dysf*$^{-/-}$ mice compared to WT mice if RD-values are not subtracted from DP or SR values. Therefore, DP was determined as highest firing rate during ramp and SR was determined as firing rate 3.25 to 3.75 sec into stretch. Again, no significant changes were observed in mutant mice compared to WT mice. The results are summarised in Table 7.

Table 7: Mean values (frequencies in imp/sec, not depending on RD) ± SD of DP and SR from BL6, *dysf*$^{-/-}$- and DMD^{mdx}-*dysf*$^{-/-}$ mice in response to ramp-and-hold stretches.

	Mean (imp/sec)			
	DP		SR	
BL6	103.9	± 37.3	48.0	± 23.2
dysf$^{-/-}$	112.6	± 56.4	52.7	± 23.7
DMD^{mdx}-*dysf*$^{-/-}$	93.4	± 33.3	49.6	± 26.3

To study the altered muscle spindle function of *dysf*$^{-/-}$ and DMD^{mdx}-*dysf*$^{-/-}$ mice more detailed during the dynamic phase of a muscle stretch, I analysed the muscle spindle afferent discharge responses to sinusoidal vibration stimuli varying in displacement as well as in frequency. I observed an increase in firing frequencies in response to sinusoidal vibration stimuli for *dysf*$^{-/-}$ and DMD^{mdx}-*dysf*$^{-/-}$ mice compared to WT mice especially at small amplitudes. Statistical analysis was performed using a three-way ANOVA (factors: mutation, amplitude and frequency) showed that the change of frequency was not statistically significant for the factor mutation ($P = 0.0838$) but significant for the factors amplitude ($P < 0.0001$) and frequency ($P < 0.0001$).

Moreover, each of the 16 sinusoidal vibrations from *dysf*$^{-/-}$ and DMD^{mdx}-*dysf*$^{-/-}$ mice were compared with the corresponding values from WT mice with a one-way ANOVA including a Dunnett´s multiple comparison test. This analysis revealed that the frequency from *dysf*$^{-/-}$ and DMD^{mdx}-*dysf*$^{-/-}$ mice were significantly increased at small amplitudes (5 µm, Figure 24 A) and slow frequencies (10 Hz and 25 Hz, Figures 24 B-D) compared to WT mice. The absolute values (imp/9 sec ± SD) for the responses to all 16 vibration stimuli are shown in Table 8.

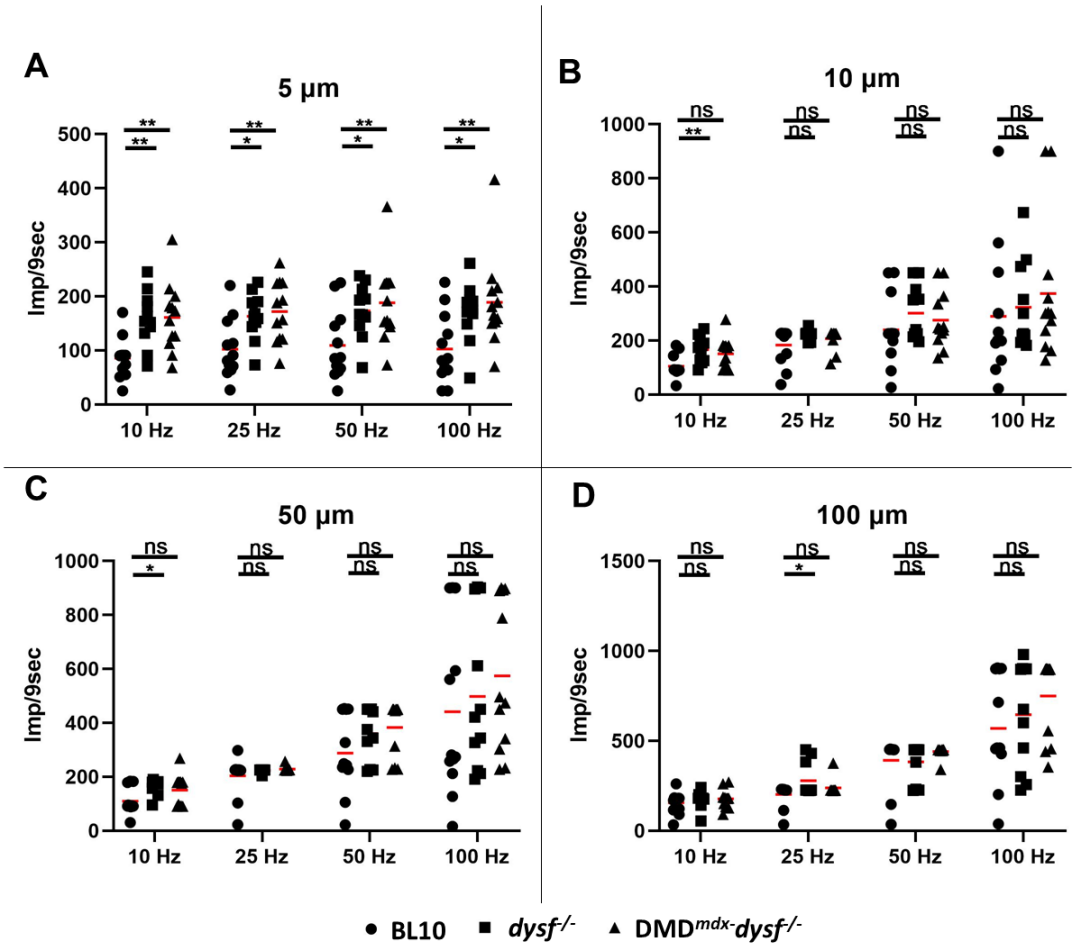

Figure 24: Muscle spindle responses to sinusoidal vibration stimuli of *dysf*$^{-/-}$ and DMD^{mdx}-*dysf*$^{-/-}$ mice compared to WT mice. *dysf*$^{-/-}$ and DMD^{mdx}-*dysf*$^{-/-}$ mice show a significantly higher firing frequency in response to small sinusoidal vibration stimuli (5 µm; A) and low frequencies (10 Hz and 25 Hz; B-D) compared to BL6 mice. Control: N=6, n=12; *dysf*$^{-/-}$: N=6, n=11; DMD^{mdx}-*dysf*$^{-/-}$: N=5, n=12; Mean is indicated as red bar; one-way ANOVA with Dunnett´s multiple comparison-test, P-values: *<0.05, **<0.01, ***<0.001, ****<0.0001.

Table 8: Mean values (in impulses per 9 sec) ± SD of the responses of muscle spindle afferents to all 16 sinusoidal vibrations from BL6, *dysf*$^{-/-}$ and DMD^{mdx}-*dysf*$^{-/-}$ mice.

	Amplitude			
Frequency	5 µm	10 µm	50 µm	100 µm
BL6				
10 Hz	85.5 ± 37.5	104,2 ± 41.4	109.3 ± 47.3	155.3 ± 57.7
25 Hz	102.4 ± 54.1	182,6 ± 67.4	204.2 ± 71.2	201.4 ± 62.1
50 Hz	109.4 ± 64.3	239,8 ± 130.5	287.8 ± 142.8	391.8 ± 142.2
100 Hz	102.8 ± 64.3	289,6 ± 242.6	440.8 ± 319.1	568.8 ± 294.0
***dysf*$^{-/-}$**				
10 Hz	158.1 ± 50.4	166.2 ± 48.5	166.2 ± 28.7	172.5 ± 45.7
25 Hz	163.0 ± 43.1	221.3 ± 17.3	223.5 ± 6.5	278.5 ± 93.1
50 Hz	173.0 ± 49.2	301.4 ± 98.6	360.5 ± 98.1	382.8 ± 102.5
100 Hz	170.4 ± 53.9	323.2 ± 160.4	498.2 ± 284.7	645.3 ± 292.5
DMD^{mdx}-*dysf*$^{-/-}$				
10 Hz	161.2 ± 63.4	150.3 ± 56.1	150.6 ± 57.3	177.0 ± 50.8
25 Hz	171.8 ± 56.7	206.8 ± 38.5	228.4 ± 9.07	237.6 ± 43.3
50 Hz	188.0 ± 73.8	275.3 ± 103.2	383.2 ± 100.1	440.3 ± 31.3
100 Hz	188.8 ± 83.9	373.6 ± 260.7	574.6 ± 278.7	749.8 ± 224.5

5.3.10 Number of muscle spindles in mouse models for muscular dystrophy

To investigate if a reduced number of muscle spindles contributes to the altered muscle spindle function in the different dystrophic mice, the exact number of muscle spindles in the M. soleus of wildtype and mutant mice was determined. My own data form DMD^{mdx}- *dysf*$^{-/-}$ mice were compared with the unpublished data from Sarah Rossmanith who analysed BL6, BL10 and DMD^{mdx}-mice. All mouse lines had approximately 10 muscle spindles per muscle (Figure 25) which agrees well with previously published results. This demonstrates that mutations in dystrophin-, utrophin- and or in the dysferlin-gene did not affect the overall number of muscle spindles per soleus muscle and that the altered muscle spindle function is likely due to other reasons. Moreover, I did not detect an additive effect of muscle spindle number in the double-transgenic mice. In other words, the degeneration of extrafusal muscle fibers is not accompanied by a similar degeneration of intrafusal fibers.

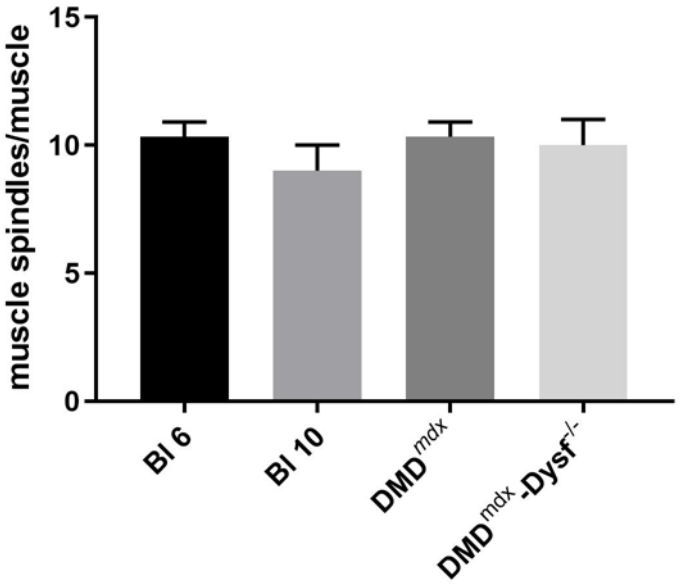

Figure 25: Number of muscle spindles in wildtype and mutant mice. No difference was observed between wildtype mice (BL6, BL10) and mutant mice (DMD^{mdx}, DMD^{mdx}-*dysf*$^{-/-}$) in soleus muscles. Results from BL6, BL10 and DMD^{mdx}-mice are unpublished data from Sarah Rossmanith. N = 3 for all mouse lines. Mean + Standard deviation; one-way ANOVA; P-values: *<0.05, **<0.01, ***<0.001, ****<0.0001. Only significant changes are indicated.

5.3.11 Tension at Lo and Lo of EDL muscles in mouse models for muscular dystrophy

To investigate if an increased tension at Lo or an increased Lo in mutant mice led to the increased action potential frequency at resting length, the tension at Lo and Lo of all mutant mice were compared with the corresponding WT data. No differences between WT and mutant mice was observed (Table 9). This result suggests that the biomechanical properties of the muscles were comparable in all mutant mouse lines.

Table 9: Mean values ± SD for Lo and Tension at Lo of EDL muscles in mouse models of muscular dystrophy and wildtype mice. N=number of EDL muscles measured.

Mutant	Lo (mm)	Tension at Lo (mN)	N
C57BL6/J	10,86 ± 0,40	3,90 ± 0,22	4
C57BL10/10sc	10,67 ± 0,08	4,00 ± 0,28	6
C57BL10/10sc/Utro	10,59 ± 0,83	4,36 ± 0,54	7
SJL-dysf C57BL/6	11,04 ± 0,23	3,88 ± 0,40	6
Dmd^{mdx}SJL-dysf C57BL/6	11,57 ± 0,33	3,96 ± 0,29	6
C57BL10/10sc/DMD^{mdx}	10,58 ± 0,31	3,83 ± 0,23	7

5.3.12 Neostigmine increases resting discharge of wildtype muscle spindles similar to mutations in dystrophin or dysferlin

One possibility to explain the changes in muscle spindle responses to stretch in dystrophic mice is the hypercontractility of extrafusal fibers described in all forms of muscular dystrophy (Cullen and Fulthorpe, 1975). To test if this hypercontractility affects not only extrafusal fibers but also intrafusal fibers, I investigated if a simulated hypercontractility induced by an increased ACh concentration, would lead to a dystrophic-like muscle spindle function. To this end, 10 µM of the AChE inhibitor neostigmine was added to the ACSF to prevent degradation of ACh through AChE. The EDL muscle in the presence of neostigmine showed spontaneous twitch contractions, suggesting an increase of the ACh concentration in extrafusal fibers.

Moreover, the hypercontractility of the dystrophic muscles is very likely due to an increased intracellular calcium concentration [Ca^{2+}] (Cullen and Fulthorpe, 1975, Millay et al., 2009, Franco and Lansman, 1990, Fong et al., 1990). To investigate if an increased intracellular [Ca^{2+}] leads to a dystrophic like hypercontractility also in intrafusal fibers, I analysed muscle spindles from WT mice before and after the administration of 20 µM nifedipine, a long- and short-acting 1,4-dihydropyridine (L-type) calcium channel blocker. Addition of nifedipine increased intracellular [Ca^{2+}] in extrafusal fibers and has been shown to affect muscle spindles in cat (Fischer and Schafer, 2002).

To investigate the function of these two drugs, I analysed individual muscle spindle afferent unit responses to a ramp-and-hold stretch (Lo plus 7.5% of Lo; ramp speed 40% Lo/sec), before and after the addition of neostigmine or nifedipine in a similar way as described for α-bungarotoxin, d-tubocurarine and hemicholinum-3. Action potential frequency were determined at four different time points before (RD) and during (DP, DI and SR) the stretch. Analysis of the overall effect of the drugs was performed by using the one-way ANOVA (factor: drug) and revealed a significant difference for RD ($P < 0.0001$), but no significant differences for DP ($P = 0.1353$), DI ($P = 0.14$) or SR ($P = 0.3519$).

For a clearer comparison of the specific effects of individual drugs, the results were expressed as Δmean, which represents the mean of the difference of the frequency (imp/sec) before compared to after drug administration. Both drugs had an effect on the resting discharge (Δmean control: 2.1 imp/sec; Δmean neostigmine: 14.4 imp/sec; Δmean nifedipine: 8.7 imp/sec; Dunnett's post hoc test relative to ACSF control: $P < 0.0001$, control vs. neostigmine; $P = 0.0367$, control vs. nifedipine; Figure 26 A). However, DP (Δmean control: -12.5 imp/sec; Δmean neostigmine: -3.4 imp/sec; Δmean nifedipine: 14.3 imp/sec; Dunnett's post hoc test relative to ACSF control: $P = 0.6601$, control vs. neostigmine; $P = 0.0921$, control vs. nifedipine; Figure 26 B), DI (Δmean control: -5.4 imp/sec; Δmean neostigmine: -9.1 imp/sec; Δmean nifedipine: 5.2 imp/sec; Dunnett's post hoc test relative

to ACSF control: P = 0.7944, control vs. neostigmine; P = 0.2426, control vs. nifedipine; Figure 26 C), and SR (Δmean control: -5.6 imp/sec; Δmean neostigmine: 9.1 imp/sec; Δmean nifedipine: 4.8 imp/sec; Dunnett's post hoc test relative to ACSF control: P = 0.2793, control vs. neostigmine; P = 0.5338, control vs. nifedipine; Figure 26 D) were not significantly different compared to the no drug control. Overall, the results demonstrate an increase of firing frequencies at resting length in the presence of neostigmine and nifedipine. Thus, both drugs had a similar effect on wildtype muscle spindles as the mutation in dystrophin and dysferlin.

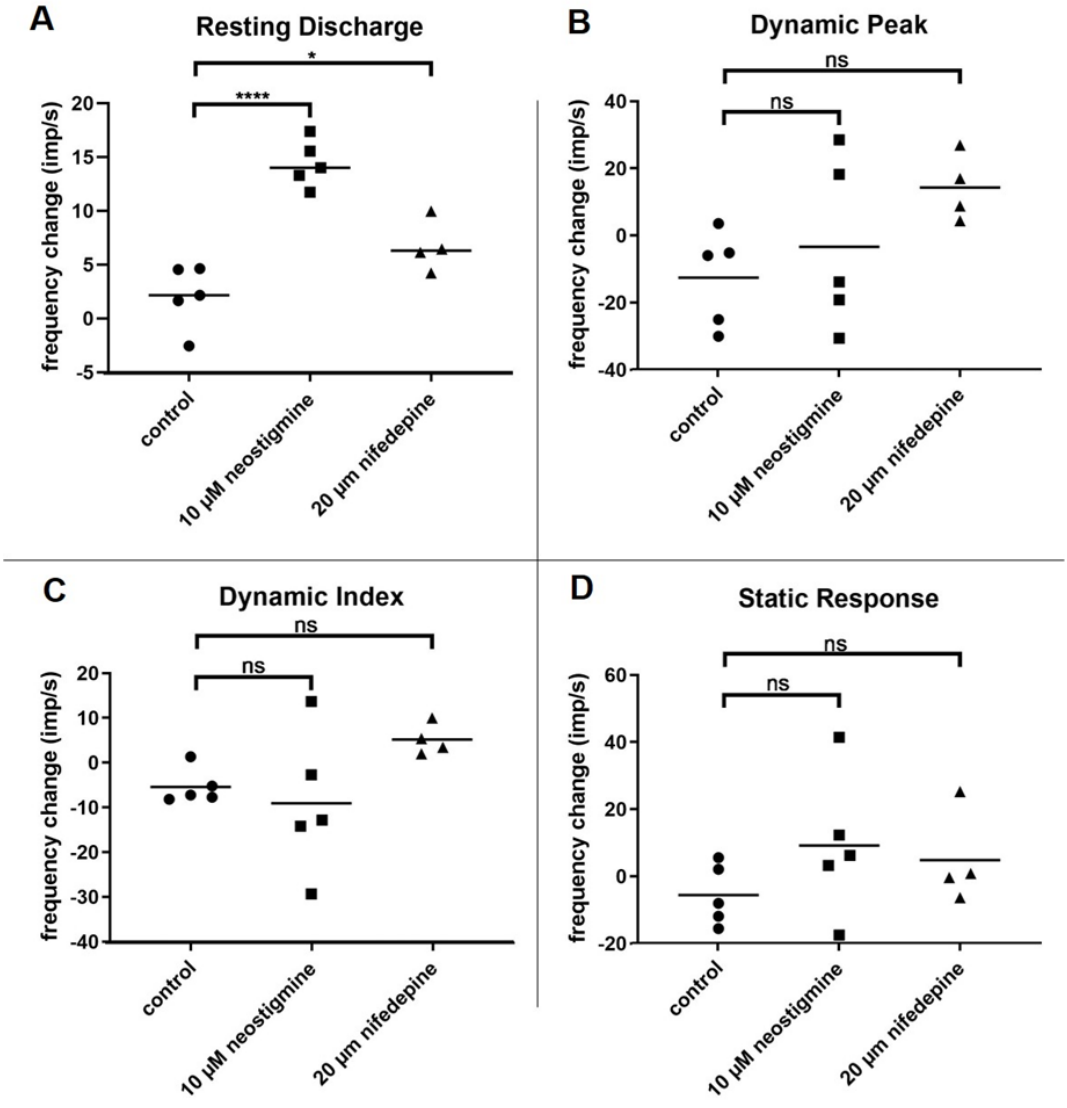

Figure 26: Change in muscle spindle response to resting length after administration of neostigmine and nifedipine. Muscle spindle firing frequency was measured before and after the addition of10 µm neostigmine or 20 µm nifedipine. The RD increased significantly (A) whereas DP (B), DI (C) and SR (D) showed no significant differences compared to the ACSF control. N=5, control, N=5 neostigmine, N=4 nifedipine; Mean is indicated by black bars. one-way ANOVA with Dunnett´s multiple comparison test, P-values: *<0.05, **<0.01, ***<0.001, ****<0.0001.

Table 10: Mean values (frequencies in imp/sec) ± SD of the responses to ramp-and-hold stretches before and after administration of ACSF (control), neostigmine or nifedipine.

	Mean (imp/sec)											
	control				10 µM neostigmine				20 µM nifedipine			
	before		after		before		after		before		after	
RD	13.0	± 6.0	15.1	± 5.8	18.3	± 4.0	30.8	± 6.6	7.3	± 2.1	11.5	± 3.8
DP	94.2	± 20.6	88.0	± 31.5	103.4	± 13.6	105.0	± 9.5	57.6	± 20.6	72.9	± 27.2
DI	37.3	± 9.3	34.2	± 11.6	55.9	± 11.9	49.8	± 16.8	25.1	± 7.4	31.7	± 7.3
SR	42.2	± 12.9	40.3	± 18.3	31.1	± 13.0	40.1	± 14.3	21.3	± 8.8	26.4	± 20.2

To investigate if the effect of both drugs is also similar when sinusoidal vibrations were used as stimulus, I applied the same 16 different vibrations to wildtype muscles in the presence and absence of nifedipine or neostigmine. I observed an increase in the firing frequency in response to sinusoidal vibration stimuli in the presence of neostigmine. Statistical analysis using the three-way ANOVA (factors: drug, amplitude and frequency) showed that the change of the frequency before and after drug addition was statistically significant for the factors drug ($P < 0.0001$) and frequency ($P = 0,0194$) but not for the factor amplitude ($P = 0.7286$).

Moreover, each of the 16 sinusoidal vibrations was analysed individually before and after drug addition with the one-way ANOVA and Dunnett's multiple comparison test. This analysis revealed that the frequency were significantly increased in the presence of neostigmine especially at small amplitudes (5 µm; Figure 27 A) and slow frequencies (10 and 25 Hz, Figure 27 B, C and D) compared to the ACSF control. Interestingly, I observed no effect of nifedipine on the response to vibrational stimuli (Figure 27 A–D), indicating that this drug affects muscle spindles in a different way, compared to neostigmine. The absolute values (imp/9 sec ± SD) for the responses to sinusoidal vibration stimuli are shown in Table 11.

Overall, neostigmine mimicked the effect of a mutation in dysferlin and dystrophin qualitatively and quantitatively during ramp-and-hold stretches as well as during sinusoidal vibration stimuli. This is consistent with the hypothesis that an altered Ca^{2+} homeostasis might be the cause for the altered resting discharge in both mutant mice.

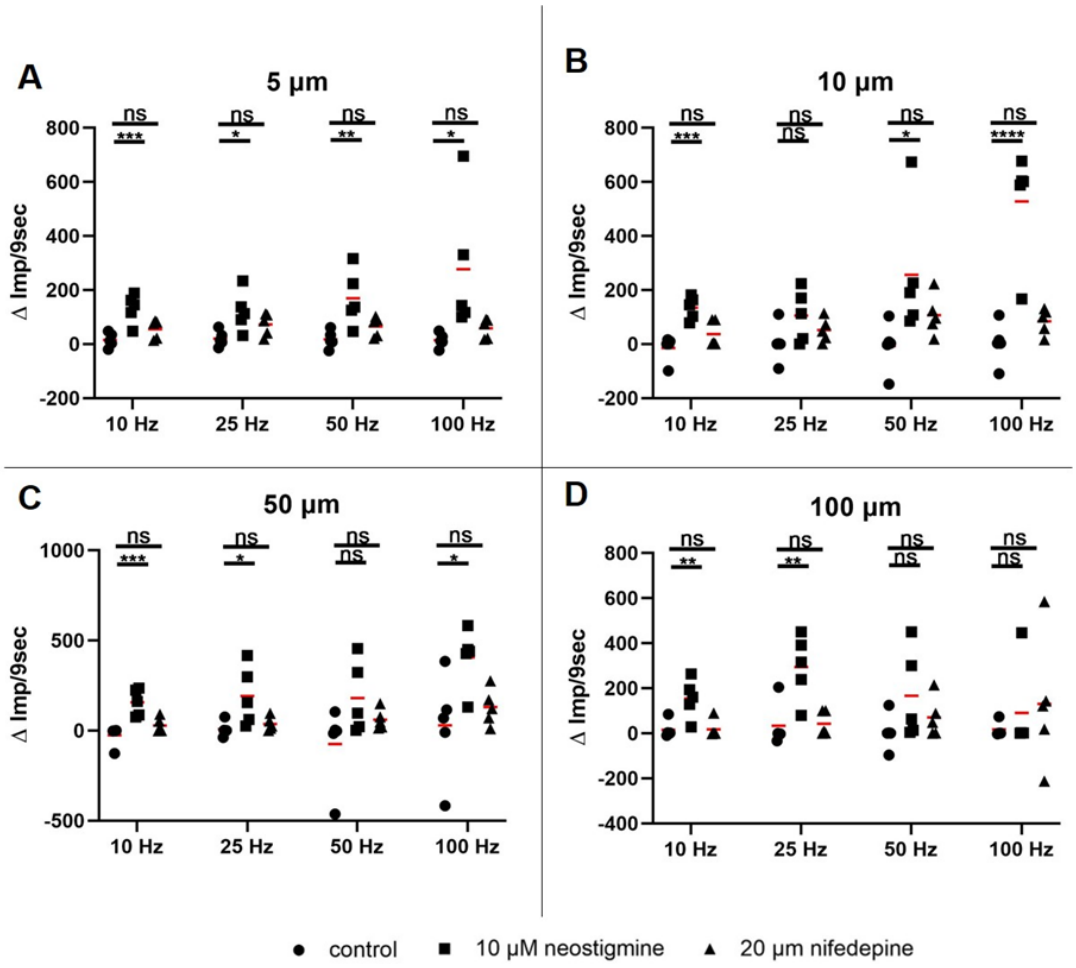

Figure 27: Response of muscle spindle sensory afferents to sinusoidal vibrations in the presence and absence of neostigmine and nifedipine. Quantification of 16 different sinusoidal vibrations (5, 25, 50 and 100 µm amplitude with each 10, 25, 50 and 100 Hz frequency). Each dot represents the difference of the impulses per 9 sec (imp/9 sec) where the values before drug (or ACSF in the case of controls) addition were subtracted from those after drug addition. An increase of firing frequencies is seen after neostigmine administration at small amplitudes (5 µm, A) and slow frequencies (10 Hz and 25 Hz, B-D). The mean is indicated as red line. One-way ANOVA (factor: drug) with Dunnett's post hoc test relative to the no drug control group, P-values: *<0.05, **<0.01, ***<0.001, ****<0.0001.

Table 11: Mean values (in impulses per 9 sec) ± SD of the responses of muscle spindle afferents to all 16 sinusoidal vibrations before and after administration of ACSF (control), neostigmine or nifedipine.

		Amplitude			
Frequency		5 µm	10 µm	50 µm	100 µm
Control					
10 Hz	before	119,5 ± 61,6	148,3 ± 80,2	155,9 ± 83,8	176,3 ± 56,7
	after	135,2 ± 49,6	133,8 ± 46,8	130,4 ± 42,7	191,6 ± 60,1
25 Hz	before	122,9 ± 65,4	207,5 ± 68,1	221,5 ± 39,1	234,5 ± 13,4
	after	143,2 ± 58,2	211,8 ± 26,4	229,4 ± 8,3	267,6 ± 76,9
50 Hz	before	125,2 ± 67,5	241,4 ± 89,6	433,2 ± 257,1	448,4 ± 71,4
	after	143,0 ± 56,3	234,4 ± 38,6	358,6 ± 79,8	454,6 ± 8,7
100 Hz	before	124,2 ± 66,9	232,8 ± 95,2	455,8 ± 239,1	887,9 ± 231,2
	after	138,8 ± 56,4	236,4 ± 43,3	484,6 ± 220,3	716,2 ± 210,8
Neostigmine					
10 Hz	before	162,2 ± 47,4	154,2 ± 37,8	154,7 ± 36,9	174,8 ± 12,5
	after	267,3 ± 58,1	260,3 ± 59,7	282,8 ± 76,4	303,5 ± 91,7
25 Hz	before	173,2 ± 42,6	209,7 ± 43,2	221,7 ± 9,3	226,2 ± 1,3
	after	269,8 ± 83,3	298,0 ± 94,9	381,5 ± 155,3	438,0 ± 219,9
50 Hz	before	179,8 ± 40,2	251,8 ± 73,3	399,0 ± 82,1	446,8 ± 8,0
	after	318,3 ± 102,1	466,7 ± 218,7	552,2 ± 209,4	588,8 ± 174,0
100 Hz	before	172,8 ± 39,1	249,0 ± 63,7	391,8 ± 88,6	815,8 ± 163,2
	after	400,3 ± 239,2	688,5 ± 278,2	733,8 ± 235,9	900,5 ± 0,5
Nifedipine					
10 Hz	before	85,5 ± 13,9	89,0 ± 2,9	90,8 ± 0,4	113,3 ± 38,5
	after	134,0 ± 43,9	135,5 ± 45,5	126,0 ± 38,4	135,3 ± 45,3
25 Hz	before	84,8 ± 18,9	141,8 ± 54,9	152,0 ± 53,7	195,5 ± 47,8
	after	154,8 ± 55,1	194,5 ± 54,0	195,5 ± 51,7	197,5 ± 48,8
50 Hz	before	87,5 ± 20,2	146,8 ± 51,7	206,0 ± 106,2	254,0 ± 117,4
	after	148,5 ± 53,6	257,0 ± 124,7	270,8 ± 126,7	319,8 ± 134,0
100 Hz	before	92,0 ± 21,5	138,8 ± 51,5	192,8 ± 85,7	376,8 ± 275,4
	after	143,3 ± 51,8	215,0 ± 92,5	337,8 ± 179,4	504,3 ± 280,6

6 Discussion

6.1 Reliability of the extracellular recordings

I established the method previously described by Wilkinson et al., (2012) to record and analyse single unit muscle spindle afferent responses to stretch. The method was used to investigate the modulatory effect of blockers of cholinergic transmission and to determine muscle spindle responses in mouse models of muscular dystrophy.

In all experiments, muscle health was ensured by comparing the maximal contractile force during a tetanic stimulation to the previously reported peak force of the EDL of 23,466 N/cm² (Larsson and Edstrom, 1986, Brooks and Faulkner, 1988). Neither the maximal force after tetanic stimulation nor the resting discharge varied significantly during the course of the recordings, suggesting that spindle afferents were not undergoing time dependent changes in firing properties and that the muscle was returning to resting length following each stretch.

To compare results between animals and to results of other species, I determined the length at which the maximum twitch contractile force was generated and set it as resting length, or Lo. In other studies muscle length was measured when knee and ankle joints were set to 90° angles (Haftel et al., 2004). The muscle length determined using this method appeared comparable to Lo (Wilkinson et al., 2012). At Lo, the majority of spindle afferents had a resting discharge and responded to an increase or a decrease in muscle length by changing their firing frequency.

To exclude the possibility that the recorded units included responses from Golgi tendon organs (type Ib fibers) or mechanosensitive group III or IV pain afferents is difficult. However, I am confident that the responses in my preparation arose from muscle spindle Ia-afferents, because Ib-afferents usually do not show a response to stretch, unless it is a very large unphysiological stretch (Houk and Henneman, 1967, Houk et al., 1971). Stretch sensitive group III or IV units show very low firing rates (0.2 imp/sec) at resting length and only slightly increase their firing rates in response to stretch (up to 1.2 imp/sec; Kindig et al., 2006). Therefore, to avoid the possibility of falsely measuring type Ib, III or IV afferents, recordings that showed no or a very low RD frequency, as well as no or a very low increase of firing rates in response to stretch, were excluded from the analysis. To further reduce the possibility of including type Ib, III or IV afferents in my analysis, only stretch sensitive signals, which showed a short pause in firing frequency after release of the stretch, the so-called time silenced, which is specific for Ia-afferents, were included in the data analysis.

In muscles of C57BL/6 mice, muscle spindle afferent responses to ramp-and-hold stretches were comparable to published data from mice (Wilkinson et al., 2012; Elahi et al., 2018; Zaytseva et al., 2018) as well as to other species (Lionikas et al., 2013).

The resting discharge in mice was similar to the reported data from Wilkinson et al., with average firing rates of 13 imp/sec in mice at room temperature (Wilkinson et al., 2012) and to cat tenuissimus spindles at 24 °C with firing rates of 13 imp/sec in primary and 20 imp/sec in secondary units at resting length (Fischer and Schafer, 1999). Moreover, comparable resting discharge frequencies at 34 °C are reported for mouse EDL (32 imp/sec; Wilkinson et al., 2012), rat soleus muscle (25 imp/sec; De-Doncker et al., 2003) and isolated cat tenuissimus spindles (25 imp/sec primary units and 38 imp/sec secondary units; Fischer and Schafer, 1999).

The static response to stretch was constant over time and did not depend on the speed of stretch. This is similar to what has been reported by Wilkinson et al. (2012) and Matthews (1963) and leads to the suggestions that once a steady state has been reached, mouse spindle afferents accurately and linearly encode the length change of a muscle stretch as well as the speed of stretching.

The dynamic response to stretch in my experimental setup was also comparable to that reported in mice and other species (Wilkinson et al., 2012, Fischer and Schafer, 1999, De-Doncker et al., 2003). Moreover, the highest firing frequency (DP) occurred during the ramp phase of a stretch and the dynamic peak as well as the dynamic index were both increased by increasing stretch length and speed. This is similar to what has been observed in mice, rats and cats

Muscle spindle afferent responses to sinusoidal vibrations were also in line with published data for mice, rats, cats and humans. The range of vibration frequency and amplitudes tested in my study demonstrated that mouse spindle afferents respond to a large dynamic range of muscle stretch. This range of firing frequency entrainment in mice was already reported by Wilkinson et al. (2012) and was observed in a similar way in cats, rats and humans (De-Doncker et al., 2003, Hunt and Ottoson, 1977, Matthews, 1964, Fallon and Macefield, 2007). These findings support the hypothesis of a common mechanosensory encoding mechanisms across vertebrate species.

In mouse, cat and frog spindles, resting spindle discharge increased with increasing temperature (Wilkinson et al., 2012, Fischer and Schafer, 1999, Ottoson, 1965). Conversely, cooling decreased firing frequencies in humans and cats (Bell and Lehmann, 1987, Michalski and Seguin, 1975). Moreover, dynamic peak, dynamic index and static response firing frequencies were higher at 34 °C compared to 24 °C in mice and cats (Wilkinson et al., 2012, Fischer and Schafer, 1999). These differences in response properties are most likely based on the fact that higher temperatures increase the rate of ion channel gating (Beam and Donaldson, 1983, Rodriguez et al., 1998) and can increase channel conductance (Peloquin et al., 2008). Therefore, room temperature was kept

constant throughout all of my experiments to avoid temperature-dependent changes in muscle spindle afferent discharge frequencies.

Weight, in particular obesity, is another factor that can influence muscle spindle firing patterns. For example, obese mice exhibit decreased muscle spindle afferent responses to muscle movement (Elahi et al., 2018). Therefore, mice with a bodyweight of more than 30 g were excluded from the experiments.

Sensory endings which innervate muscle spindles are in general classified into two types of units, primary (Ia) and secondary (II), based on their anatomical location, their functional responses to stretch and their conduction velocity (Hunt, 1954, Ruffini, 1898). So far it has not been possible to distinguish between group I and II afferents in mice by using the difference in conduction velocity (Wenk and McCleskey, 2007). Functional analyses of spindle afferent responses to stretch can generally be used to separate primary and secondary endings in humans and cats (Edin and Vallbo, 1990, Fischer and Schafer, 1999, Matthews, 1963, Cody et al., 1972), though in rats it is less clear. While Bullinger et al. report that 34 % of their stretch sensitive units were not classifiable (Bullinger et al., 2011). De-Doncker et al. reported that in de-efferented rats *in vivo*, the slope of the linear regression of the dynamic index during various stretch speeds produced a bimodal distribution of stretch sensitive units. This slope closely matched the classification based on the conduction velocity (De-Doncker et al., 2003). Wilkinson et al. (2012) did not observe a bimodal distribution of the dynamic index slope in mice at any stretch length tested. Recordings from identified spindle primary and secondary afferents may be required to generate classification criteria for unit determination in mice. Alternatively, the innervation patterns of spindle afferents during the development of rodents may explain the difficulty in unit classification. In cat, primary fibers innervate the developing muscle spindle before chain fibers have formed. In contrast the secondary endings innervate the muscle spindle at a later developmental stage. In rat, the time course for innervation is much shorter and many afferents have primary as well as secondary-like terminals or even more multiple primary units than in the cat (Banks et al., 2009). This may be an explanation for the large number of units in the rat that cannot be clearly characterised as a primary or a secondary afferent. Mouse spindle anatomy has been investigated lately and primary and secondary afferents were described (Sonner et al., 2017). However, the evidence for the presence of secondary afferent endings was not completely satisfying. Nevertheless, the non-bimodal distribution of stretch responses described by Wilkinson et al. (2012) would be consistent with the innervation pattern which was observed in rat. It was suggested that there may be no consistent way to separate units into primary and secondary by conduction velocity, instead a third hybrid afferent population may emerge with response properties characteristic for both types of afferents. Future studies are necessary to investigate the

electrophysiological differences and similarities between primary and secondary endings in mice and it remains possible that type II afferents may not exist in rodents. This would be consistent with the fact that I never recorded exclusively dynamic muscle spindle afferent responses to stretch – a feature that would be predicted if type II afferents would exist in mice – and that I never observed structures comparable to typical type II endings in my immunohistochemical analysis.

6.2 The role of the AChR at the central part of the muscle spindle (based on the publication Gerwin et al. 2019)

So far, the simultaneous presence of the fetal (γ-subunit containing AChR) and the adult (ε-subunit containing AChR) forms of the AChR have been described in the central region of intrafusal fibers at the contact site with the sensory nerve ending of the muscle spindle. Moreover, the AChR associated protein rapsyn as well as the machinery for ACh uptake in vesicles and their exocytosis have been described at the central part of the muscle spindle via immunohistochemical staining (Zhang et al., 2014) as well as glutamate containing synaptic-like vesicles (Bewick et al., 2005). Other studies described an excitatory effect of ACh and succinylcholine on muscle spindles, which might be due to a direct depolarising action on the intrafusal fibers via the γ-motoneuron endplate (for review see Carr and Proske 1996). The function of the cholinergic specialisations at the contact site between sensory neuron and intrafusal muscle fiber remained unknown. To investigate the function of these AChR at the central part of the muscle spindle, I blocked AChR ion permeability using a non-competitive (α-bungarotoxin) as well as a competitive (d-tubocurarine) antagonist while applying two different kinds of stretches, ramp-and-hold stretches and sinusoidal vibration stimuli, respectively (Gerwin et al., 2019). During both kinds of stretch protocols, the action potential frequency was increased in the presence of either drug. In contrast, no changes of the resting discharge frequency were detected. I observed a similar effect in muscle spindle sensitivity during stretch after the inhibition of the high-affinity choline uptake mechanism by using hemicholinium-3. Collectively, these results provide the first evidence for a function of AChRs in the central region of muscle spindles and suggest that ACh might modulate muscle spindle responses to stretch.

Several studies previously analysed the effects of cholinergic agonists and antagonists in muscle spindle firing behaviour (Carr and Proske, 1996). Direct application of ACh to muscle spindle for example induced a strong excitatory activity in cat soleus muscles *in vivo*, which could be blocked by d-tubocurarine. These results are probably due to a contraction of the polar regions of intrafusal muscle fibers rather than activity acting directly on sensory nerve terminals. Additionally, intravenous injections of d-tubocurarine

into anesthetised cats followed by a fusimotor stimulation resulted in a transient increase of the discharge frequency in 55 % of the cases, a decrease in the frequency in 29 % and an unchanged discharge frequency in 15 % of the cases during the first 20 minutes after d-tubocurarine administration (Smith and Albuquerque, 1967). In these and other studies summarised by Carr and Proske (1996), the drugs were either applied systemically, i.e. by intravenous infusion or stretch-evoked action potentials were not recorded. Therefore, these studies could not distinguish if the observed effects were due to an activity of neuromuscular junctions on extrafusal fibers, γ-motoneuron endplates or on AChRs in the equatorial region of intrafusal fibers (Gerwin et al., 2019). In consequence of this ambiguity, I specifically analysed the effect of antagonists instead of agonists. This excludes any influence of neuromuscular junction activity and on the fusimotor innervation of intrafusal fibers. Moreover, I analysed stretch-induced afferent changes instead of changes, induced by γ-motoneuron stimulation. Eliminating the influence of γ-motoneuron endplate activity on sensory afferents allowed for selective analysis of AChR function in the central region of muscle fibers. Additionally, I used single unit muscle spindle afferent recordings with a much higher sensitivity allowing me to detect small modulatory activities that probably have escaped detection in previous studies (Ganguly et al., 1978, Akoev, 1980).

Addition of d-tubocurarine, α-bungarotoxin or hemicholinium-3 did not change the resting discharge frequency. Since the resting discharge depends on γ-motoneuron activity (Proske et al., 1991), the results strongly suggest that neither drug directly activated fusimotor activity at γ-motoneuron endplates. Additionally, the absence of an effect of all drugs on the resting discharge level makes a potential agonistic activity of d-tubocurarine on intrafusal muscle fibers very unlikely (Takeda and Trautmann, 1984, Ziskind and Dennis, 1978). The effect of d-tubocurarine, α-bungarotoxin and hemicholinium-3 specifically on stretch-evoked responses also excludes other possible sites of action of these drugs, including the sympathetic innervation (Santini and Ibata, 1971) or nociceptive fibers (Lund et al., 2010b). Therefore, it is very likely that I examined the effect of the drugs exclusively on the AChRs that are concentrated at the contact site between intrafusal muscle fibers and proprioceptive sensory neurons.

Previous studies have proven that in addition to the AChR, the acetylcholine receptor-associated protein rapsyn is concentrated in the central region of the intrafusal muscle fibers at the contact site with the sensory neuron (Zhang et al., 2014). Sensory nerve terminals also contain the vesicular acetylcholine transporter as well as the choline acetyl transferase, the key enzyme of acetylcholine synthesis (Zhang et al., 2014). Moreover, sensory nerve terminals contain synapse-like vesicles (Bewick et al., 2005) and the molecular machinery required for their exocytosis. These include the presynaptic cytomatrix protein bassoon, the vesicle clustering protein synapsin I, and synaptophysin,

synaptotagmin, VAMP/synaptobrevin I and II, as well as syntaxin (Aguado et al., 1999, De Camilli et al., 1988, Li et al., 1996, Bewick et al., 2005, Simon et al., 2010, Zhang et al., 2014, Bewick, 2015). Functional proof of vesicle exo- and endocytosis in the sensory nerve terminal was provided by using the styryl dye FM1-43 (Banks et al., 2002, Bewick et al., 2005). The vesicle turnover was 4-fold increased in response to stretch and depended on the presence of extracellular calcium ions (Bewick et al., 2005). All together, these previously published results as well as the present study suggest that the terminals of the stretch-sensitive muscle spindle afferents have a molecular specialisation reminiscent of cholinergic synapses and incorporate the molecular machinery which is required to release vesicles.

The high-affinity choline transporter (ChT) is essential for proper signalling at cholinergic synapses due to the transporter's rate-limiting reuptake of choline which is required to sustain ACh synthesis and release (Lund et al., 2010a, Carpenter and Woodruff, 1987). At cholinergic synapses, the majority of this transporter is present on synaptic vesicles (Nakata et al., 2004). Accordingly, the treatment of neuromuscular junctions with the high-affinity choline transporter antagonist hemicholinium-3 reduced ACh levels in NMJ presynaptic vesicles (Yu and Van der Kloot, 1991). Here I demonstrate that incubation of muscle spindles with hemicholinium-3 resulted in an increase in the firing frequency during the dynamic peak and the dynamic index by about 30 % as well as to a lesser extend during the static phase. Thus, the effect of blocking AChR or inhibiting ACh release from the sensory neuron are very similar and suggest a vesicular release of ACh from sensory neurons. These results further support the hypothesis that the ACh-mediated signalling is part of a stretch-dependent modulatory feedback system which can possibly regulate muscle spindle sensitivity.

Previously Zhang et al. (2014) discussed that AChRs at the central region of intrafusal muscle fibers are very likely located in the muscle fiber plasma membrane, rather than in the sensory nerve terminal. Therefore, it appears likely that α-bungarotoxin and d-tubocurarine affect AChRs which are located there. Based on the results of the present study, I propose that some of the vesicles that are located in the sensory nerve terminal contain ACh. A stretch-dependent release of this ACh could activate AChRs in the intrafusal muscle fiber membrane directly opposite to the sensory nerve terminal. If this release is calcium-dependent (Bewick et al., 2005) and either involves the stretch-sensitive calcium channel which has been described in the sensory nerve terminal (Hunt et al., 1978, Kruse and Poppele, 1991) or the Piezo2 channel (Woo et al., 2015), remains to be determined. Since an effect of d-tubocurarine and α-bungarotoxin on firing rates of resting muscle spindles was not observed, I assume that ACh is released primarily during mechanical

activity, consistent with the stretch-induced increase in vesicle turnover (Bewick et al., 2005).

Binding of sensory neuron-derived ACh to the AChR would most likely result in a depolarisation of the intrafusal fiber. In addition, the fetal (γ-subunit-containing) as well as the adult (ε-subunit-containing) AChR have been detected in the central region of intrafusal fibers (Zhang et al., 2014). Both types of AChRs are permeable for calcium, although the adult type has a higher permeability (Grassi and Fucile, 2019). Thus, above threshold depolarisation or direct influx of calcium via the AChRs might elevate the calcium concentration in intrafusal fibers. Since nuclear bag- and nuclear chain fibers both contain a cylinder of myofilaments directly underneath the plasma membrane in their equatorial regions (Ovalle, 1972), this Ca^{2+} influx would lead to a contraction of the subsarcolemmal sarcomeres and, thus, to a contraction of the central part of the intrafusal muscle fibers. This would counteract the γ-motoneuron-mediated contraction of the polar regions and might therefore be considered a negative feedback signal. This AChR-mediated negative feedback system could be a control system modulating the stretch-induced muscle spindle afferent firing rate to reduce the potential damage to the central region of intrafusal fibers caused for example by excessive contraction of the polar regions. Alternatively, the contraction in the central part of intrafusal fibers might lead to a lengthening of the polar regions, thereby enabling the subsequent γ-motoneuron-mediated contraction of this part of the intrafusal fiber. In any case, these results strengthen the hypothesis that in addition to the afferent activity of proprioceptive neurons, their terminals might have synapse-like functions and thus, have efferent activity as well.

A termination of the AChR activation could be mediated by acetylcholinesterase (AChE), although there have been conflicting results regarding the presence of this enzyme at the central region of intrafusal muscle fibers (Giacobini, 1959, Schober and Thomas, 1978, Zhang et al., 2014). Alternatively, a long-lasting presence of ACh, due to the absence of AChE in the equatorial part of intrafusal muscle fibers, might generate a background intrafusal fiber tone, counteracting the mechanical tension generated by the fusimotor activity in the polar regions.

Proprioceptive sensory afferents have been shown to contain glutamate-filled synapse-like vesicles, suggesting that they might release glutamate. This glutamate could, via an unusual phospholipase D-linked metabotropic glutamate receptor that is located within the sensory nerve terminal, modulate the stretch-induced sensory afferent excitability (Bewick, 2015, Bewick et al., 2005, Simon et al., 2010, Bewick and Banks, 2015). The results from my study suggest that ACh has very likely a different effect. In contrast to glutamate, ACh possibly modulates the stretch-induced response via the nicotinic AChR in the intrafusal muscle fiber plasma membrane. Moreover, ACh is likely to act as a negative

feedback mechanism, reducing stretch-induced sensitivity. These results certainly do not exclude the possibility that mechanical activity releases glutamate- as well as ACh-containing vesicles and that both modulate the sensitivity of the proprioceptive sensory neuron responses to stretch.

6.3 Increased resting discharge in murine models for muscular dystrophy

An impaired muscle spindle function contributes to several neurodegenerative and neuromuscular diseases (Blecher et al., 2018; for review see Kröger, 2018). An example for neuromuscular diseases are muscular dystrophies, a heterogeneous group of hereditary myogenic disorders. Since extrafusal and intrafusal fibers are very similar in several aspects, including structure, ATPase or myosin subgroups (Yellin, 1969, Ovalle, 1972) I tested the hypothesis if intrafusal fibers and muscle spindle function are similarly affected as extrafusal fibers in mouse models for muscular dystrophies. To this end, I analysed muscle spindle afferent responses to ramp-and-hold stretches as well as to sinusoidal vibrations in three mouse models for muscular dystrophies. I show that proprioceptive sensory afferents from all three different dystrophic mouse lines with mutations in different genes and different molecular mechanisms for the muscle degeneration have a qualitatively and quantitatively similar increase in the resting discharge frequency and in the response to sinusoidal vibrations. I also show that the response to ramp and hold stretches were not affected by the mutations, as was the overall structure and the total number of muscle spindles. My results demonstrate that intrafusal fibers are less affected by the degenerative events compared to extrafusal fibers and that muscle spindles from dystrophic mice have functional deficits. Moreover, they represent the first description of a possible contribution of muscle spindles to the unstable gait and frequent falls observed in patients with muscular dystrophy.

Three different mouse models for muscular dystrophy were used in this study: the DMD^{mdx}-mouse, the SJL-Dysf$^{-/-}$ mouse and the DMD^{mdx}-*dysf*$^{-/-}$ mouse line. The *utro*$^{-/-}$ line was used to control for unspecific loss of function effects due to mutations in proteins expressed in skeletal muscle tissue. The DMD^{mdx}-mouse is a well-characterised mouse-model for DMD, the most common and severe form of muscular dystrophy (Bulfield et al., 1984, Chamberlain et al., 2007, Connolly et al., 2001, Messina et al., 2006, Raymackers et al., 2003). Mutations in dystrophin affect the mechanical stability of muscle fibers, rendering them mechanically labile, so that the sarcolemmal membrane has a higher susceptibility to damage particularly during contraction (Waite et al., 2009). Despite the less severe phenotype of DMD^{mdx}-mice compared to DMD patients, this mouse model is recommended as the model of choice for preclinical tests and proof-of-concept studies (Willmann et al., 2009).

The SJL-Dysf$^{-/-}$ mouse is a model for dysferlinopathies, another form of muscular dystrophy with a completely different molecular origin. This mouse develops a mild, progressive myopathy (Bittner et al., 1999) due to a 171-bp deletion in the *DYSF* gene (Vafiadaki et al., 2001) and a reduction of 75 % in dysferlin expression compared to wild type mice. Despite the residual 25 % of dysferlin histological changes observed in these mice display many of the features seen in the corresponding patients (Hornsey et al., 2013).

The DMD^{mdx}-*dysf*$^{-/-}$ double transgenic mouse is a cross breading of the DMD^{mdx} and the *dysf*$^{-/-}$ mouse. This mouse model exhibits a more severe muscle pathology than either DMD^{mdx}-mice or *dysf*$^{-/-}$ mice and the onset of the muscle pathology occurs much earlier than in *dysf*$^{-/-}$ mice. These mice show a greater number of regenerating muscle fibers, higher serum creatine kinase levels and elevated Evans blue dye uptake into skeletal muscles compared to either DMD^{mdx} or *dysf*$^{-/-}$ mice. (Han et al., 2011).

The three mouse models for muscular dystrophy were analysed with respect to muscle spindle morphology and muscle spindle function. DMD^{mdx}- and *utro*$^{-/-}$ mice are bred on a BL10 background whereas the *dysf*$^{-/-}$ and DMD^{mdx}-*dysf*$^{-/-}$ mice had a BL6 background. Data from mice with different genetic background are not always comparable since they differ in various details (Lionikas et al., 2013). However, the morphology as well as the function of muscle spindles were similar if not identical between the BL6 and BL10 mice (probably due to their close genetic relationship). Nevertheless, I cannot rule out the possibility that very minor differences are due to a different genetic background of the mice and not due to an altered muscle spindle function.

In a previous study, the distribution of dystrophin-deficient segments alternating with positive-stained domains along the sarcolemma in the central part of intrafusal fibers has been reported (Nahirney and Ovalle, 1993). I confirmed this finding using a different anti-dystrophin antibody and additionally show that other components of the DGC are similarly subcellularly concentrated in the same segments of the sarcoplasmic membrane. These segments coextend with the parts of intrafusal fibers that are in direct contact with the basal lamina (Maier and Mayne, 1995). In contrast, the intrafusal fiber plasma membrane is separated from the basal lamina by the sensory nerve terminal in the DGC-deficient segments. Thus, it is tempting to speculate that the DGC in intrafusal fibers is stabilised in the regions between the sensory nerve terminals by the direct contact to the extracellular matrix. The absence of dystrophin and β-dystroglycan immunoreactivity in the contact region between the sensory neuron and the intrafusal fiber also suggests that the DGC is not directly involved in the mechanotransduction process but instead is more likely to provide a mechanical link between intrafusal fiber plasma membrane and the basal lamina. It remains to be shown if the DGC is actively excluded from the sensory neuron to the

intrafusal fiber contact zone or if it is selectively stabilised in regions where intrafusal fibers have contact to the basal lamina.

Several studies have previously analysed the effect of muscular dystrophy on extrafusal fibers in humans and mice (Barohn et al., 1998, Barohn et al., 1991, Emery, 1993, Galassi et al., 1987, Meryon, 1852, Rosales et al., 2010). Due to a reduced mechanical stability of skeletal muscle fibers or a limited membrane repair, extrafusal fibers degenerate and subsequently, due to satellite cell proliferation and differentiation, regenerate (Anderson et al., 1999, Kunkel et al., 1985, Ray et al., 1985). These (vicious) cycles of degeneration and regeneration lead to the diagnostic hallmarks of muscular dystrophy, including variable fiber diameter, centralised nuclei and an increase of connective tissue infiltration between muscle fibers (Grounds and Torrisi, 2004, Messina et al., 2006).

Analysis of muscle tissue from DMD patients has revealed conflicting results regarding the overall morphology of muscle spindles. Some studies reported that muscle spindle morphology in post mortem muscle tissue was slightly atrophic and that due to the loss of intrafusal fibers and due to a reduced intrafusal fiber diameter, the periaxial space was increased and the connective tissue capsule was widened (Kararizou et al., 2007, Swash and Fox, 1976). In contrast, other studies, analysing intrafusal fibers in biopsy material from patients, showed a normal diameter and an unaltered thickness of the connective tissue capsule (Cazzato and Walton, 1968, Skuk et al., 2010). It is therefore possible, that the morphological changes observed in the first two studies were not a direct consequence of the mutation but instead caused by secondary effects, including age, immobilisation or post-mortem tissue autolysis. In any case, compared to extrafusal fibers, intrafusal fibers and muscle spindle function appear much less affected by the mutation. This is consistent with my finding that in the DMD^{mdx}-mouse, the morphological changes appeared to be considerably less pronounced compared to those described for extrafusal fibers as well as with previous studies (Gossrau and Grozdanovic, 1997, Johnson and Ovalle, 1986, Nahirney and Ovalle, 1993, Ovalle and Dow, 1986).

I observed no centrally localised nuclei and no apparent degeneration of intrafusal fibers or a reduction in the total number of muscle spindles per soleus muscle. Likewise, the distribution and intensity of the vGluT1 immunoreactivity in the central region of intrafusal fibers was not apparently different in muscle spindles from the various dystrophic mice. One potential explanation for the mild phenotypic effect might be that intrafusal fibers have a much smaller mechanical burden and are thus less likely to suffer from mechanical damage. An additional possibility is suggested by the finding from Sara Rossmanith (unpublished data) that utrophin expression was severely upregulated in the DMD^{mdx}-mice. Utrophin is an autosomally encoded homologue of dystrophin which shares more than 80% amino acid sequence similarity to dystrophin, has a very similar domain structure and like

dystrophin can interact with actin filaments and with β-dystroglycan (Tinsley et al., 1992). In skeletal muscle, utrophin is highly expressed in fetal and regenerating muscle fibers (Khurana et al., 1991, Lin et al., 1998). In adult wildtype muscle fibers, utrophin is replaced by dystrophin along the entire sarcolemmal membrane but remains present at the neuromuscular junction, the myotendenous junction and blood vessels (Nguyen et al., 1991, Ohlendieck et al., 1991, Schofield et al., 1993). In DMD^{mdx}-mice, utrophin is severely upregulated in extrafusal fibers and can be found along the entire sarcolemma (Keep, 2000). The passive stiffness of the EDL and the soleus muscle is slightly different in *utro*$^{-/-}$ mice compared to wildtype mice (Rajaganapathy et al., 2019). However, several studies have demonstrated that utrophin overexpression can lessen or even prevent the dystrophic phenotype in DMD^{mdx}-mice and muscular dystrophy patients (Amenta et al., 2011, Gilbert et al., 1999, Guiraud et al., 2019, Krag et al., 2004, Tinsley et al., 1998, Tinsley et al., 2011). I therefore suggest that a similar functional compensation occurs endogenously in intrafusal fibers, resulting in a less severe phenotype in DMD^{mdx}-mice. In contrast, utrophin is only slightly increased in human MD patients at the sarcolemma of regenerating extrafusal fibers as part of the repair process and their regeneration (Guiraud et al., 2019, Helliwell et al., 1992). Likewise, intrafusal fibers in DMD patients do not apparently upregulate utrophin expression (Skuk et al., 2010), predicting more severe functional deficits in human muscle spindles compared to those from DMD^{mdx}-mice.

Muscle spindle afferent responses to stretch from all three mouse strains with muscular dystrophy were, despite the extensive differences between *dysf*$^{-/-}$ and DMD^{mdx} mice, strikingly similar affected. All showed an increase in the resting discharge and an altered response to sinusoidal vibrations particularly at small amplitudes but no change in the response to ramp-and-hold stretches. Moreover, there was no additive effect in double transgenic mice and no change in the distribution of dystrophin in *dysf*$^{-/-}$ mice, suggesting that both mutations phenotypically converge onto a common intracellular signaling mechanism.

The molecular mechanism underlying the increase in the resting discharge in dystrophic muscles is unclear. After shortening, muscle spindles fall silent, but the original resting discharge frequency is gradually reached again after several seconds. In cat soleus muscle, an early recovery could be induced by stimulating static- but not dynamic β-motoneurons suggesting that the resting discharge frequency in cat muscle spindles is primarily mediated by Bag2 fibers (Proske et al., 1991). Thus, a selective effect of the mutations on Bag2 fibers could be one way to explain the increased resting discharge. I did not observe a difference in the distribution of dystrophin or β-dystroglycan in wildtype or dystrophic mice between nuclear bag and nuclear chain fibers. Nor did Sarah Rossmanith observe a difference in the distribution of utrophin in wildtype or dystrophic mice between

nuclear bag and nuclear chain fibers, suggesting that the mutations in these proteins are unlikely to selectively affect Bag2 intrafusal fibers. However, I cannot exclude an effect of the mutations on the viscoelastic properties specifically of Bag2 fibers.

The only similarity between these groups are the dystrophic changes of the extrafusal fibers, suggesting that this could be the reason for the altered muscle spindle function observed in all three mouse models. One of the first symptoms of muscular dystrophies is the hypercontractility of the skeletal muscles (Cullen and Fulthorpe, 1975). To simulate an increased contraction of intrafusal as well as extrafusal fibers, the ACh concentration was increased by incubating the EDL muscle with neostigmine, an AChE inhibitor. ACh can be released tonically or phasically from the presynapse into the synaptic cleft after an action potential arrives at the presynaptic terminal. Additionally, due to the muscle dissection for the experiment, ACh could leak from damaged muscles surrounding the EDL into the bathing solution and increase the ACh concentration over time. Electrophysiological analyses were performed at least half an hour after the first twitch contractions of the muscle were observed, indicating a complete diffusion of neostigmine into the muscle. After drug administration muscle spindle RD increased, whereas the DP, DI and SR remained unchanged, leading to the same changes in muscle spindle function as observed in dystrophic mice during ramp-and-hold stretches as well as during sinusoidal vibrations. These results are in line with previously reported results from Ganguly et al. (1978) using physostigmine, another AChE inhibitor, in rats (Ganguly et al., 1978).

The hypercontractility in muscular dystrophy could be due to a change in the intracellular calcium ion concentration [Ca^{2+}]. Several studies have shown an abnormal calcium ion homeostasis in extrafusal fibers in murine models of both types of muscular dystrophies (Flix et al., 2013, Franco and Lansman, 1990, Kerr et al., 2013, Klinge et al., 2010, Turner et al., 1993, Turner et al., 1988, Mallouk et al., 2000, Robert et al., 2001, Vandebrouck et al., 2002). An increase of intracellular calcium concentration via calcium leak channels (Fong et al., 1990, Franco and Lansman, 1990, Millay et al., 2009) and shorter calcium channels close times in dystrophic muscles of mice and humans (Franco and Lansman, 1990) have been reported. This results in an increase of the intracellular calcium concentration in myotubes, resulting in hypercontractility of the muscle fiber (Fong et al., 1990). Moreover, Millay et al. (2009) showed that a dystrophic-like phenotype similar to the one observed in DMD^{mdx}-mice can be induced when TRPC3 channels, very likely the calcium leak channel, were overexpressed in wildtype muscle tissue (Millay et al., 2009). Dysferlin is localised in the t-tubule membrane and physically associated with the dihydropyridine receptor and several other proteins involved in Ca^{2+}-based signalling (Ampong et al., 2005, Kerr et al., 2013, Klinge et al., 2010, Matsuda et al., 2001, de Morree et al., 2010, Waddell et al., 2011,). In addition, blocking of L-type Ca^{2+} channels using

diltiazem improves the recovery of *dysf*$^{-/-}$ muscle fibers from injury (Kerr et al., 2013). Collectively, these results suggest that calcium ions might play a pivotal role in the etiology of the dystrophic phenotype in extrafusal fibers from both mouse strains.

I tested this hypothesis by recording muscle spindle Ia afferents in the presence and absence of nifedipine. Nifedipine is a long- and short-acting 1,4-dihydropyridine (L-type) calcium channel blocker. However, an excitatory effect of low concentrations of nifedipine on extrafusal and intrafusal fibers of cats and frogs was described previously and suggests that nifedipine could promote the contractility of skeletal muscle fibers through a yet unknown mechanism (Fischer and Schafer, 2002, Neuhaus et al., 1990). After drug administration RD increased significantly whereas DP, DI and SR showed no statistically significant difference compared to the no drug control. Thus, I observed similar changes in muscle spindle function as in experiments with an increased ACh-concentration as well as in dystrophic mice. On the contrary no changes were observed during sinusoidal vibrations.

Overall, my results show that muscle spindle function is altered in mouse models of muscular dystrophy. In line with these findings, I hypothesize that an elevated cytosolic [Ca^{2+}] under resting conditions as the mechanistic link between the genetic defect and the dystrophic phenotype in muscle spindles from the tested mouse models of muscular dystrophy. An increased Ca^{2+} concentration in intrafusal fibers would presumably lead to a contraction in the polar regions. This would exert stretch in the central region causing an elevated discharge frequency of the proprioceptive sensory neuron. It will therefore be interesting to investigate, if the intracellular [Ca^{2+}] concentration is elevated and if the Ca^{2+} homeostasis is perturbed in both dystrophic mouse lines.

Postural abnormalities have been reported previously in patients with muscular dystrophy of the Duchenne type and in dysferlinopathies (Hsu and Furumasu, 1993, Pradhan et al., 2006, Mahjneh et al., 2001). In general, muscular dystrophy patients suffer from sudden spontaneous falls, balance problems, as well as gait and posture abnormalities (Barrett et al., 1988) or kinematic and mechanical deficits as well as a peripheral areflexia (Fukuda et al., 1999, Umakhanova et al., 2017). Some of these symptoms can certainly be attributed to the muscle weakness. However, a disturbance in proprioception may also contribute to the impaired postural control in these patients. Analyses of the perception of body segment movement and control of posture in patients suffering from various types of muscular dystrophy failed to reveal differences between MD patients and healthy subjects (Ribot-Ciscar et al., 2004). Both the MD patients and healthy subjects perceived passive movements and experienced sensations of illusory movement induced by vibratory stimulation applied to muscle tendons, suggesting that muscle spindles are still responsive to vibratory stimulation and that proprioception in general might be spared in MD patients (Ribot-Ciscar et al., 2004). Moreover, the effects of reinforcement manoeuvres that are

known to increase muscle spindle sensitivity via fusimotor drive in healthy subjects were unaltered in MD patents, suggesting that the intrafusal muscle fibers preserve their contractile abilities in slowly progressive MDs (Aimonetti et al., 2005). My results of an unaltered dynamic and static response to stretch in DMD^{mdx}-mice is in agreement with these studies. However, I observed a strong increase in the resting discharge of muscle spindle afferents. It is unclear how much this increase in the afferent discharge frequency affects conscious proprioception, since muscle spindle afferent information is highly processed in the central nervous system (Proske and Gandevia, 2012, Proske and Gandevia, 2018). However, the increased resting discharge frequency could directly feed back on skeletal muscle tissue via the monosynaptic stretch reflex. An increased resting discharge is likely to cause an increase in the muscle tone in the patients. This would probably not only cause postural problems but also enhance the degeneration of extrafusal fibers.

Therefore, muscle spindle activity might contribute to the instable gait and the increased frequency of falling in patients with muscular dystrophy. Since frequent falls often lead to injuries which are more severe in patients with muscular dystrophy and often cause hospitalisation, I would therefore propose to include proprioceptive training into the clinical treatment of DMD patients – at least during the time while they are still able to walk.

References

AGUADO, F., MAJO, G., RUIZ-MONTASELL, B., LLORENS, J., MARSAL, J. & BLASI, J. 1999. Syntaxin 1A and 1B display distinct distribution patterns in the rat peripheral nervous system. *Neuroscience,* 88**,** 437-46.

AIMONETTI, J. M., RIBOT-CISCAR, E., ROSSI-DURAND, C., ATTARIAN, S., POUGET, J. & ROLL, J. P. 2005. Functional sparing of intrafusal muscle fibers in muscular dystrophies. *Muscle Nerve,* 32**,** 88-94.

AKOEV, G. N. 1980. Catecholamines, acetylcholine and excitability of mechanoreceptors. *Prog Neurobiol,* 15**,** 269-94.

ALLIKIAN, M. J. & MCNALLY, E. M. 2007. Processing and assembly of the dystrophin glycoprotein complex. *Traffic,* 8**,** 177-83.

AMENTA, A. R., YILMAZ, A., BOGDANOVICH, S., MCKECHNIE, B. A., ABEDI, M., KHURANA, T. S. & FALLON, J. R. 2011. Biglycan recruits utrophin to the sarcolemma and counters dystrophic pathology in mdx mice. *Proc Natl Acad Sci U S A,* 108**,** 762-7.

AMPONG, B. N., IMAMURA, M., MATSUMIYA, T., YOSHIDA, M. & TAKEDA, S. 2005. Intracellular localization of dysferlin and its association with the dihydropyridine receptor. *Acta Myol,* 24**,** 134-44.

ANDERSON, L. V., DAVISON, K., MOSS, J. A., YOUNG, C., CULLEN, M. J., WALSH, J., JOHNSON, M. A., BASHIR, R., BRITTON, S., KEERS, S., ARGOV, Z., MAHJNEH, I., FOUGEROUSSE, F., BECKMANN, J. S. & BUSHBY, K. M. 1999. Dysferlin is a plasma membrane protein and is expressed early in human development. *Hum Mol Genet,* 8**,** 855-61.

AOKI, M., LIU, J., RICHARD, I., BASHIR, R., BRITTON, S., KEERS, S. M., OELTJEN, J., BROWN, H. E., MARCHAND, S., BOURG, N., BELEY, C., MCKENNA-YASEK, D., ARAHATA, K., BOHLEGA, S., CUPLER, E., ILLA, I., MAJNEH, I., BAROHN, R. J., URTIZBEREA, J. A., FARDEAU, M., AMATO, A., ANGELINI, C., BUSHBY, K., BECKMANN, J. S. & BROWN, R. H., JR. 2001. Genomic organization of the dysferlin gene and novel mutations in Miyoshi myopathy. *Neurology,* 57**,** 271-8.

ASHRAFI, S., LALANCETTE-HEBERT, M., FRIESE, A., SIGRIST, M., ARBER, S., SHNEIDER, N. A. & KALTSCHMIDT, J. A. 2012. Wnt7A identifies embryonic gamma-motor neurons and reveals early postnatal dependence of gamma-motor neurons on a muscle spindle-derived signal. *J Neurosci,* 32**,** 8725-31.

AUERBACH, A. 2015. Activation of endplate nicotinic acetylcholine receptors by agonists. *Biochem Pharmacol,* 97**,** 601-608.

BANKS, R. W. 1986. Observations on the primary sensory ending of tenuissimus muscle spindles in the cat. *Cell Tissue Res,* 246**,** 309-19.

BANKS, R. W. 1994a. Intrafusal motor innervation: a quantitative histological analysis of tenuissimus muscle spindles in the cat. *J Anat,* 185 (Pt 1)**,** 151-72.

BANKS, R. W. 1994b. The motor innervation of mammalian muscle spindles. *Prog Neurobiol,* 43**,** 323-62.

BANKS, R. W. 2015. The innervation of the muscle spindle: a personal history. *J Anat,* 227**,** 115-35.

BANKS, R. W., BARKER, D. & STACEY, M. J. 1982. Form and distribution of sensory terminals in cat hindlimb muscle spindles. *Philos Trans R Soc Lond B Biol Sci,* 299**,** 329-64.

BANKS, R. W., BEWICK, G. S., REID, B. & RICHARDSON, C. 2002. Evidence for activity-dependent modulation of sensory-terminal excitability in spindles by glutamate release from synaptic-like vesicles. *Adv Exp Med Biol,* 508**,** 13-8.

BANKS, R. W., HULLIGER, M., SAED, H. H. & STACEY, M. J. 2009. A comparative analysis of the encapsulated end-organs of mammalian skeletal muscles and of their sensory nerve endings. *J Anat,* 214**,** 859-87.

BAROHN, R. J., AMATO, A. A. & GRIGGS, R. C. 1998. Overview of distal myopathies: from the clinical to the molecular. *Neuromuscul Disord,* 8**,** 309-16.

BAROHN, R. J., MILLER, R. G. & GRIGGS, R. C. 1991. Autosomal recessive distal dystrophy. *Neurology,* 41**,** 1365-70.

BARRETT, R., HYDE, S. A., SCOTT, O. M. & DUBOWITZ, V. 1988. Changes in center of gravity in boys with Duchenne muscular dystrophy. *Muscle Nerve,* 11**,** 1157-63.

BASHIR, R., BRITTON, S., STRACHAN, T., KEERS, S., VAFIADAKI, E., LAKO, M., RICHARD, I., MARCHAND, S., BOURG, N., ARGOV, Z., SADEH, M., MAHJNEH, I., MARCONI, G., PASSOS-BUENO, M. R., MOREIRA EDE, S., ZATZ, M., BECKMANN, J. S. & BUSHBY, K. 1998. A gene related to Caenorhabditis elegans spermatogenesis factor fer-1 is mutated in limb-girdle muscular dystrophy type 2B. *Nat Genet,* 20**,** 37-42.

BEAM, K. G. & DONALDSON, P. L. 1983. A quantitative study of potassium channel kinetics in rat skeletal muscle from 1 to 37 degrees C. *J Gen Physiol,* 81**,** 485-512.

BELL, K. R. & LEHMANN, J. F. 1987. Effect of cooling on H- and T-reflexes in normal subjects. *Arch Phys Med Rehabil,* 68**,** 490-3.

BEWICK, G. S. 2015. Synaptic-like vesicles and candidate transduction channels in mechanosensory terminals. *J Anat,* 227**,** 194-213.

BEWICK, G. S. & BANKS, R. W. 2015. Mechanotransduction in the muscle spindle. *Pflugers Arch,* 467**,** 175-90.

BEWICK, G. S., REID, B., RICHARDSON, C. & BANKS, R. W. 2005. Autogenic modulation of mechanoreceptor excitability by glutamate release from synaptic-like vesicles: evidence from the rat muscle spindle primary sensory ending. *J Physiol,* 562**,** 381-94.

BHATTACHARYYA, B., SOKOLL, M. D., CANNON, J. G. & LONG, J. P. 1988. Neuromuscular blocking action of two hemicholinium-3 analogs. *Eur J Pharmacol,* 146**,** 155-65.

BITTNER, R. E., ANDERSON, L. V., BURKHARDT, E., BASHIR, R., VAFIADAKI, E., IVANOVA, S., RAFFELSBERGER, T., MAERK, I., HOGER, H., JUNG, M., KARBASIYAN, M., STORCH, M., LASSMANN, H., MOSS, J. A., DAVISON, K., HARRISON, R., BUSHBY, K. M. & REIS, A. 1999. Dysferlin deletion in SJL mice (SJL-Dysf) defines a natural model for limb girdle muscular dystrophy 2B. *Nat Genet,* 23**,** 141-2.

BLECHER, R., HEINEMANN-YERUSHALMI, L., ASSARAF, E., KONSTANTIN, N., CHAPMAN, J. R., COPE, T. C., BEWICK, G. S., BANKS, R. W. & ZELZER, E. 2018. New functions for the proprioceptive system in skeletal biology. *Philos Trans R Soc Lond B Biol Sci,* 373.

BLECHER, R., KRIEF, S., GALILI, T., ASSARAF, E., STERN, T., ANEKSTEIN, Y., AGAR, G. & ZELZER, E. 2017a. The Proprioceptive System Regulates Morphologic Restoration of Fractured Bones. *Cell Rep,* 20**,** 1775-1783.

BLECHER, R., KRIEF, S., GALILI, T., BITON, I. E., STERN, T., ASSARAF, E., LEVANON, D., APPEL, E., ANEKSTEIN, Y., AGAR, G., GRONER, Y. & ZELZER, E. 2017b. The Proprioceptive System Masterminds Spinal Alignment: Insight into the Mechanism of Scoliosis. *Dev Cell,* 42**,** 388-399 e3.

BROOKS, S. V. & FAULKNER, J. A. 1988. Contractile properties of skeletal muscles from young, adult and aged mice. *J Physiol,* 404**,** 71-82.

BROWN, M. C., ENGBERG, I. & MATTHEWS, P. B. 1967. The relative sensitivity to vibration of muscle receptors of the cat. *J Physiol,* 192**,** 773-800.

BULFIELD, G., SILLER, W. G., WIGHT, P. A. & MOORE, K. J. 1984. X chromosome-linked muscular dystrophy (mdx) in the mouse. *Proc Natl Acad Sci U S A,* 81**,** 1189-92.

BULLINGER, K. L., NARDELLI, P., WANG, Q., RICH, M. M. & COPE, T. C. 2011. Oxaliplatin neurotoxicity of sensory transduction in rat proprioceptors. *J Neurophysiol,* 106**,** 704-9.

CARPENTER, F. G. & WOODRUFF, C. R. 1987. Blockade and recovery of cholinergic transmission in rats treated with hemicholinium 3. *Eur J Pharmacol,* 141**,** 179-86.

CARR, R. W. & PROSKE, U. 1996. Action of cholinesters on sensory nerve endings in skin and muscle. *Clin Exp Pharmacol Physiol,* 23**,** 355-62.

CAZZATO, G. & WALTON, J. N. 1968. The pathology of the muscle spindle. A study of biopsy material in various muscular and neuromuscular diseases. *J Neurol Sci,* 7**,** 15-70.

CHAMBERLAIN, J. S., METZGER, J., REYES, M., TOWNSEND, D. & FAULKNER, J. A. 2007. Dystrophin-deficient mdx mice display a reduced life span and are susceptible to spontaneous rhabdomyosarcoma. *FASEB J,* 21**,** 2195-204.

CHAN, Y. M., BONNEMANN, C. G., LIDOV, H. G. & KUNKEL, L. M. 1998. Molecular organization of sarcoglycan complex in mouse myotubes in culture. *J Cell Biol,* 143**,** 2033-44.

CHANG, N. C., CHEVALIER, F. P. & RUDNICKI, M. A. 2016. Satellite Cells in Muscular Dystrophy - Lost in Polarity. *Trends Mol Med,* 22**,** 479-496.

CHYATTE, S. B., VIGNOS, P. J., JR. & WATKINS, M. 1966. Early muscular dystrophy: differential patterns of weakness in duchenne, limb-girdle and facioscapulohumeral types. *Arch Phys Med Rehabil,* 47**,** 499-503.

CODY, F. W., LEE, R. W. & TAYLOR, A. 1972. A functional analysis of the components of the mesencephalic nucleus of the fifth nerve in the cat. *J Physiol,* 226**,** 249-61.

CONNOLLY, A. M., KEELING, R. M., MEHTA, S., PESTRONK, A. & SANES, J. R. 2001. Three mouse models of muscular dystrophy: the natural history of strength and fatigue in dystrophin-, dystrophin/utrophin-, and laminin alpha2-deficient mice. *Neuromuscul Disord,* 11**,** 703-12.

CONSTANTIN, B. 2014. Dystrophin complex functions as a scaffold for signalling proteins. *Biochim Biophys Acta,* 1838**,** 635-42.

CULLEN, M. J. & FULTHORPE, J. J. 1975. Stages in fibre breakdown in Duchenne muscular dystrophy. An electron-microscopic study. *J Neurol Sci,* 24**,** 179-200.

DE-DONCKER, L., PICQUET, F., PETIT, J. & FALEMPIN, M. 2003. Characterization of spindle afferents in rat soleus muscle using ramp-and-hold and sinusoidal stretches. *J Neurophysiol,* 89**,** 442-9.

DE CAMILLI, P., VITADELLO, M., CANEVINI, M. P., ZANONI, R., JAHN, R. & GORIO, A. 1988. The synaptic vesicle proteins synapsin I and synaptophysin (protein P38) are concentrated both in efferent and afferent nerve endings of the skeletal muscle. *J Neurosci,* 8**,** 1625-31.

DE MORREE, A., HENSBERGEN, P. J., VAN HAAGEN, H. H., DRAGAN, I., DEELDER, A. M., T HOEN, P. A., FRANTS, R. R. & VAN DER MAAREL, S. M. 2010. Proteomic analysis of the dysferlin protein complex unveils its importance for sarcolemmal maintenance and integrity. *PLoS One,* 5**,** e13854.

DECONINCK, A. E., POTTER, A. C., TINSLEY, J. M., WOOD, S. J., VATER, R., YOUNG, C., METZINGER, L., VINCENT, A., SLATER, C. R. & DAVIES, K. E. 1997. Postsynaptic abnormalities at the neuromuscular junctions of utrophin-deficient mice. *J Cell Biol,* 136**,** 883-94.

DIETZ, V. 2002. Proprioception and locomotor disorders. *Nat Rev Neurosci,* 3**,** 781-90.

DUANN, P., LI, H., LIN, P., TAN, T., WANG, Z., CHEN, K., ZHOU, X., GUMPPER, K., ZHU, H., LUDWIG, T., MOHLER, P. J., ROVIN, B., ABRAHAM, W. T., ZENG, C. & MA, J. 2015. MG53-mediated cell membrane repair protects against acute kidney injury. *Sci Transl Med,* 7**,** 279ra36.

DUTERTRE, S., NICKE, A. & TSETLIN, V. I. 2017. Nicotinic acetylcholine receptor inhibitors derived from snake and snail venoms. *Neuropharmacology,* 127**,** 196-223.

EDIN, B. B. & VALLBO, A. B. 1990. Dynamic response of human muscle spindle afferents to stretch. *J Neurophysiol,* 63**,** 1297-306.

ELAHI, L. S., SHAMAI, K. N., ABTAHIE, A. M., CAI, A. M., PADMANABHAN, S., BREMER, M. & WILKINSON, K. A. 2018. Diet induced obesity alters muscle spindle afferent function in adult mice. *PLoS One,* 13**,** e0196832.

EMERY, A. E. 1993. Duchenne muscular dystrophy--Meryon's disease. *Neuromuscul Disord,* 3**,** 263-6.

ERVASTI, J. M. 2003. Costameres: the Achilles' heel of Herculean muscle. *J Biol Chem,* 278**,** 13591-4.

ERVASTI, J. M. & CAMPBELL, K. P. 1991. Membrane organization of the dystrophin-glycoprotein complex. *Cell,* 66**,** 1121-31.
FALLON, J. B. & MACEFIELD, V. G. 2007. Vibration sensitivity of human muscle spindles and Golgi tendon organs. *Muscle Nerve,* 36**,** 21-9.
FERGUSON, S. M., BAZALAKOVA, M., SAVCHENKO, V., TAPIA, J. C., WRIGHT, J. & BLAKELY, R. D. 2004. Lethal impairment of cholinergic neurotransmission in hemicholinium-3-sensitive choline transporter knockout mice. *Proc Natl Acad Sci U S A,* 101**,** 8762-7.
FISCHER, M. & SCHAFER, S. S. 1999. Temperature effects on the discharge frequency of primary and secondary endings of isolated cat muscle spindles recorded under a ramp-and-hold stretch. *Brain Res,* 840**,** 1-15.
FISCHER, M. & SCHAFER, S. S. 2002. Effects of the calcium antagonist nifedipine on the afferent impulse activity of isolated cat muscle spindles. *Brain Res,* 954**,** 256-76.
FLIX, B., DE LA TORRE, C., CASTILLO, J., CASAL, C., ILLA, I. & GALLARDO, E. 2013. Dysferlin interacts with calsequestrin-1, myomesin-2 and dynein in human skeletal muscle. *Int J Biochem Cell Biol,* 45**,** 1927-38.
FONG, P. Y., TURNER, P. R., DENETCLAW, W. F. & STEINHARDT, R. A. 1990. Increased activity of calcium leak channels in myotubes of Duchenne human and mdx mouse origin. *Science,* 250**,** 673-6.
FRANCO, A., JR. & LANSMAN, J. B. 1990. Calcium entry through stretch-inactivated ion channels in mdx myotubes. *Nature,* 344**,** 670-3.
FRANCO, J. A., KLOEFKORN, H. E., HOCHMAN, S. & WILKINSON, K. A. 2014. An in vitro adult mouse muscle-nerve preparation for studying the firing properties of muscle afferents. *J Vis Exp***,** 51948.
FRIESE, A., KALTSCHMIDT, J. A., LADLE, D. R., SIGRIST, M., JESSELL, T. M. & ARBER, S. 2009. Gamma and alpha motor neurons distinguished by expression of transcription factor Err3. *Proc Natl Acad Sci U S A,* 106**,** 13588-93.
FUKUDA, H., KUDO, Y. & WATANABE, K. 1972. Effects of anticholinergics on the afferent discharges from the muscle spindle of the bullfrog in vitro. *Jpn J Pharmacol,* 22**,** 381-9.
FUKUDA, K., KOTO, A., FUKUUCHI, Y. & ISHIHARA, T. 1999. Characteristic form of standing up from squatting in Miyoshi's distal muscular dystrophy. *Clin Neurol Neurosurg,* 101**,** 249-52.
GALASSI, G., ROWLAND, L. P., HAYS, A. P., HOPKINS, L. C. & DIMAURO, S. 1987. High serum levels of creatine kinase: asymptomatic prelude to distal myopathy. *Muscle Nerve,* 10**,** 346-50.
GANGULY, D. K., NATH, D. N., ROSS, H. G. & VEDASIROMONI, J. R. 1978. Rat isolated phrenic nerve-diaphragm preparation for pharmacological study of muscle spindle afferent activity: effect of oxotremorine. *Br J Pharmacol,* 64**,** 47-52.
GERWIN, L., HAUPT, C., WILKINSON, K. A. & KROGER, S. 2019. Acetylcholine receptors in the equatorial region of intrafusal muscle fibres modulate mouse muscle spindle sensitivity. *J Physiol,* 597**,** 1993-2006.
GIACOBINI, E. 1959. Quantitative determination of cholinesterase in individual spinal ganglion cells. *Acta Physiol Scand,* 45**,** 238-54.
GILBERT, R., NALBANTOGLU, J., PETROF, B. J., EBIHARA, S., GUIBINGA, G. H., TINSLEY, J. M., KAMEN, A., MASSIE, B., DAVIES, K. E. & KARPATI, G. 1999. Adenovirus-mediated utrophin gene transfer mitigates the dystrophic phenotype of mdx mouse muscles. *Hum Gene Ther,* 10**,** 1299-310.
GOSSRAU, R. & GROZDANOVIC, Z. 1997. NO is not substantially involved in afferent signalling in rat muscle spindles. *Acta Histochem,* 99**,** 445-58.
GRADY, R. M., MERLIE, J. P. & SANES, J. R. 1997. Subtle neuromuscular defects in utrophin-deficient mice. *J Cell Biol,* 136**,** 871-82.
GRASSI, F. & FUCILE, S. 2019. Calcium influx through muscle nAChR-channels: One route, multiple roles. *Neuroscience*.
GROUNDS, M. D. & TORRISI, J. 2004. Anti-TNFalpha (Remicade) therapy protects dystrophic skeletal muscle from necrosis. *FASEB J,* 18**,** 676-82.

GUIRAUD, S., EDWARDS, B., BABBS, A., SQUIRE, S. E., BERG, A., MOIR, L., WOOD, M. J. & DAVIES, K. E. 2019. The potential of utrophin and dystrophin combination therapies for Duchenne muscular dystrophy. *Hum Mol Genet*.

GUIRAUD, S., SQUIRE, S. E., EDWARDS, B., CHEN, H., BURNS, D. T., SHAH, N., BABBS, A., DAVIES, S. G., WYNNE, G. M., RUSSELL, A. J., ELSEY, D., WILSON, F. X., TINSLEY, J. M. & DAVIES, K. E. 2015. Second-generation compound for the modulation of utrophin in the therapy of DMD. *Hum Mol Genet,* 24**,** 4212-24.

HADDIX, S. G., LEE, Y. I., KORNEGAY, J. N. & THOMPSON, W. J. 2018. Cycles of myofiber degeneration and regeneration lead to remodeling of the neuromuscular junction in two mammalian models of Duchenne muscular dystrophy. *PLoS One,* 13**,** e0205926.

HAFTEL, V. K., BICHLER, E. K., NICHOLS, T. R., PINTER, M. J. & COPE, T. C. 2004. Movement reduces the dynamic response of muscle spindle afferents and motoneuron synaptic potentials in rat. *J Neurophysiol,* 91**,** 2164-71.

HAN, R., RADER, E. P., LEVY, J. R., BANSAL, D. & CAMPBELL, K. P. 2011. Dystrophin deficiency exacerbates skeletal muscle pathology in dysferlin-null mice. *Skelet Muscle,* 1**,** 35.

HELLIWELL, T. R., MAN, N. T., MORRIS, G. E. & DAVIES, K. E. 1992. The dystrophin-related protein, utrophin, is expressed on the sarcolemma of regenerating human skeletal muscle fibres in dystrophies and inflammatory myopathies. *Neuromuscul Disord,* 2**,** 177-84.

HIPPENMEYER, S., SHNEIDER, N. A., BIRCHMEIER, C., BURDEN, S. J., JESSELL, T. M. & ARBER, S. 2002. A role for neuregulin1 signaling in muscle spindle differentiation. *Neuron,* 36**,** 1035-1049.

HO, M., POST, C. M., DONAHUE, L. R., LIDOV, H. G., BRONSON, R. T., GOOLSBY, H., WATKINS, S. C., COX, G. A. & BROWN, R. H., JR. 2004. Disruption of muscle membrane and phenotype divergence in two novel mouse models of dysferlin deficiency. *Hum Mol Genet,* 13**,** 1999-2010.

HORNSEY, M. A., LAVAL, S. H., BARRESI, R., LOCHMULLER, H. & BUSHBY, K. 2013. Muscular dystrophy in dysferlin-deficient mouse models. *Neuromuscul Disord,* 23**,** 377-87.

HOSUR, V., KAVIRAYANI, A., RIEFLER, J., CARNEY, L. M., LYONS, B., GOTT, B., COX, G. A. & SHULTZ, L. D. 2012. Dystrophin and dysferlin double mutant mice: a novel model for rhabdomyosarcoma. *Cancer Genet,* 205**,** 232-41.

HOUK, J. & HENNEMAN, E. 1967. Responses of Golgi tendon organs to active contractions of the soleus muscle of the cat. *J Neurophysiol,* 30**,** 466-81.

HOUK, J. C., SINGER, J. J. & HENNEMAN, E. 1971. Adequate stimulus for tendon organs with observations on mechanics of ankle joint. *J Neurophysiol,* 34**,** 1051-65.

HSU, J. D. & FURUMASU, J. 1993. Gait and posture changes in the Duchenne muscular dystrophy child. *Clin Orthop Relat Res***,** 122-5.

HUNT, C. C. 1954. Relation of function to diameter in afferent fibers of muscle nerves. *J Gen Physiol,* 38**,** 117-31.

HUNT, C. C. 1990. Mammalian muscle spindle: peripheral mechanisms. *Physiol Rev,* 70**,** 643-63.

HUNT, C. C. & KUFFLER, S. W. 1951a. Further study of efferent small-nerve fibers to mammalian muscle spindles; multiple spindle innervation and activity during contraction. *J Physiol,* 113**,** 283-97.

HUNT, C. C. & KUFFLER, S. W. 1951b. Stretch receptor discharges during muscle contraction. *J Physiol,* 113**,** 298-315.

HUNT, C. C. & OTTOSON, D. 1977. Responses of primary and secondary endings of isolated mammalian muscle spindles to sinusoidal length changes. *J Neurophysiol,* 40**,** 1113-20.

HUNT, C. C., WILKINSON, R. S. & FUKAMI, Y. 1978. Ionic basis of the receptor potential in primary endings of mammalian muscle spindles. *J Gen Physiol,* 71**,** 683-98.

JOHNSON, M. I. & OVALLE, W. K. 1986. A comparative study of muscle spindles in slow and fast neonatal muscles of normal and dystrophic mice. *Am J Anat,* 175**,** 413-27.

KARARIZOU, E. G., MANTA, P., KALFAKIS, N., GKIATAS, K. A. & VASSILOPOULOS, D. 2007. Morphologic and morphometrical study of the muscle spindle in muscular dystrophy. *Anal Quant Cytol Histol,* 29**,** 148-52.

KEEP, N. H. 2000. Structural comparison of actin binding in utrophin and dystrophin. *Neurol Sci,* 21**,** S929-37.

KENNEDY, T. L., MOIR, L., HEMMING, S., EDWARDS, B., SQUIRE, S., DAVIES, K. & GUIRAUD, S. 2017. Utrophin influences mitochondrial pathology and oxidative stress in dystrophic muscle. *Skelet Muscle,* 7**,** 22.

KERR, J. P., ZIMAN, A. P., MUELLER, A. L., MURIEL, J. M., KLEINHANS-WELTE, E., GUMERSON, J. D., VOGEL, S. S., WARD, C. W., ROCHE, J. A. & BLOCH, R. J. 2013. Dysferlin stabilizes stress-induced Ca2+ signaling in the transverse tubule membrane. *Proc Natl Acad Sci U S A,* 110**,** 20831-6.

KHURANA, T. S., WATKINS, S. C., CHAFEY, P., CHELLY, J., TOME, F. M., FARDEAU, M., KAPLAN, J. C. & KUNKEL, L. M. 1991. Immunolocalization and developmental expression of dystrophin related protein in skeletal muscle. *Neuromuscul Disord,* 1**,** 185-94.

KINDIG, A. E., HAYES, S. G., HANNA, R. L. & KAUFMAN, M. P. 2006. P2 antagonist PPADS attenuates responses of thin fiber afferents to static contraction and tendon stretch. *Am J Physiol Heart Circ Physiol,* 290**,** H1214-9.

KLINGE, L., HARRIS, J., SEWRY, C., CHARLTON, R., ANDERSON, L., LAVAL, S., CHIU, Y. H., HORNSEY, M., STRAUB, V., BARRESI, R., LOCHMULLER, H. & BUSHBY, K. 2010. Dysferlin associates with the developing T-tubule system in rodent and human skeletal muscle. *Muscle Nerve,* 41**,** 166-73.

KRAG, T. O., BOGDANOVICH, S., JENSEN, C. J., FISCHER, M. D., HANSEN-SCHWARTZ, J., JAVAZON, E. H., FLAKE, A. W., EDVINSSON, L. & KHURANA, T. S. 2004. Heregulin ameliorates the dystrophic phenotype in mdx mice. *Proc Natl Acad Sci U S A,* 101**,** 13856-60.

KRÖGER, S. 2018. Proprioception 2.0: novel functions for muscle spindles. *Curr Opin Neurol,* 31**,** 592-598.

KRUSE, M. N. & POPPELE, R. E. 1991. Components of the dynamic response of mammalian muscle spindles that originate in the sensory terminals. *Exp Brain Res,* 86**,** 359-66.

KUNKEL, L. M., MONACO, A. P., MIDDLESWORTH, W., OCHS, H. D. & LATT, S. A. 1985. Specific cloning of DNA fragments absent from the DNA of a male patient with an X chromosome deletion. *Proc Natl Acad Sci U S A,* 82**,** 4778-82.

LARSSON, L. & EDSTROM, L. 1986. Effects of age on enzyme-histochemical fibre spectra and contractile properties of fast- and slow-twitch skeletal muscles in the rat. *J Neurol Sci,* 76**,** 69-89.

LE RUMEUR, E., WINDER, S. J. & HUBERT, J. F. 2010. Dystrophin: more than just the sum of its parts. *Biochim Biophys Acta,* 1804**,** 1713-22.

LI, J. Y., EDELMANN, L., JAHN, R. & DAHLSTROM, A. 1996. Axonal transport and distribution of synaptobrevin I and II in the rat peripheral nervous system. *J Neurosci,* 16**,** 137-47.

LIN, S. & BURGUNDER, J. M. 2000. Utrophin may be a precursor of dystrophin during skeletal muscle development. *Brain Res Dev Brain Res,* 119**,** 289-95.

LIN, S., GASCHEN, F. & BURGUNDER, J. M. 1998. Utrophin is a regeneration-associated protein transiently present at the sarcolemma of regenerating skeletal muscle fibers in dystrophin-deficient hypertrophic feline muscular dystrophy. *J Neuropathol Exp Neurol,* 57**,** 780-90.

LIONIKAS, A., SMITH, C. J., SMITH, T. L., BUNGER, L., BANKS, R. W. & BEWICK, G. S. 2013. Analyses of muscle spindles in the soleus of six inbred mouse strains. *J Anat,* 223**,** 289-96.

LIU, J., AOKI, M., ILLA, I., WU, C., FARDEAU, M., ANGELINI, C., SERRANO, C., URTIZBEREA, J. A., HENTATI, F., HAMIDA, M. B., BOHLEGA, S., CULPER, E. J., AMATO, A. A., BOSSIE, K., OELTJEN, J., BEJAOUI, K., MCKENNA-YASEK, D., HOSLER, B. A., SCHURR, E., ARAHATA, K., DE JONG, P. J. & BROWN, R. H.,

JR. 1998. Dysferlin, a novel skeletal muscle gene, is mutated in Miyoshi myopathy and limb girdle muscular dystrophy. *Nat Genet,* 20**,** 31-6.
LOVE, D. R., HILL, D. F., DICKSON, G., SPURR, N. K., BYTH, B. C., MARSDEN, R. F., WALSH, F. S., EDWARDS, Y. H. & DAVIES, K. E. 1989. An autosomal transcript in skeletal muscle with homology to dystrophin. *Nature,* 339**,** 55-8.
LUND, D., RUGGIERO, A. M., FERGUSON, S. M., WRIGHT, J., ENGLISH, B. A., REISZ, P. A., WHITAKER, S. M., PELTIER, A. C. & BLAKELY, R. D. 2010a. Motor neuron-specific overexpression of the presynaptic choline transporter: impact on motor endurance and evoked muscle activity. *Neuroscience,* 171**,** 1041-53.
LUND, J. P., SADEGHI, S., ATHANASSIADIS, T., CARAM SALAS, N., AUCLAIR, F., THIVIERGE, B., ARSENAULT, I., ROMPRE, P., WESTBERG, K. G. & KOLTA, A. 2010b. Assessment of the potential role of muscle spindle mechanoreceptor afferents in chronic muscle pain in the rat masseter muscle. *PLoS One,* 5**,** e11131.
MAH, J. K., KORNGUT, L., DYKEMAN, J., DAY, L., PRINGSHEIM, T. & JETTE, N. 2014. A systematic review and meta-analysis on the epidemiology of Duchenne and Becker muscular dystrophy. *Neuromuscul Disord,* 24**,** 482-91.
MAHJNEH, I., MARCONI, G., BUSHBY, K., ANDERSON, L. V., TOLVANEN-MAHJNEH, H. & SOMER, H. 2001. Dysferlinopathy (LGMD2B): a 23-year follow-up study of 10 patients homozygous for the same frameshifting dysferlin mutations. *Neuromuscul Disord,* 11**,** 20-6.
MAIER, A. & MAYNE, R. 1995. Basal lamina development in chicken muscle spindles. *Dev Dyn,* 202**,** 284-93.
MALLOUK, N., JACQUEMOND, V. & ALLARD, B. 2000. Elevated subsarcolemmal Ca2+ in mdx mouse skeletal muscle fibers detected with Ca2+-activated K+ channels. *Proc Natl Acad Sci U S A,* 97**,** 4950-5.
MATSUDA, C., HAYASHI, Y. K., OGAWA, M., AOKI, M., MURAYAMA, K., NISHINO, I., NONAKA, I., ARAHATA, K. & BROWN, R. H., JR. 2001. The sarcolemmal proteins dysferlin and caveolin-3 interact in skeletal muscle. *Hum Mol Genet,* 10**,** 1761-6.
MATSUDA, C., MIYAKE, K., KAMEYAMA, K., KEDUKA, E., TAKESHIMA, H., IMAMURA, T., ARAKI, N., NISHINO, I. & HAYASHI, Y. 2012. The C2A domain in dysferlin is important for association with MG53 (TRIM72). *PLoS Curr,* 4**,** e5035add8caff4.
MATTHEWS, P. B. 1963. The Response of De-Efferented Muscle Spindle Receptors to Stretching at Different Velocities. *J Physiol,* 168**,** 660-78.
MATTHEWS, P. B. 1964. Muscle Spindles and Their Motor Control. *Physiol Rev,* 44**,** 219-88.
MCGEACHIE, J. K., GROUNDS, M. D., PARTRIDGE, T. A. & MORGAN, J. E. 1993. Age-related changes in replication of myogenic cells in mdx mice: quantitative autoradiographic studies. *J Neurol Sci,* 119**,** 169-79.
MCNEIL, P. 2009. Membrane repair redux: redox of MG53. *Nat Cell Biol,* 11**,** 7-9.
MERCURI, E. & MUNTONI, F. 2013. Muscular dystrophy: new challenges and review of the current clinical trials. *Curr Opin Pediatr,* 25**,** 701-7.
MERYON, E. 1852. On Granular and Fatty Degeneration of the Voluntary Muscles. *Med Chir Trans,* 35**,** 73-84 1.
MESSINA, S., BITTO, A., AGUENNOUZ, M., MINUTOLI, L., MONICI, M. C., ALTAVILLA, D., SQUADRITO, F. & VITA, G. 2006. Nuclear factor kappa-B blockade reduces skeletal muscle degeneration and enhances muscle function in Mdx mice. *Exp Neurol,* 198**,** 234-41.
MICHALSKI, W. J. & SEGUIN, J. J. 1975. The effects of muscle cooling and stretch on muscle spindle secondary endings in the cat. *J Physiol,* 253**,** 341-56.
MILLAY, D. P., GOONASEKERA, S. A., SARGENT, M. A., MAILLET, M., ARONOW, B. J. & MOLKENTIN, J. D. 2009. Calcium influx is sufficient to induce muscular dystrophy through a TRPC-dependent mechanism. *Proc Natl Acad Sci U S A,* 106**,** 19023-8.
NAHIRNEY, P. C. & OVALLE, W. K. 1993. Distribution of dystrophin and neurofilament protein in muscle spindles of normal and Mdx-dystrophic mice: an immunocytochemical study. *Anat Rec,* 235**,** 501-10.

NAKATA, K., OKUDA, T. & MISAWA, H. 2004. Ultrastructural localization of high-affinity choline transporter in the rat neuromuscular junction: enrichment on synaptic vesicles. *Synapse,* 53**,** 53-6.

NEELY, G. A. & KOHLI, A. 2017. Neostigmine. *StatPearls.* Treasure Island (FL).

NEUHAUS, R., ROSENTHAL, R. & LUTTGAU, H. C. 1990. The effects of dihydropyridine derivatives on force and Ca2+ current in frog skeletal muscle fibres. *J Physiol,* 427**,** 187-209.

NGUYEN, T. M., ELLIS, J. M., LOVE, D. R., DAVIES, K. E., GATTER, K. C., DICKSON, G. & MORRIS, G. E. 1991. Localization of the DMDL gene-encoded dystrophin-related protein using a panel of nineteen monoclonal antibodies: presence at neuromuscular junctions, in the sarcolemma of dystrophic skeletal muscle, in vascular and other smooth muscles, and in proliferating brain cell lines. *J Cell Biol,* 115**,** 1695-700.

OHLENDIECK, K., ERVASTI, J. M., MATSUMURA, K., KAHL, S. D., LEVEILLE, C. J. & CAMPBELL, K. P. 1991. Dystrophin-related protein is localized to neuromuscular junctions of adult skeletal muscle. *Neuron,* 7**,** 499-508.

OTTOSON, D. 1965. The effects of temperature on the isolated muscle spindle. *J Physiol,* 180**,** 636-48.

OVALLE, W. K. & DOW, P. R. 1986. Alterations in muscle spindle morphology in advanced stages of murine muscular dystrophy. *Anat Rec,* 216**,** 111-26.

OVALLE, W. K., JR. 1972. Fine structure of rat intrafusal muscle fibers. The equatorial region. *J Cell Biol,* 52**,** 382-96.

OZAWA, E., NOGUCHI, S., MIZUNO, Y., HAGIWARA, Y. & YOSHIDA, M. 1998. From dystrophinopathy to sarcoglycanopathy: evolution of a concept of muscular dystrophy. *Muscle Nerve,* 21**,** 421-38.

PELOQUIN, J. B., DOERING, C. J., REHAK, R. & MCRORY, J. E. 2008. Temperature dependence of Cav1.4 calcium channel gating. *Neuroscience,* 151**,** 1066-83.

PILGRAM, G. S., POTIKANOND, S., BAINES, R. A., FRADKIN, L. G. & NOORDERMEER, J. N. 2010. The roles of the dystrophin-associated glycoprotein complex at the synapse. *Mol Neurobiol,* 41**,** 1-21.

PRADHAN, S., GHOSH, D., SRIVASTAVA, N. K., KUMAR, A., MITTAL, B., PANDEY, C. M. & SINGH, U. 2006. Prednisolone in Duchenne muscular dystrophy with imminent loss of ambulation. *J Neurol,* 253**,** 1309-16.

PROSKE, U. 1997. The mammalian muscle spindle. *News Physiol. Sci,* 12**,** 37–42.

PROSKE, U. & GANDEVIA, S. C. 2012. The proprioceptive senses: their roles in signaling body shape, body position and movement, and muscle force. *Physiol Rev,* 92**,** 1651-97.

PROSKE, U. & GANDEVIA, S. C. 2018. Kinesthetic Senses. *Compr Physiol,* 8**,** 1157-1183.

PROSKE, U., GREGORY, J. E. & MORGAN, D. L. 1991. Where in the muscle spindle is the resting discharge generated? *Exp Physiol,* 76**,** 777-85.

RAJAGANAPATHY, S., MCCOURT, J. L., GHOSAL, S., LINDSAY, A., MCCOURT, P. M., LOWE, D. A., ERVASTI, J. M. & SALAPAKA, M. V. 2019. Distinct mechanical properties in homologous spectrin-like repeats of utrophin. *Sci Rep,* 9**,** 5210.

RAY, P. N., BELFALL, B., DUFF, C., LOGAN, C., KEAN, V., THOMPSON, M. W., SYLVESTER, J. E., GORSKI, J. L., SCHMICKEL, R. D. & WORTON, R. G. 1985. Cloning of the breakpoint of an X;21 translocation associated with Duchenne muscular dystrophy. *Nature,* 318**,** 672-5.

RAYMACKERS, J. M., DEBAIX, H., COLSON-VAN SCHOOR, M., DE BACKER, F., TAJEDDINE, N., SCHWALLER, B., GAILLY, P. & GILLIS, J. M. 2003. Consequence of parvalbumin deficiency in the mdx mouse: histological, biochemical and mechanical phenotype of a new double mutant. *Neuromuscul Disord,* 13**,** 376-87.

RIBOT-CISCAR, E., TREFOURET, S., AIMONETTI, J. M., ATTARIAN, S., POUGET, J. & ROLL, J. P. 2004. Is muscle spindle proprioceptive function spared in muscular dystrophies? A muscle tendon vibration study. *Muscle Nerve,* 29**,** 861-6.

ROBERT, V., MASSIMINO, M. L., TOSELLO, V., MARSAULT, R., CANTINI, M., SORRENTINO, V. & POZZAN, T. 2001. Alteration in calcium handling at the subcellular level in mdx myotubes. *J Biol Chem,* 276**,** 4647-51.

ROCHE, I., TURMO, M. & MERLIO, J. P. 2000. [One heat-induced antigen retrieval step allows the sequential detection of two antigens on the same slide of tissue fixed and enclosed in paraffin]. *Ann Pathol,* 20**,** 171-5.

RODRIGUEZ, B. M., SIGG, D. & BEZANILLA, F. 1998. Voltage gating of Shaker K+ channels. The effect of temperature on ionic and gating currents. *J Gen Physiol,* 112**,** 223-42.

ROSALES, X. Q., GASTIER-FOSTER, J. M., LEWIS, S., VINOD, M., THRUSH, D. L., ASTBURY, C., PYATT, R., RESHMI, S., SAHENK, Z. & MENDELL, J. R. 2010. Novel diagnostic features of dysferlinopathies. *Muscle Nerve,* 42**,** 14-21.

RUFFINI, A. 1898. On the Minute Anatomy of the Neuromuscular Spindles of the Cat, and on their Physiological Significance. *J Physiol,* 23**,** 190-208 3.

SANES, J. R., JOHNSON, Y. R., KOTZBAUER, P. T., MUDD, J., HANLEY, T., MARTINOU, J. C. & MERLIE, J. P. 1991. Selective expression of an acetylcholine receptor-lacZ transgene in synaptic nuclei of adult muscle fibers. *Development,* 113**,** 1181-1191.

SANTINI, M. & IBATA, Y. 1971. The fine structure of thin unmyelinated axons within muscle spindles. *Brain Res,* 33**,** 289-302.

SCHINDELIN, J., ARGANDA-CARRERAS, I., FRISE, E., KAYNIG, V., LONGAIR, M., PIETZSCH, T., PREIBISCH, S., RUEDEN, C., SAALFELD, S., SCHMID, B., TINEVEZ, J. Y., WHITE, D. J., HARTENSTEIN, V., ELICEIRI, K., TOMANCAK, P. & CARDONA, A. 2012. Fiji: an open-source platform for biological-image analysis. *Nat Methods,* 9**,** 676-82.

SCHMIDT, W. M., UDDIN, M. H., DYSEK, S., MOSER-THIER, K., PIRKER, C., HOGER, H., AMBROS, I. M., AMBROS, P. F., BERGER, W. & BITTNER, R. E. 2011. DNA damage, somatic aneuploidy, and malignant sarcoma susceptibility in muscular dystrophies. *PLoS Genet,* 7**,** e1002042.

SCHOBER, R. & THOMAS, E. 1978. The fine structural localization of acetylcholinesterase in the muscle spindle of the rat. *Cell Tissue Res,* 186**,** 39-52.

SCHOFIELD, J., HOUZELSTEIN, D., DAVIES, K., BUCKINGHAM, M. & EDWARDS, Y. H. 1993. Expression of the dystrophin-related protein (utrophin) gene during mouse embryogenesis. *Dev Dyn,* 198**,** 254-64.

SHERRINGTON, C. S. 1894. On the Anatomical Constitution of Nerves of Skeletal Muscles; with Remarks on Recurrent Fibres in the Ventral Spinal Nerve-root. *J Physiol,* 17**,** 210 2-258.

SHNEIDER, N. A., BROWN, M. N., SMITH, C. A., PICKEL, J. & ALVAREZ, F. J. 2009. Gamma motor neurons express distinct genetic markers at birth and require muscle spindle-derived GDNF for postnatal survival. *Neural Dev,* 4**,** 42.

SIMON, A., SHENTON, F., HUNTER, I., BANKS, R. W. & BEWICK, G. S. 2010. Amiloride-sensitive channels are a major contributor to mechanotransduction in mammalian muscle spindles. *J Physiol,* 588**,** 171-85.

SKUK, D., GOULET, M. & TREMBLAY, J. P. 2010. Preservation of muscle spindles in a 27-year-old Duchenne muscular dystrophy patient: importance for regenerative medicine strategies. *Muscle Nerve,* 41**,** 729-30.

SMITH, C. M. & ALBUQUERQUE, E. X. 1967. Differences in the tubocurarine antagonism of the activation of muscle spindle afferents by siccinylcholine, acetylcholine and nicotine. *J Pharmacol Exp Ther,* 156**,** 573-84.

SONNER, M. J., WALTERS, M. C. & LADLE, D. R. 2017. Analysis of Proprioceptive Sensory Innervation of the Mouse Soleus: A Whole-Mount Muscle Approach. *PLoS One,* 12**,** e0170751.

SWASH, M. & FOX, K. P. 1976. The pathology of the muscle spindle in Duchenne muscular dystrophy. *J Neurol Sci,* 29**,** 17-32.

TAKEDA, K. & TRAUTMANN, A. 1984. A patch-clamp study of the partial agonist actions of tubocurarine on rat myotubes. *J Physiol,* 349**,** 353-74.

TAKEOKA, A., VOLLENWEIDER, I., COURTINE, G. & ARBER, S. 2014. Muscle spindle feedback directs locomotor recovery and circuit reorganization after spinal cord injury. *Cell,* 159**,** 1626-39.

TALY, A., CORRINGER, P. J., GUEDIN, D., LESTAGE, P. & CHANGEUX, J. P. 2009. Nicotinic receptors: allosteric transitions and therapeutic targets in the nervous system. *Nat Rev Drug Discov,* 8**,** 733-50.

TIDBALL, J. G. 2011. Mechanisms of muscle injury, repair, and regeneration. *Compr Physiol,* 1**,** 2029-62.

TINSLEY, J., DECONINCK, N., FISHER, R., KAHN, D., PHELPS, S., GILLIS, J. M. & DAVIES, K. 1998. Expression of full-length utrophin prevents muscular dystrophy in mdx mice. *Nat Med,* 4**,** 1441-4.

TINSLEY, J. M., BLAKE, D. J., ROCHE, A., FAIRBROTHER, U., RISS, J., BYTH, B. C., KNIGHT, A. E., KENDRICK-JONES, J., SUTHERS, G. K., LOVE, D. R. & ET AL. 1992. Primary structure of dystrophin-related protein. *Nature,* 360**,** 591-3.

TINSLEY, J. M., FAIRCLOUGH, R. J., STORER, R., WILKES, F. J., POTTER, A. C., SQUIRE, S. E., POWELL, D. S., COZZOLI, A., CAPOGROSSO, R. F., LAMBERT, A., WILSON, F. X., WREN, S. P., DE LUCA, A. & DAVIES, K. E. 2011. Daily treatment with SMTC1100, a novel small molecule utrophin upregulator, dramatically reduces the dystrophic symptoms in the mdx mouse. *PLoS One,* 6**,** e19189.

TURNER, P. R., SCHULTZ, R., GANGULY, B. & STEINHARDT, R. A. 1993. Proteolysis results in altered leak channel kinetics and elevated free calcium in mdx muscle. *J Membr Biol,* 133**,** 243-51.

TURNER, P. R., WESTWOOD, T., REGEN, C. M. & STEINHARDT, R. A. 1988. Increased protein degradation results from elevated free calcium levels found in muscle from mdx mice. *Nature,* 335**,** 735-8.

TUTHILL, J. C. & AZIM, E. 2018. Proprioception. *Curr Biol,* 28**,** R194-R203.

UMAKHANOVA, Z. R., BARDAKOV, S. N., MAVLIKEEV, M. O., CHERNOVA, O. N., MAGOMEDOVA, R. M., AKHMEDOVA, P. G., YAKOVLEV, I. A., DALGATOV, G. D., FEDOTOV, V. P., ISAEV, A. A. & DEEV, R. V. 2017. Twenty-Year Clinical Progression of Dysferlinopathy in Patients from Dagestan. *Front Neurol,* 8**,** 77.

VAFIADAKI, E., REIS, A., KEERS, S., HARRISON, R., ANDERSON, L. V., RAFFELSBERGER, T., IVANOVA, S., HOGER, H., BITTNER, R. E., BUSHBY, K. & BASHIR, R. 2001. Cloning of the mouse dysferlin gene and genomic characterization of the SJL-Dysf mutation. *Neuroreport,* 12**,** 625-9.

VANDEBROUCK, C., MARTIN, D., COLSON-VAN SCHOOR, M., DEBAIX, H. & GAILLY, P. 2002. Involvement of TRPC in the abnormal calcium influx observed in dystrophic (mdx) mouse skeletal muscle fibers. *J Cell Biol,* 158**,** 1089-96.

WADDELL, L. B., LEMCKERT, F. A., ZHENG, X. F., TRAN, J., EVESSON, F. J., HAWKES, J. M., LEK, A., STREET, N. E., LIN, P., CLARKE, N. F., LANDSTROM, A. P., ACKERMAN, M. J., WEISLEDER, N., MA, J., NORTH, K. N. & COOPER, S. T. 2011. Dysferlin, annexin A1, and mitsugumin 53 are upregulated in muscular dystrophy and localize to longitudinal tubules of the T-system with stretch. *J Neuropathol Exp Neurol,* 70**,** 302-13.

WAITE, A., BROWN, S. C. & BLAKE, D. J. 2012. The dystrophin-glycoprotein complex in brain development and disease. *Trends Neurosci,* 35**,** 487-96.

WAITE, A., TINSLEY, C. L., LOCKE, M. & BLAKE, D. J. 2009. The neurobiology of the dystrophin-associated glycoprotein complex. *Ann Med,* 41**,** 344-59.

WENK, H. N. & MCCLESKEY, E. W. 2007. A novel mouse skeletal muscle-nerve preparation and in vitro model of ischemia. *J Neurosci Methods,* 159**,** 244-51.

WILKINSON, K. A., KLOEFKORN, H. E. & HOCHMAN, S. 2012. Characterization of muscle spindle afferents in the adult mouse using an in vitro muscle-nerve preparation. *PLoS One,* 7**,** e39140.

WILLMANN, R., POSSEKEL, S., DUBACH-POWELL, J., MEIER, T. & RUEGG, M. A. 2009. Mammalian animal models for Duchenne muscular dystrophy. *Neuromuscul Disord,* 19**,** 241-9.

WOO, S. H., LUKACS, V., DE NOOIJ, J. C., ZAYTSEVA, D., CRIDDLE, C. R., FRANCISCO, A., JESSELL, T. M., WILKINSON, K. A. & PATAPOUTIAN, A. 2015. Piezo2 is the principal mechanotransduction channel for proprioception. *Nat Neurosci,* 18**,** 1756-62.

WU, S. X., KOSHIMIZU, Y., FENG, Y. P., OKAMOTO, K., FUJIYAMA, F., HIOKI, H., LI, Y. Q., KANEKO, T. & MIZUNO, N. 2004. Vesicular glutamate transporter immunoreactivity in the central and peripheral endings of muscle-spindle afferents. *Brain Res,* 1011**,** 247-51.

YELLIN, H. 1969. Unique intrafusal and extraocular muscle fibers exhibiting dual actomyosin ATPase activity. *Exp Neurol,* 25**,** 153-63.

YOSHIDA, M., HAMA, H., ISHIKAWA-SAKURAI, M., IMAMURA, M., MIZUNO, Y., ARAISHI, K., WAKABAYASHI-TAKAI, E., NOGUCHI, S., SASAOKA, T. & OZAWA, E. 2000. Biochemical evidence for association of dystrobrevin with the sarcoglycan-sarcospan complex as a basis for understanding sarcoglycanopathy. *Hum Mol Genet,* 9**,** 1033-40.

YU, S. P. & VAN DER KLOOT, W. 1991. Increasing quantal size at the mouse neuromuscular junction and the role of choline. *J Physiol,* 433**,** 677-704.

ZHANG, Y., WESOLOWSKI, M., KARAKATSANI, A., WITZEMANN, V. & KRÖGER, S. 2014. Formation of cholinergic synapse-like specializations at developing murine muscle spindles. *Developmental Biology,* 393**,** 227-35.

ZISKIND, L. & DENNIS, M. J. 1978. Depolarising effect of curare on embryonic rat muscles. *Nature,* 276**,** 622-3.

Appendix A: List of figures

Appendix B: List of tables

Appendix C: Authors approval

JOHN WILEY AND SONS LICENSE TERMS AND CONDITIONS

Sep 20, 2018

This Agreement between Laura Gerwin ("You") and John Wiley and Sons ("John Wiley and Sons") consists of your license details and the terms and conditions provided by John Wiley and Sons and Copyright Clearance Center.

License Number	4433180053693
License date	Sep 20, 2018
Licensed Content Publisher	John Wiley and Sons
Licensed Content Publication	The Anatomical Record: Advances in Integrative Anatomy and Evolutionary Biology
Licensed Content Title	Distribution of dystrophin and neurofilament protein in muscle spindles of normal and mdx-dystrophic mice: An immunocytochemical study
Licensed Content Author	Patrick C. Nahirney, William K. Ovalle
Licensed Content Date	Jan 26, 2005
Licensed Content Volume	235
Licensed Content Issue	4
Licensed Content Pages	10
Type of use	Dissertation/Thesis
Requestor type	University/Academic
Format	Print and electronic
Portion	Figure/table
Number of figures/tables	1
Original Wiley figure/table number(s)	Figure 7
Will you be translating?	No
Title of your thesis / dissertation	The function of the acetylcholine receptor at the central part of the muscle spindle and the functional changes of muscles spindles in murine models of muscular dystrophy
Expected completion date	Nov 2018
Expected size (number of pages)	100
Requestor Location	Laura Gerwin [redacted] [redacted] Germany Attn: Laura Gerwin
Publisher Tax ID	EU826007151
Total	0.00 EUR
Terms and Conditions	

TERMS AND CONDITIONS

This copyrighted material is owned by or exclusively licensed to John Wiley & Sons, Inc. or one of its group companies (each a"Wiley Company") or handled on behalf of a society with which a Wiley Company has exclusive publishing rights in relation to a particular work